Technical Report Documentation Page

1. Report No.	2. Government Accession No.	3. Recipient's Catalog No.
FHWA/TX-96/1409-1		

4. Title and Subtitle	5. Report Date
HYDRAULIC CHARACTERISTICS OF FLUSH DEPRESSED CURB INLETS AND BRIDGE DECK DRAINS	December 1995
	6. Performing Organization Code

7. Author(s)	8. Performing Organization Report No.
Mark Alan Hammonds and Edward Holley	Research Report 1409-1

9. Performing Organization Name and Address	10. Work Unit No. (TRAIS)
Center for Transportation Research The University of Texas at Austin 3208 Red River, Suite 200 Austin, Texas 78705-2650	11. Contract or Grant No. Research Study 0-1409
	13. Type of Report and Period Covered Interim
12. Sponsoring Agency Name and Address Texas Department of Transportation Research and Technology Transfer Office P. O. Box 5080 Austin, Texas 78763-5080	14. Sponsoring Agency Code

15. Supplementary Notes

Study conducted in cooperation with the U.S. Department of Transportation, Federal Highway Administration. Research study title: "Hydraulic Characteristics of Recessed Curb Inlets and Bridge Drains: Phase 2"

16. Abstract

This report presents the results of a research project to determine the hydraulic characteristics of and to develop design equations for two types of stormwater drainage structures: flush depressed curb inlets and bridge deck drains. Flush depressed curb inlets are so named because the lip of the inlet opening is flush with the curb line and the gutter section adjacent to the inlet opening is depressed. Bridge deck drains consist of grated openings in the bridge deck supported by a drain pan. All of the drainage structure designs tested in this project are used by the Texas Department of Transportation in the State of Texas. Except for one of the bridge deck drains, no empirical design information existed previously for any of the drainage structures tested in this project. One of the bridge deck drains had been tested previously in a different orientation.

To determine the hydraulic characteristics of the drainage structures, models of the structures were tested on a large roadway model. Curb inlets were tested at 3/4 scale; bridge deck drains were tested at full scale. The measurements made during the model studies were correlated to the capacity of the inlets and drains to develop empirical design equations.

The performance of curb inlets is usually divided into the following two categories: (1) 100% efficiency, in which the inlet is capturing all of the approach flow, and (2) less than 100% efficiency, in which there is carryover flow. The design method developed in this project for flush depressed curb inlets utilized a new empirical equation for the 100% efficiency capacity of the inlets on the basis of the effective length of the inlet. For less than 100% efficiency, an existing TxDOT design equation was used, also on the basis of the effective inlet length.

Two types of bridge deck drains were tested. Empirical design equations were developed for both drains. The equations are a function of the roadway geometry and approach flow conditions.

17. Key Words	18. Distribution Statement
Flush depressed curb inlets, bridge deck drains, hydraulic behavior	No restrictions. This document is available to the public through the National Technical Information Service, Springfield, Virginia 22161.

19. Security Classif. (of this report)	20. Security Classif. (of this page)	21. No. of Pages	22. Price
Unclassified	Unclassified	170	

HYDRAULIC CHARACTERISTICS OF FLUSH DEPRESSED CURB INLETS AND BRIDGE DECK DRAINS

by

Mark Alan Hammons
Edward R. Holley

Research Report 0-1409-01

Research Project 0-1409
Hydraulic Characteristics of Recessed Curb Inlets and Bridge Drains
Phase 2

conducted for the

Texas Department of Transportation

in cooperation with the

U.S. Department of Transportation
Federal Highway Administration

by the

CENTER FOR TRANSPORTATION RESEARCH
Bureau of Engineering Research
THE UNIVERSITY OF TEXAS AT AUSTIN

December 1995

IMPLEMENTATION STATEMENT

Experiments using Type C and Type D depressed curb inlets showed that the capacity equations used by TxDOT are not applicable for these inlets. The primary problem is with the equation for 100% efficiency which overestimated the capacity of the inlets. The equation for less than 100% efficiency has acceptable accuracy if an accurate equation is used for 100% efficiency. The appropriate equation (Equation 4.6) for Type C and Type D inlets for 100% efficiency is

$$q_{L,eff} = \frac{Q}{L_{r,eff}} = 0.196 y_n - 0.0023$$

where $q_{L,eff}$ = flow captured per unit of effective length of the inlet ($m^3/s/m$), Q = approach flow rate (m^3/s), $L_{r,eff}$ = required effective length of the inlet opening to capture 100% of the approach flow (m) (and also $L_{r,eff}$ = actual effective length at 100% efficiency), and y_n = normal depth for approach flow (m). The effective length is the actual opening length plus the 3.05 m combined length of the upstream and downstream depression transitions. For less than 100% efficiency, the design equation (Equation 4.7) is

$$\frac{Q}{Q_a} = \frac{\left(\frac{a}{y_n}+1\right)^{5/2} - \left(\frac{a}{y_n}+1-\frac{L_{eff}}{L_{r,eff}}\right)^{5/2}}{\left(\frac{a}{y_n}+1\right)^{5/2} - \left(\frac{a}{y_n}\right)^{5/2}}$$

where Q = captured flow rate (m^3/s), Q_a = approach flow rate (m^3/s), a = depression depth (m), and L_{eff} = actual effective length (m). These equations are valid for inlet lengths from 1.52 m to 4.57 m, longitudinal slopes from 0.004 to 0.06, transverse slopes from 0.0208 (1:48) to 0.0417 (1:24), approach flow rates up to 0.25 m^3/s, and captured flow rates up to 0.15 m^3/s.

One of the design capacity equations (namely, Equation 5.1) developed from the experiments for the bridge deck drain called Drain 2B is

$$Q_{2B} = 0.201\, y_n^{1.32} \frac{S^{0.16}}{S_x^{0.60}}$$

where Q_{2B} = flow rate captured by the drain (m^3/s), S = longitudinal slope, and S_x = cross slope. An alternate equation which has a 40% smaller standard error but which is a little more difficult to use is

$$Q_{2B} = -0.00646 + 2.04f - 33.5f^2$$

where $f = 0.201 y_n^{1.32} S^{0.16} S_x^{-0.60}$. These equations are valid for longitudinal slopes from 0.004 to 0.06, transverse slopes from 0.0208 (1:48) to 0.0417 (1:24), approach flow rates up to 0.12 m^3/s, and captured flow rates up to 0.025 m^3/s. Drain 4, which is larger and deeper than Drain 2B and also has a larger outlet pipe size, is more efficient than Drain 2B. The design capacity equations for Drain 4 are

$$Q_{4,low} = 8.63 y_n^{2.44} \frac{S^{0.42}}{S_x^{0.93}}$$

for low flows ($Q_{4,low} < 0.027$ m^3/s) and

$$Q_{4,high} = 0.420 y_n^{2.44} \frac{S^{0.42}}{S_x^{0.93}}$$

for higher flows ($Q_{4,high} > 0.027$ m^3/s). These equations are valid for longitudinal slopes from 0.004 to 0.06, transverse slopes from 0.0208 (1:48) to 0.0417 (1:24), approach flow rates up to 0.20 m^3/s, and captured flow rates up to 0.068 m^3/s.

Prepared in cooperation with the Texas Department of Transportation and the
U.S. Department of Transportation, Federal Highway Administration.

DISCLAIMERS

The contents of this report reflect the views of the authors, who are responsible for the facts and the accuracy of the data presented herein. The contents do not necessarily reflect the official views or policies of the Federal Highway Administration or the Texas Department of Transportation. This report does not constitute a standard, specification, or regulation.

NOT INTENDED FOR CONSTRUCTION,
BIDDING, OR PERMIT PURPOSES

E.R. Holley
Research Supervisor

SUMMARY

This report presents the results of a research project to determine the hydraulic characteristics of and to develop design equations for two types of stormwater drainage structures: flush depressed curb inlets and bridge deck drains. Flush depressed curb inlets are so named because the lip of the inlet opening is flush with the curb line and the gutter section adjacent to the inlet opening is depressed. Bridge deck drains consist of grated openings in the bridge deck supported by a drain pan. All of the drainage structure designs tested in this project are used by the Texas Department of Transportation in the State of Texas. Except for one of the bridge deck drains, no empirical design information existed previously for any of the drainage structures tested in this project. One of the bridge deck drains had been tested previously in a different orientation.

To determine the hydraulic characteristics of the drainage structures, models of the structures were tested on a large roadway model. Curb inlets were tested at 3/4 scale; bridge deck drains were tested at full scale. The measurements made during the model studies were correlated to the capacity of the inlets and drains to develop empirical design equations.

The performance of curb inlets is usually divided into the following two categories: (1) 100% efficiency, in which the inlet is capturing all of the approach flow, and (2) less than 100% efficiency, in which there is carryover flow. The design method developed in this project for flush depressed curb inlets utilized a new empirical equation for the 100% efficiency capacity of the inlets on the basis of the effective length of the inlet. For less than 100% efficiency, an existing TxDOT design equation was used, also on the basis of the effective inlet length.

Two types of bridge deck drains were tested. Empirical design equations were developed for both drains. The equations are a function of the roadway geometry and approach flow conditions.

TABLE OF CONTENTS

1. INTRODUCTION

1.1 BACKGROUND

One of the many concerns about roadway safety is how to remove runoff, from the roadway surface and adjacent areas, quickly and efficiently. On uncurbed roadways, water simply drains into adjacent ditches. On curbed roadways, water flows down the gutter until it reaches an inlet structure, where it flows away from the roadway through a piped drainage system. Similarly, runoff from bridge decks is captured by bridge deck drains. The water intercepted by a bridge deck drain flows downward through a piping system and is discharged onto the ground or into a subsurface drainage system.

The inability of inlets and drains to adequately intercept and convey the runoff, results in water standing on the roadway and possibly on the adjacent property. Standing water threatens traffic safety by causing vehicles to hydroplane. Standing water is also an economic problem. It accelerates the deterioration of pavement due to the seepage of water and also causes sediment and debris to accumulate in low areas, which must then be swept clean. Furthermore, standing water is a nuisance to pedestrians.

Several types of inlet structures are used for roadways. Two of the primary types are grate inlets and curb inlets. A grate inlet uses metal bars placed in the roadway surface with the bars parallel and/or perpendicular to the flow of water. Flush curb inlets are simply vertical openings in the curb face which may or may not have a depression in the roadway adjacent to the inlet. One drawback of grate inlets is their high probability of clogging, since the opening between the bars is smaller than the opening for a curb inlet. Another potential problem is interference with traffic, especially bicycles. Clogging is not frequently a problem with curb inlets, and unlike grate inlets, the curb inlets do not interfere with traffic. A third type of inlet is a combination inlet, which uses a curb opening inlet and a grate inlet. One of the purposes of combining the two types of inlets is to achieve good efficiency, while minimizing the potential for clogging.

Similarly, several types of bridge deck drains exist. Most bridge deck drains consist of a grate supported by a drain pan. A variety of geometries exists for the grates, the pans beneath the grates, and the subsequent drain pipes.

1.2 OBJECTIVES

The research described in this report focused on flush depressed curb inlets and bridge deck drains. Flush depressed curb inlets are vertical openings in the curb face with an adjacent depression of the roadway surface (Figure 1.1). The inlet lip is flush with the curb face. Typically, depression transitions are placed upstream and downstream of the inlet section. The pavement surface changes gradually from the undepressed gutter into the fully depressed section

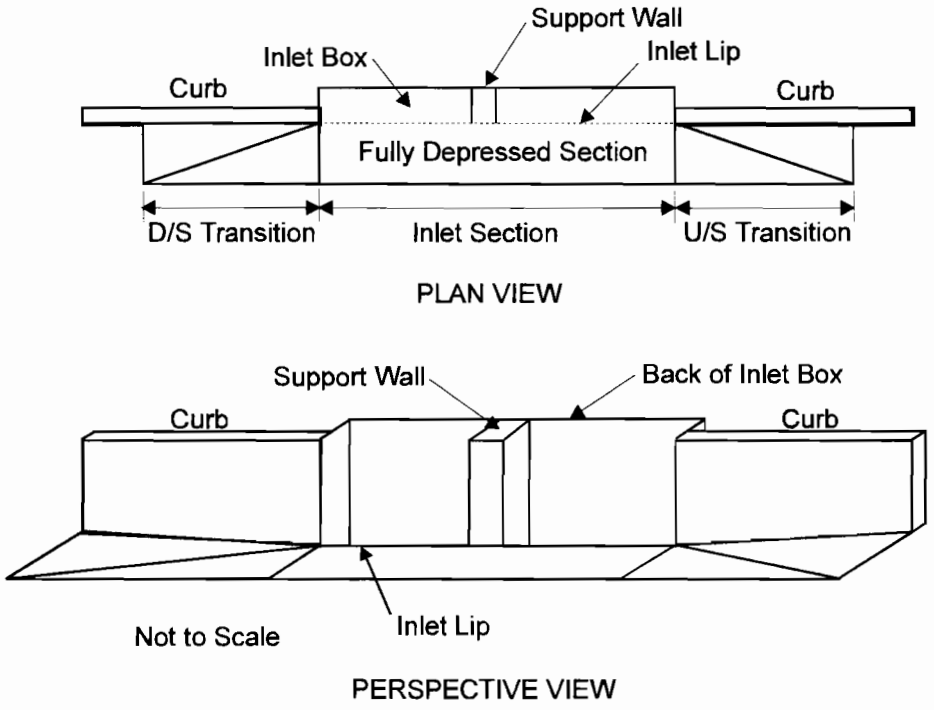

Figure 1.1 Typical Flush Depressed Curb Inlet

over the length of the depression transition. The upstream transition helps to increase the inlet capacity by concentrating more water against the curb upstream of the inlet opening. If the slope of the downstream depression transition is steep enough, some of the water that enters the downstream transition will turn around and flow back upstream and over the inlet lip.

The bridge deck drains analyzed in this project consisted of grates supported by a drain pan beneath the grate (e.g., Figure 1.2). The bottom surface of the drain pan is inclined towards the entrance to the outlet pipe. Two different types of bridge deck drains were analyzed. The geometries of the drain pans of the two drain pans were similar, except one was significantly larger. The smaller drain had grate slots oriented in the longitudinal direction and had a 0.15-cm outlet pipe, while the larger drain had grate slots oriented in the transverse direction and had an 0.203 m outlet pipe.

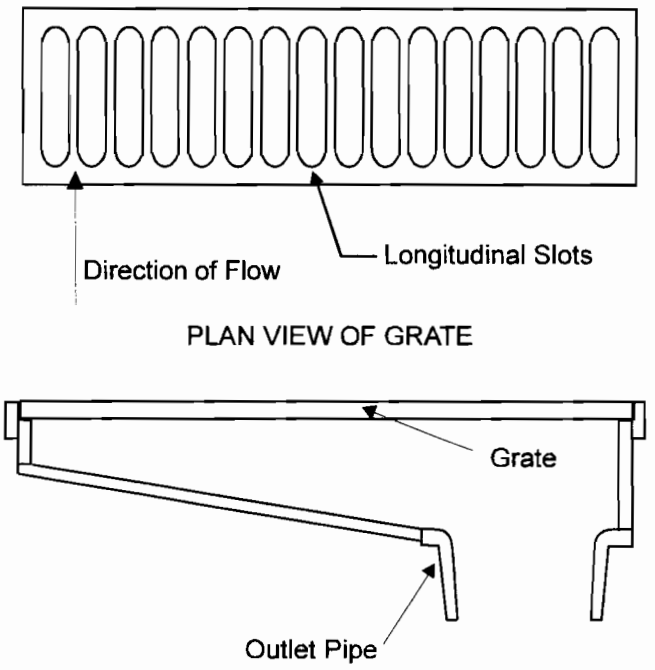

Figure 1.2 Typical Bridge Deck Drain

The primary objectives of this research project were

1. to determine the hydraulic characteristics of flush depressed curb inlets for different flow conditions and geometries,
2. to determine the hydraulic characteristics of two types of bridge deck drains for different flow conditions and geometries, and
3. to develop design equations related to objectives 1 and 2.

With the exception of one of the bridge deck drains, all of the inlets and drains tested in this research project are currently used by the Texas Department of Transportation (TxDOT) on roadways in the State of Texas.

1.3 APPROACH

The primary variables which influence the amount of flow captured by inlets and drains are the longitudinal roadway slope, the transverse roadway slope and geometry, the flow rate in the gutter, the hydraulic roughness of the pavement material, the flow regime (i.e., whether the flow is subcritical or supercritical), and inlet or drain size and geometry. Obtaining analytical solutions for the discharge capacity of inlets and drains is a very complex problem. In fact, the computational approach is so complex that it would require verification against experimental results before complete confidence could be placed in the results of the computations. Thus, the primary approach for accomplishing the project objectives (Section 1.2) was to utilize a large, versatile physical model of a roadway, and to conduct a large number of experiments to cover the expected flow conditions and geometries of flush depressed curb inlets and bridge deck drains. In the past, most new inlet designs have been designed by inference from the results of studies conducted on other types of inlets. The research performed in this project provided necessary design information for TxDOT inlets.

This report presents the results of the experimental work performed on curb inlets and bridge deck drains. Chapter 2, contains a comprehensive review of the relevant literature for curb inlets and bridge deck drains; Chapter 3, describes in detail the apparatus and the methods used for the experimental work; Chapter 4, presents the results and analysis of the curb inlet tests; Chapter 5, presents the results and analysis of the bridge deck drain tests; and Chapter 6, summarizes the major findings of this research work.

Some of the equations presented in this report are given as dimensionally consistent equations; such equations may be used with any set of consistent units. When specific units are needed for the equations which are not dimensionally consistent, SI units are used throughout.

This research was funded by TxDOT through the Center for Transportation Research (CTR) at the University of Texas at Austin. The project number was 705XXA4004-0-1409.

2. LITERATURE REVIEW

A literature review was performed to identify the references relevant to flush depressed curb inlets and bridge deck drains. Many of the references discovered were not fully applicable to the inlet designs tested in this research project, but were useful in providing background information and general conclusions about inlet behavior. A primary objective of the literature review was to determine the source of the procedures used by TxDOT to design curb inlets and bridge deck drains. These sources were identified and are described where appropriate in the following sections.

The literature review revealed that there is a definite need for up-to-date design information on curb inlets and bridge deck drains. As new drain designs are developed, their capacity is often estimated by inference from previous designs. This practice can result in inaccurate predictions of the capacity of new inlets. The research project described in this report provided much-needed specific design information for several types of inlets used by TxDOT.

2.1 FLUSH CURB INLETS

The complexity of the hydraulics of roadway curb inlets makes the analytical description of the flow impractical. Consequently, most of the available literature presents empirical capacity equations resulting from experimental investigations on existing curb inlet designs. In the references located during the literature review, all of the attempts to describe the flow into curb inlets analytically required modification when compared with experimental data. Empirical equations can predict the behavior of physical systems very accurately when applied within the conditions for which the equations were developed and tested. The main drawback of empirical equations is that they cannot be applied with confidence outside of the conditions for which they were tested.

The two curb inlet investigations summarized in detail in this report are Izzard's (1950) and Li's (1954). These two investigations were chosen in part because of their application of basic hydraulic theory to the problem of flow into curb inlets. Both of these investigations began with a few basic assumptions to develop a theory, which was tested against experimental

evidence. Both Izzard and Li modified their analytical equations to match experimental data. Since Izzard's design procedure is used by TxDOT, Izzard's equations were used extensively in the analysis of the TxDOT curb inlets tested in this research project (see Chapter 4). A comparison of the predictions of Izzard's and Li's equations is presented in Section 2.1.3, along with some possible explanations for the differences in the predictions.

Several other curb inlet investigations are briefly summarized in Section 2.1.4. These references are described to show how different researchers presented their results and to illustrate how researchers have expanded upon the ideas of others.

2.1.1 Izzard (1950)

Izzard (1950) analyzed the flow into flush curb inlets as flow over a broad-crested weir. Because TxDOT uses Izzard's equations for curb inlet design, the curb inlet research described in this report, focuses on the application of Izzard's equations to TxDOT Types C and D curb inlets (see Section 4.1 and Figures 4.1-4.2).

The basic premise of Izzard's analysis is that the flow over the lip of a flush curb inlet is analogous to flow over a broad-crested weir. A number of simplifying assumptions were made in the analysis. First, Izzard assumed that the velocity of the approach gutter flow is parallel to the plane of the inlet opening; i.e., that there is no transverse component of the approach flow velocity, so the approach flow velocity is ineffective in causing flow over the inlet lip. Second, for undepressed curb inlets, he assumed that the head on the inlet lip at the upstream end of the inlet is equal to the depth of the approach flow. For depressed curb inlets, the head on the inlet lip at the upstream end of the inlet opening was assumed to be the depth of the approach flow plus the depth of gutter depression. Third, a linear head distribution along the length of the weir (inlet lip) was assumed. Thus, for an undepressed curb inlet to capture all of the approach flow, Izzard assumed the head decreased linearly to zero at the downstream end of the inlet opening. For depressed curb inlets, Izzard assumed that the inlet would intercept all of the approach flow if the head at the downstream end of the inlet opening was equal to the depth of the depression. Finally, he assumed uniform flow existed upstream of the inlet section. Although not specifically stated, implicit in Izzard's analysis is the assumption that the longitudinal roadway

slope has a negligible effect on the hydraulic behavior of the inlets; the analysis is performed as if the longitudinal roadway slope were zero.

2.1.1.1 Undepressed Curb Inlets

A typical undepressed curb inlet is shown in Figure 2.1. In the following discussion and throughout this report, the longitudinal direction is oriented along the length of the roadway, with the transverse direction oriented normal to the longitudinal direction. The convention is illustrated in Figure 2.1. Assuming uniform flow in the gutter upstream of the inlet, y_n is the normal depth of flow in the approach gutter, h is the hydraulic head on the inlet lip at any distance x from the upstream end of the inlet opening, and L_r is the length of inlet opening required to capture all of the approach flow (100% inlet efficiency). The hydraulic head is used because Izzard assumed that the velocity of the approach flow is zero in the transverse direction. In this case, the hydraulic head is equal to the total head. For 100% efficiency, the head on the weir at any point along the inlet length can be expressed as

$$h = y_n\left(1-\frac{x}{L_r}\right) \tag{2.1}$$

The normal depth y_n is calculated from Izzard's modified Manning's equation for gutter flows (Equation 2.4). The usual form of Manning's equation for open channel (Equation 3.4) can be written for flow in triangular channels such as street gutters. With a uniform cross slope, it can be assumed that the wetted perimeter is equal to the ponded width of gutter flow without introducing significant error. With this assumption, the hydraulic radius is $y_n/2$. Thus, Manning's equation in SI units can be rearranged as

$$Q_a = \frac{0.316 y_n^{8/3} S_f^{1/2}}{n S_x} \tag{2.2}$$

where Q_a = approach flow rate, S_f = slope of the energy grade line, S_x = transverse slope of roadway, and n = Manning's roughness coefficient. For uniform flow, S_f = S, where S = the

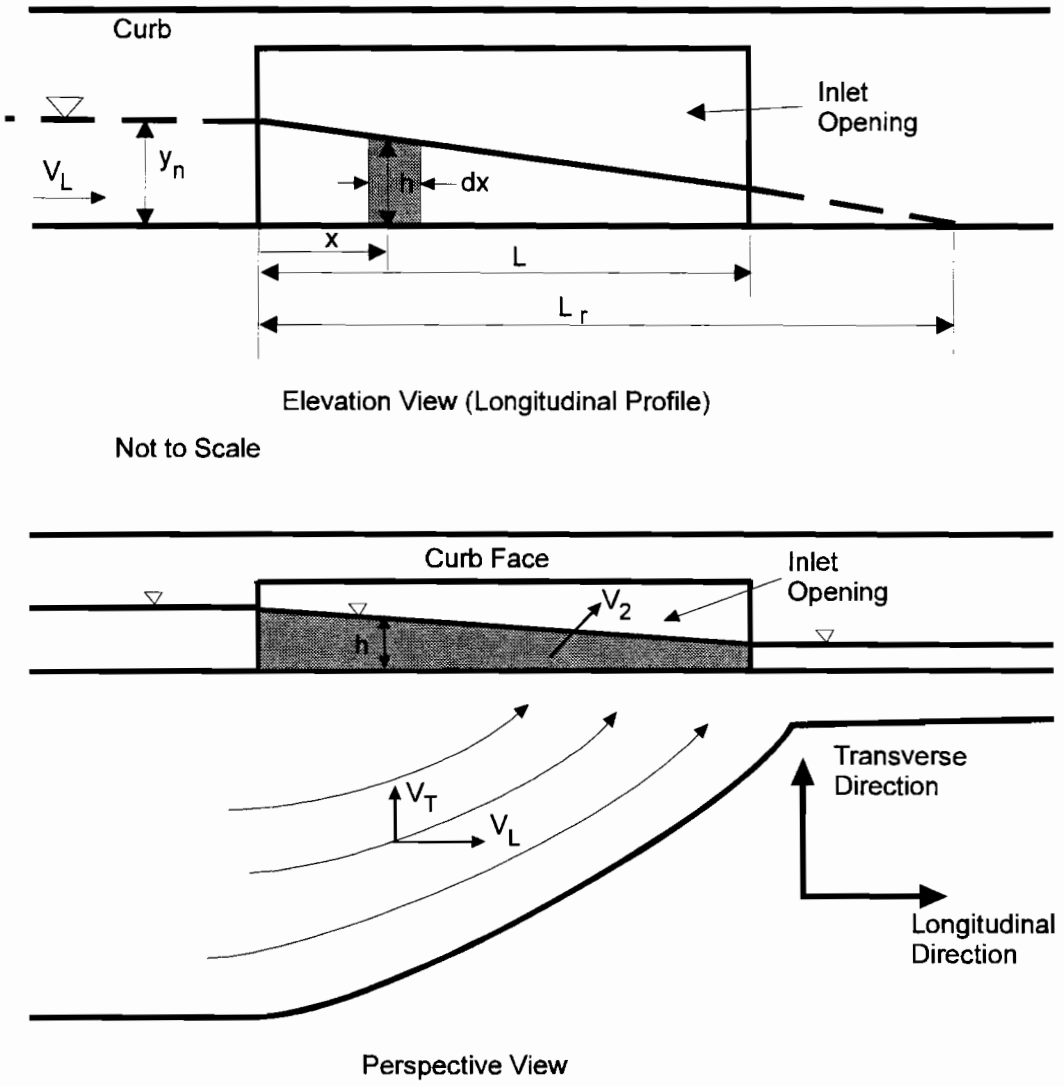

Figure 2.1 Typical Undepressed Curb Inlet

longitudinal slope of the roadway. Because it was believed that the standard definition of the hydraulic radius did not adequately describe the wide, shallow cross-section of street gutter flow, Izzard (1946) developed an alternative form of Manning's equation. The cross-section of gutter flow shown in Figure 2.2 defines the variables used in the analysis. In Figure 2.2, w is the distance from the curb face in the transverse direction as previously defined in Figure 2.1. y_n is

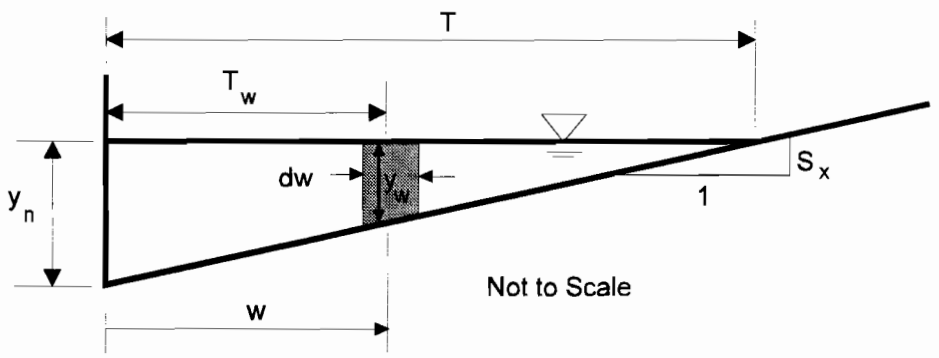

Figure 2.2 Cross-Section of Gutter Flow

the normal depth of flow at the curb face. The ponded width in the gutter (T) can be expressed as $T = y_n/S_x$.

Izzard applied the usual form of Manning's equation in a local sense rather than an average sense, as it is normally used. That is, he assumed that the longitudinal velocity at each distance (w) from the curb could be calculated by Manning's equation for the velocity based on the local depth (y_w) at that point being equal to the hydraulic radius. Thus, at each w where the depth is y_w, he had

$$V_L = \frac{1}{n} y_w^{2/3} S^{1/2} \tag{2.3}$$

where V_L = velocity of flow in the longitudinal direction and y_w = depth of flow at a distance w from the curb face. The flow through an incremental area at each w is $dQ = V_L dA$. At each w, the incremental area dA is given by $dA = y_w dw$. The depth y_w can be written as a function of w, namely $y_w = (T- w)S_x$ (see Figure 2.2). Thus, the flow through an incremental area becomes $dQ = (V_L y_w)dw = V_L(T - w)S_x dw$. Using Equation 2.3 and the expression for dQ, Izzard integrated dQ with respect to w and across the flow area with a uniform cross slope. The result is

$$Q_a = \int_0^T \frac{1}{n}[(T-w)S_x]^{5/3} S^{1/2}\, dw$$
$$Q_a = \frac{3}{8}\frac{y_n^{8/3} S^{1/2}}{nS_x} \tag{2.4}$$

Equation 2.4 is the form of Manning's equation in SI units traditionally used for gutter flows. The only difference between Equations 2.2 and 2.4 is the numerical coefficient. Thus, for a given set of hydraulic conditions (Q_a, S, S_x, and n), y_n calculated from Equation 2.2 is about 7% larger than when calculated from Equation 2.4. In this research project, Equation 2.4 was used to calculate the normal depth for all conditions except when applying Li's curb inlet equations, as explained in Section 2.1.2.1.

The transverse profile of flow over the inlet lip is shown in Figure 2.3. Assuming that the pressure distribution in the flow is hydrostatic and that the flow passes through critical depth at the inlet lip, Bernoulli's equation written from point 1 to point 2 yields

$$h_1 = y_c + \frac{V_{T,2}^2}{2g} \tag{2.5}$$

where h_1 = hydraulic head at point 1, y_c = critical depth of flow at point 2, and $V_{T,2}^2/2g$ = velocity head at point 2, where $V_{T,2}$ = transverse velocity at point 2. Equation 2.5 implies that $V_{L,2} = 0$;

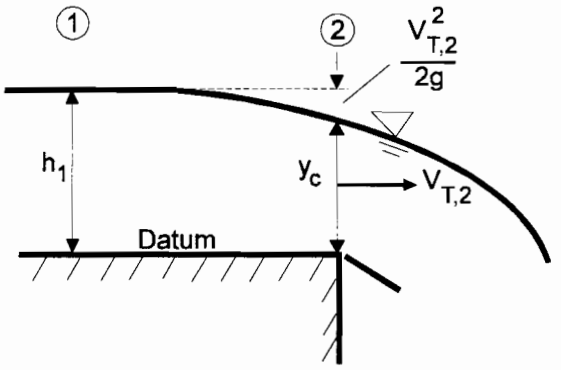

Figure 2.3 Transverse Profile View of Flow Over the Inlet Lip

i.e., that the total velocity at point 2 is perpendicular to the x direction. The assumption of critical depth at the inlet lip is not applicable for all approach flows because the longitudinal slopes of many streets are steep enough to create supercritical flow in the approach gutter. Equation 2.5 may be solved for $V_{T,2}$:

$$V_{T,2} = \sqrt{2g(h_1 - y_c)} \tag{2.6}$$

By continuity, the flow over the inlet lip through an incremental strip dx (Figure 2.1) is

$$dQ = V_{T,2}\, dA = \sqrt{2g(h_1 - y_c)}\, dA \tag{2.7}$$

where

$$dA = y_c\, dx \tag{2.8}$$

Equation 2.7 is the differential form of the standard broad-crested weir equation as given by Bos (1989), except in the standard weir equation, the hydraulic head h_1 is replaced by the total head H_1. Substituting Equation 2.8 into Equation 2.7 gives

$$dQ = y_c \sqrt{2g(h_1 - y_c)}\, dx \tag{2.9}$$

The critical depth y_c can be expressed as

$$y_c = \frac{2}{3} h_1 \tag{2.10}$$

Equation 2.10 is valid only for rectangular open channels or for channels in which the flow width is extremely wide compared to the depth (Henderson, 1966). Since one or both of these conditions is met for flow through the inlet opening, Equation 2.10 is applicable if critical depth actually occurs at the inlet lip and under the conditions of previously stated assumptions.

Substituting the expressions for h_1 and y_c from Equations 2.1 and 2.10 into Equation 2.9 gives

$$dQ = \frac{2}{3} h_1 \left[2g\left(h_1 - \frac{2}{3} h_1 \right) \right]^{0.5} dx = \frac{2}{3}\sqrt{\frac{2}{3} g}\, h_1^{3/2}\, dx$$
$$dQ = \frac{2}{3}\sqrt{\frac{2}{3} g}\, y_n^{3/2} \left(1 - \frac{x}{L_r} \right)^{3/2} dx \qquad (2.11)$$

Izzard integrated Equation 2.11 between the limits x = 0 and x = L to give

$$Q = \frac{2}{3}\sqrt{\frac{2}{3} g}\, y_n^{3/2} \int_0^L \left(1 - \frac{x}{L_r} \right)^{3/2} dx$$
$$Q = \frac{4}{15}\sqrt{\frac{2}{3} g}\, y_n^{3/2} L_r \left[1 - \left(1 - \frac{L}{L_r} \right)^{5/2} \right] \qquad (2.12)$$

where Q is the flow intercepted by an undepressed inlet of length L. For SI units with g = 9.81 m/s^2, Equation 2.12 reduces to

$$Q = 0.679 y_n^{3/2} L_r \left[1 - \left(1 - \frac{L}{L_r} \right)^{5/2} \right] \qquad (2.13)$$

Equation 2.13 gives the flow intercepted by an undepressed inlet of length L. For 100% inlet efficiency, the inlet length L is equal to L_r. Thus, the 100% efficiency capacity of the inlet is calculated to be

$$Q_a = 0.679\, L_r y_n^{3/2} \qquad (2.14)$$

where Q_a is the approach gutter flow rate. For inlet lengths less than L_r, the fraction of the approach flow intercepted by the inlet is found by dividing Equation 2.13 by Equation 2.14:

$$\frac{Q}{Q_a} = 1 - \left(1 - \frac{L}{L_r} \right)^{5/2} \qquad (2.15)$$

Izzard compared Equations 2.14 and 2.15 to unpublished data from less than 100% efficiency experiments on undepressed curb inlets conducted at the University of Illinois. He found that the equation fit the data reasonably well if the numerical coefficient in Equation 2.14

was reduced from 0.682 to 0.39. Thus, the empirically adjusted equation for 100% efficiency became

$$Q_a = 0.39\, L_r y_n^{3/2} \tag{2.16}$$

A comparison plot of the Illinois experimental data and Equation 2.15 is shown in Izzard's report. Considerable scatter is evident in the figure, especially for higher values of Q/Q_a, but Izzard concluded that Equation 2.15 was a reasonable approximation of the entire range of data. However, a diagram included in Izzard's report reveals that the Illinois inlet had a composite transverse slope as shown in Figure 2.4. The effect of the composite transverse slope of the Illinois inlet on the experimental results is unknown, but it probably caused the Illinois inlet to be more efficient than an inlet of equal length on a constant transverse slope. This possibility was not discussed in Izzard's report.

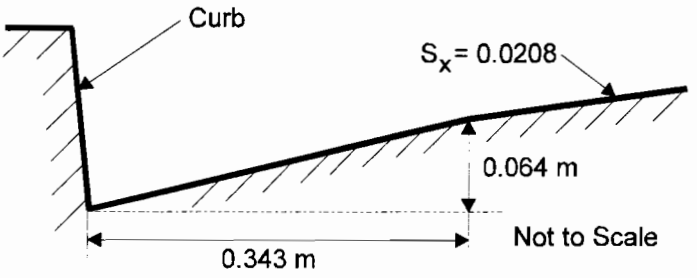

Figure 2.4 Cross-Section of Illinois Approach Gutter and Curb Inlet

Izzard's empirical equation (Equation 2.16) indicates that for 100% efficiency the inlet actually captures about 60% of the flow predicted by the analytical equation (Equation 2.14). It seems reasonable to conclude that the simplifying assumptions used in the analysis led to this discrepancy. One possible explanation noted by Holley et al. (1992) was Izzard's assumption that gravity was the only force influencing the flow over the inlet lip. While gravity is the primary force causing water to flow over the lip, the momentum of the approach flow is actually tending to carry the water past the inlet opening. Another possible reason for the discrepancy is Izzard's assumption of critical depth at the inlet lip. If the flow approaching the inlet lip is

supercritical, as it often is, the depth is less than critical depth and the head is less than Izzard assumed. Thus, it can be expected that the actual flow captured by the inlet would be less than that predicted by the analytical equation. Further, the incremental captured flow is $dQ = V_{T,2}dA$ as stated in Equation 2.7, but the momentum of the flow in the approach gutter causes the flow to go through cross section 2 at an angle (Figure 2.1), so that $V_{L,2}$ is not zero. Thus, $V_{T,2}$ is actually less than that given by Equation 2.6.

The use of Izzard's equations for the design of undepressed curb inlets is straightforward. Typically, the street geometry (longitudinal and transverse slopes) and pavement material (Manning's n) are known beforehand. The design approach flow rate can be estimated from hydrologic analysis. Once these quantities are known, the normal depth of the approach gutter flow (y_n) can be calculated from Equation 2.4. The inlet length required to capture 100% of the approach flow (L_r) can then be calculated from Equation 2.16. Because the cost of constructing inlets long enough to capture 100% of the approach flow is usually prohibitive, inlets are typically designed to function at less than 100% efficiency for the design storm. In the inlet design process, the carryover flow from an upstream inlet is added to the inflow before the next inlet, and so on.

2.1.1.2 Depressed Curb Inlets

A depressed curb inlet with a length of inlet opening L, and a depression of depth a, is shown in Figure 2.5. For 100% efficiency, Izzard assumed that the head on the inlet lip at the downstream end of the inlet opening was equal to the depth of the depression, a. The length of inlet opening required for 100% efficiency is L_r. For 100% efficiency, the equation for the head along the length of the inlet is

$$h = (a + y_n) - \frac{x}{L_r} y_n = a + \left(1 - \frac{x}{L_r}\right) y_n \qquad (2.17)$$

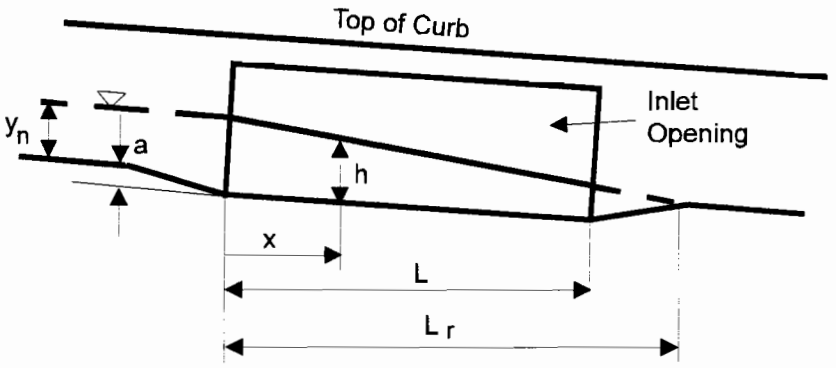

Figure 2.5 Elevation View of Depressed Curb Inlet

With the assumption of critical depth at the inlet lip, the flow through an incremental strip dx is

$$dQ = \sqrt{\frac{2}{3}gh}\left(\frac{2}{3}h\right)dx = \frac{2}{3}\sqrt{\frac{2}{3}g}\,h^{3/2}\,dx$$

$$dQ = \frac{2}{3}\sqrt{\frac{2}{3}g}\,y_n^{3/2}\left[a + \left(1 - \frac{x}{L_r}\right)y_n\right]^{3/2} \tag{2.18}$$

(see Equation 2.11). The assumption of critical depth at the lip of a depressed inlet may be even less valid than for an undepressed inlet, because the increased slopes in the upstream transition section and in the fully depressed section, can cause the flow to accelerate and enter the supercritical regime in the inlet section for even subcritical approach flows.

Integrating Equation 2.18 between the limits of x = 0 and x = L yields

$$Q = \frac{4}{15}\sqrt{\frac{2}{3}g}\,L_r y_n^{3/2}\left[\left(\frac{a}{y_n} + 1\right)^{5/2} - \left(\frac{a}{y_n} + 1 - \frac{L}{L_r}\right)^{5/2}\right] \tag{2.19}$$

for the flow intercepted by a depressed inlet of length L. Izzard also changed the numerical coefficient in Equation 2.19 based on experimental results (see Equation 2.16). Thus, the empirical equation for the flow intercepted by a depressed curb inlet of length L was written as

$$Q = 0.39\, L_r y_n^{3/2}\left[\left(\frac{a}{y_n}+1\right)^{5/2} - \left(\frac{a}{y_n}+1-\frac{L}{L_r}\right)^{5/2}\right] \tag{2.20}$$

For 100% efficiency, the inlet length is L_r and the inlet captures the entire approach flow Q_a. With this substitution, Equation 2.20 becomes

$$\begin{aligned} Q_a &= 0.39\, L_r y_n^{3/2}\left[\left(\frac{a}{y_n}+1\right)^{5/2} - \left(\frac{a}{y_n}\right)^{5/2}\right] \\ Q_a &= \frac{0.39}{y_n} L_r\left[(a+y_n)^{5/2} - a^{5/2}\right] \end{aligned} \tag{2.21}$$

Equation 2.21 is used by TxDOT for the 100% efficiency capacity of depressed curb inlets. The efficiency of inlets of length L less than L_r is found by dividing Equation 2.20 by Equation 2.21:

$$\frac{Q}{Q_a} = \frac{\left(\frac{a}{y_n}+1\right)^{5/2} - \left(\frac{a}{y_n}+1-\frac{L}{L_r}\right)^{5/2}}{\left(\frac{a}{y_n}+1\right)^{5/2} - \left(\frac{a}{y_n}\right)^{5/2}} \tag{2.22}$$

Equation 2.22 is used by TxDOT for the less than 100% efficiency capacity of depressed curb inlets.

Izzard compared Equations 2.21 and 2.22 with data from 100% efficiency tests conducted on curb inlets used in North Carolina and with data from less than 100% efficiency tests conducted by the St. Paul District of the U.S. Army Corps of Engineers in 1949. Figure 2.6 shows the North Carolina and the Corps of Engineers' pavement cross-sections. The North Carolina tests were conducted for inlets with a depression depth (a) of 0.076 m and a depression width (W) of 0.61 m. In the tests, the inlet length was varied from 0.30 m to 2.13 m and the longitudinal slope was varied from 0.005 to 0.1. The North Carolina inlet was not a standard depressed inlet such as the TxDOT Type C and Type D inlets described in Section 4.1,

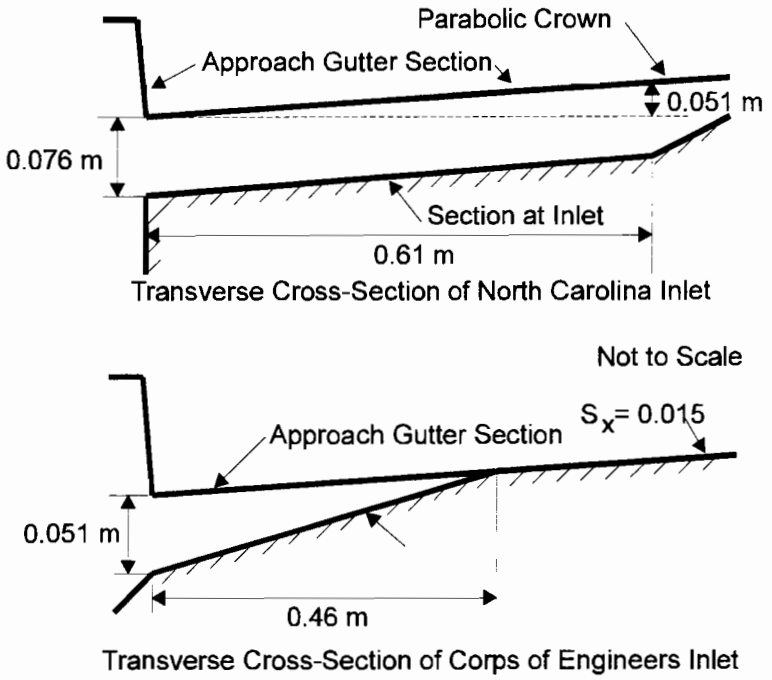

Figure 2.6 Cross-Sections of North Carolina and Corps of Engineers Inlets

but could be called a compound depressed inlet because the cross-section of the depression did not have a constant slope (Figure 2.6). The Corps of Engineers inlet was a standard depressed curb inlet with a depth of 0.051 m and a width of 0.46 m (Figure 2.6). Tests were conducted at 1/2 scale with a transverse roadway slope of 0.015 and longitudinal slopes of 0.0075, 0.01, and 0.02. The inlet lengths tested were 0.91 m and 2.72 m. Izzard found that his equations overestimated the 100% capacity of the North Carolina inlets and underestimated the less than 100% capacity data of the Corps of Engineers tests. When Izzard compared his equations with the combined data from the University of Illinois, North Carolina, and Corps of Engineers inlet tests, he concluded that the scatter of the data was significant and that other variables not analyzed in his approach were affecting the results. However, he concluded that the equations were adequate to represent the data available at that time.

The use of Izzard's equations for the design of depressed curb inlets is very similar to the method described in Section 2.1.1.1 for undepressed curb inlets. Because TxDOT uses Izzard's

equations for curb inlet design in Texas, a comparison of the predictions of the equations with experimental data from TxDOT Type C and Type D curb inlets is presented in Chapter 4.

2.1.2 Li (1954) and Li et al. (1951b)

Li (1954) analyzed the flow into flush curb inlets by analogy with open-channel flow over a free drop. The basic methodology used in the analysis was to compare the elevation view of open-channel flow over a free drop to the plan view of flow into a curb inlet.

An elevation view of supercritical open-channel flow over a free drop is shown in Figure 2.7. It is assumed that there is a uniform velocity distribution in the flow. Neglecting friction and using the equations of motion for a particle on the free surface, the length L_r of the trajectory of the free surface is

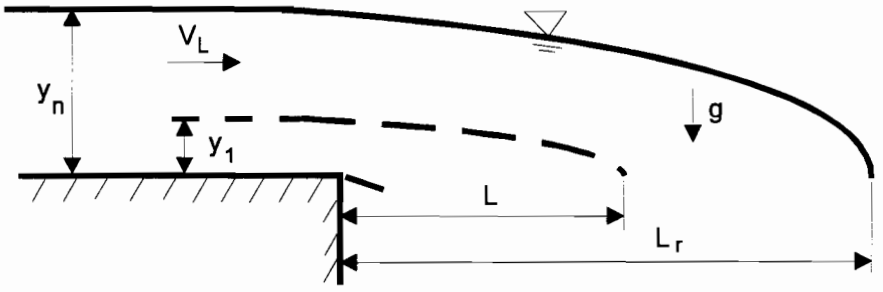

Figure 2.7 Elevation View of Open-Channel Flow Over a Free Drop

$$L_r = V_L\sqrt{\frac{2y_n}{g}} \tag{2.23}$$

where V_L = longitudinal velocity of the flow. The length of opening L in the channel bottom required to capture flow of depth y_1 is

$$L = V_L\sqrt{\frac{2y_1}{g}} \tag{2.24}$$

Dividing Equation 2.23 by Equation 2.24 gives

$$\frac{y_1}{y_n} = \left(\frac{L}{L_r}\right)^2 \tag{2.25}$$

Li used Equations 2.23-2.25 to develop equations for flow into flush curb inlets, as discussed in the next two subsections.

2.1.2.1 Undepressed Curb Inlets

Li observed that the plan view of flow into an undepressed curb inlet was similar to the elevation view of open channel flow over a free drop shown in Figure 2.7. Figure 2.8 shows the plan view of flow into a curb inlet and defines the variables used in the analysis. The width of flow T in Figure 2.8 is $y_n \tan\theta_o$. Neglecting resistance due to the surface roughness, the acceleration towards the curb opening is $g \cos\theta_o$. Thus, by analogy with Equation 2.23,

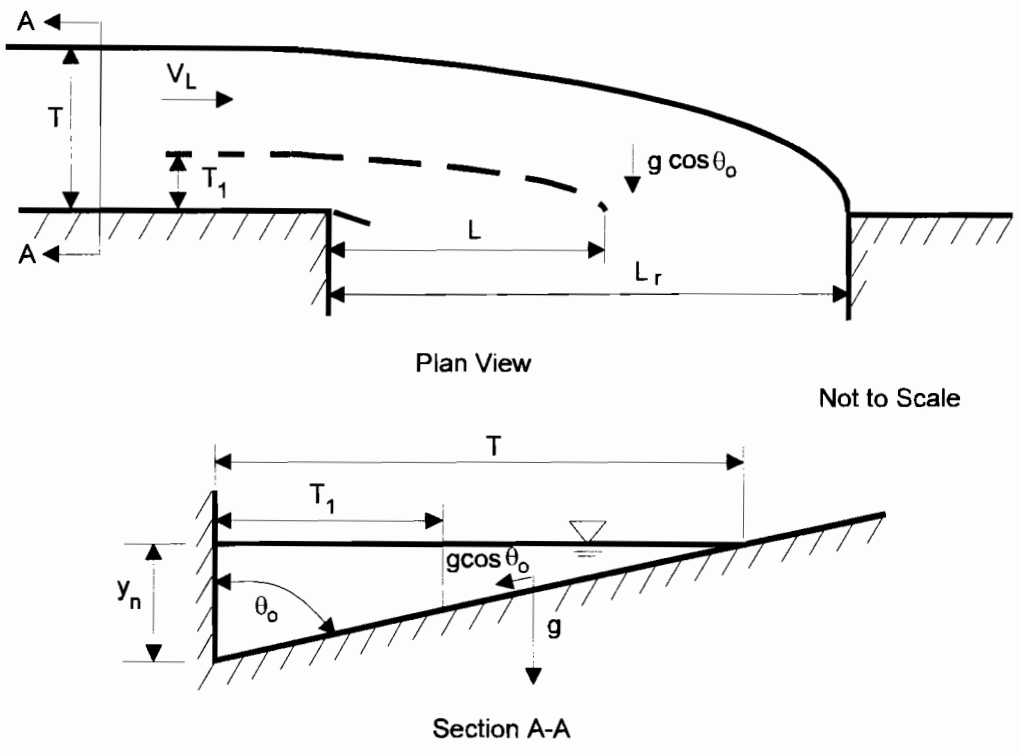

Figure 2.8 Flow Into an Undepressed Curb Inlet

$$L_r = V_T \sqrt{\frac{2y_n \tan\theta_o}{g \cos\theta_o}} \tag{2.26}$$

The normal depth in the approach gutter (y_n) is calculated by Manning's equation. In the development of his equations, Li wrote Manning's equation for a triangular channel in terms of the angle θ_o (Figure 2.8). With the standard definition of the hydraulic radius (cross-sectional area of flow divided by the full wetted perimeter), Manning's equation in SI units in terms of θ_o is

$$Q_a = \frac{0.5}{n} y_n^2 \tan\theta_o \left[\frac{y_n \tan\theta_o}{2(1+\sec\theta_o)}\right]^{2/3} \sqrt{S} \tag{2.27}$$

Equation 2.27 can be solved for y_n to give

$$y_n = \frac{1.54(1+\sec\theta_o)^{1/4}}{(\tan\theta_o)^{5/8}} \left(\frac{Q_a n}{\sqrt{S}}\right)^{3/8} \tag{2.28}$$

In this research project, Equation 2.28 was used to calculate y_n when using Li's curb inlet equations because Equation 2.28 was used in the development of Li's equations. Equation 2.28 gives greater calculated normal depths than those calculated from Izzard's modified Manning's equation (Equation 2.4). The difference between the two equations varies depending on the channel geometry.

The approach flow rate in the gutter, Q_a, can be expressed by

$$Q_a = V_L A = \frac{V_L y_n^2 \tan\theta_o}{2} \tag{2.29}$$

Solving Equations 2.26 and 2.29 for V_L, equating, and simplifying yields

$$\frac{Q_a}{L_r y_n \sqrt{g y_n}} = \sqrt{\frac{\sin\theta_o}{8}} \tag{2.30}$$

For most highway cross slopes, $\sin\theta_o$ is very near unity. Thus, Equation 2.30 becomes

$$\frac{Q_a}{L_r y_n \sqrt{g y_n}} = \sqrt{\frac{1}{8}} \cong 0.35 \tag{2.31}$$

Therefore, the theoretical equation for the 100% efficiency capacity of an undepressed flush curb inlet is

$$Q_a = 0.35 L_r y_n \sqrt{g y_n} \tag{2.32}$$

After comparing Equation 2.32 with experimental data, Li modified the constant coefficient in the equation. This modification was justified by noting that friction was neglected in the analysis. Li's empirical 100% efficiency equation for undepressed curb inlets is

$$Q_a = K L_r y_n \sqrt{g y_n} \tag{2.33}$$

where K = 0.23 for a transverse roadway slope of 0.0833 and K = 0.20 for transverse roadway slopes of 0.0417 and 0.0208. These values of K supposedly gave a good fit to the experimental data Li used for comparison; however, no table of experimental data or comparison plot was included in Li's report.

For a curb inlet of length L less than L_r, the width of flow captured is T_1 (Figure 2.8). By analogy with Equation 2.25,

$$\frac{T_1}{y_n \tan\theta_o} = \left(\frac{L}{L_r}\right)^2 \tag{2.34}$$

The area of flow A_1 for a width T_1 is

$$A_1 = y_n T_1 - \frac{T_1^2}{2\tan\theta_o} \tag{2.35}$$

The flow Q captured by an opening of length L is

$$\frac{Q}{Q_a} = \frac{A_1}{A} = \frac{y_n T_1 - \frac{T_1^2}{2\tan\theta_o}}{\frac{y_n^2 \tan\theta_o}{2}}$$

$$\frac{Q}{Q_a} = 2\left(\frac{L}{L_r}\right)^2 - \left(\frac{L}{L_r}\right)^4 \qquad (2.36)$$

Equation 2.36 is Li's general equation for the less than 100% efficiency capacity of undepressed curb inlets. Li reported that for $L/L_r \geq 0.6$, Equation 2.36 can be approximated as

$$\frac{Q}{Q_a} \cong \frac{L}{L_r} \qquad (2.37)$$

Therefore, as long as the carryover flow is less than 40% of the approach flow, the capacity of the inlet is proportional to the inlet length. By analogy to Equation 2.33, the flow captured at less than 100% efficiency is

$$Q = KLy_n\sqrt{gy_n} \qquad (2.38)$$

where K has the same values as for the 100% efficiency equation. Li reported that the accuracy of Equation 2.38 was verified by many tests under various conditions, but no data or plots were shown for comparison in the report. No range of applicability for any of the above equations was given in Li's report; however, it can be assumed that only transverse roadway slopes of 0.0208, 0.0417, or 0.0833 may be used because values of K were given for these slopes only.

In an earlier journal article Li et al. (1951b), presented much of the above derivation from a dimensional analysis approach and described a series of experiments used to verify the equations. Those experiments presumably resulted in the data to which Li referred in his 1954 report. Tests were conducted at 1/3 scale for supercritical approach flows only, with Froude numbers ranging from 1 to 3. Both 100% efficiency and less than 100% efficiency tests were conducted, with a maximum carryover flow rate of 70% of the approach flow rate. Experimental data are tabulated in the paper for inlet lengths varying from 0.91 to 2.74 m, longitudinal

roadway slopes varying from 0.005 to 0.04, and a transverse roadway slope of 0.0833. The experimental data exhibited close agreement with the predictions of the equations, as shown in Figure 2.9. Note that this figure includes comparisons for both 100% efficiency and less than 100% efficiency.

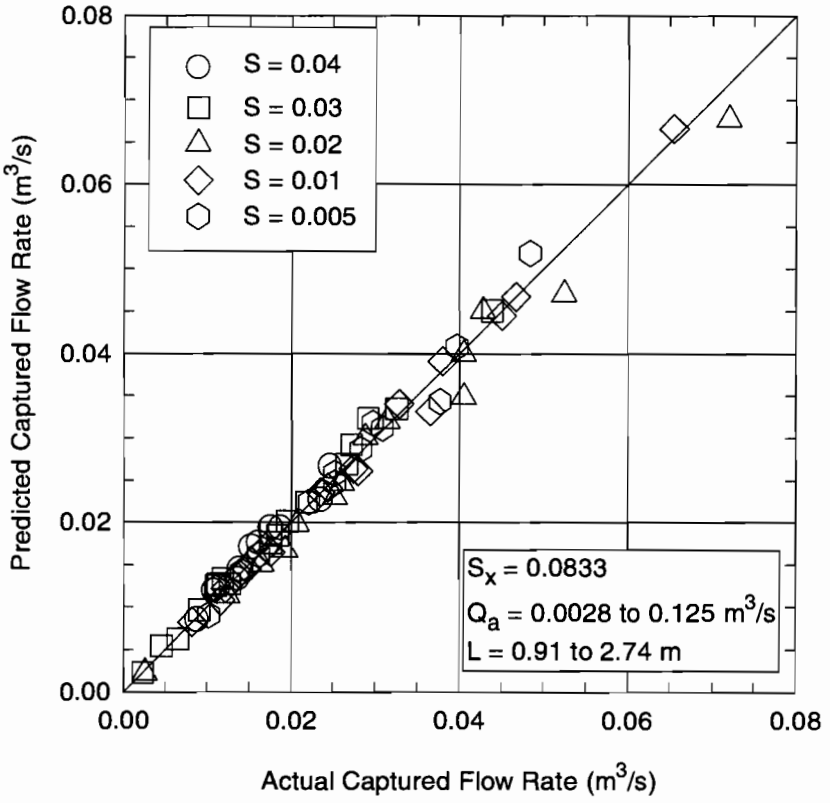

Figure 2.9 Comparison of Equations 2.33 and 2.36 with Data Published in Li et al. (1951b) for Undepressed Curb Inlets

2.1.2.2 Depressed Curb Inlets

Li et al. made a few modifications to the method for undepressed curb inlets presented in Section 2.1.2.1 to apply it to depressed curb inlets. In the following development, it is assumed that all of the approach flow is contained within the depressed gutter of width W (Figure 2.10).

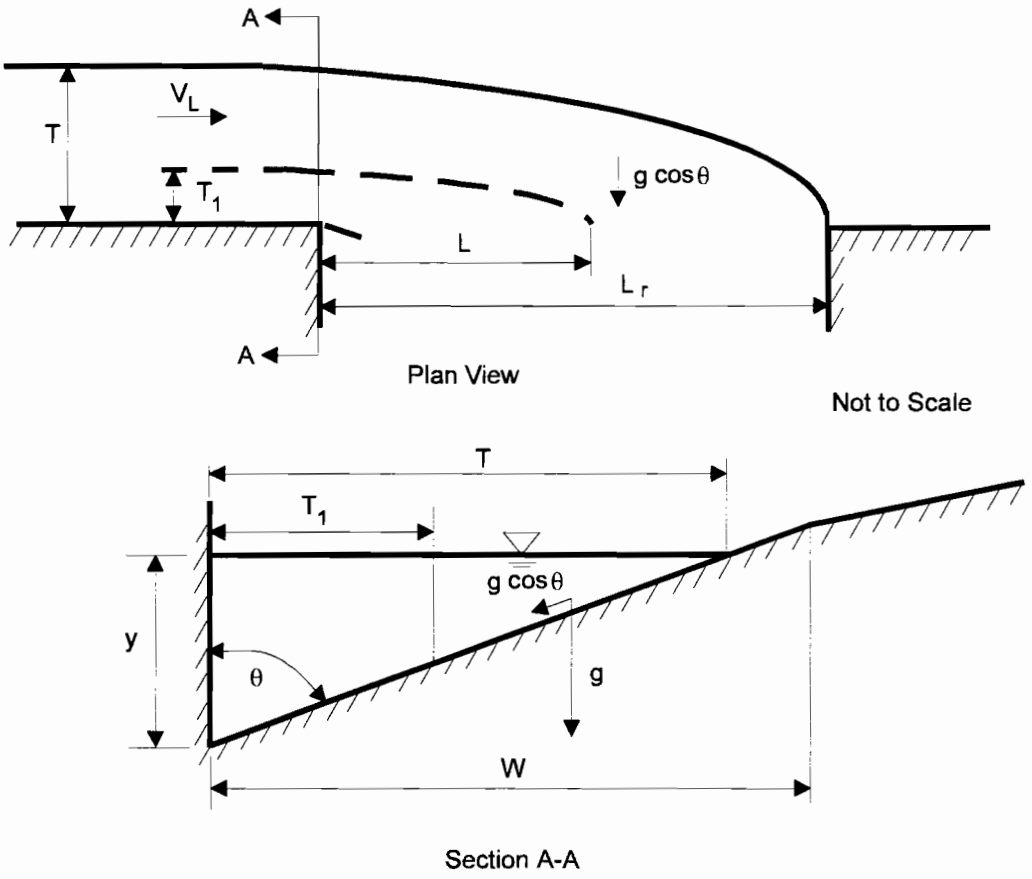

Figure 2.10 Flow Into Depressed Curb Inlet

This assumption simplifies the approach, but it limits the applicability of the equations because many higher flow rates may not be contained within the depressed gutter.

To apply Equation 2.29 to depressed curb inlets, Li replaced the calculated normal depth, y_n, in the equation by y, the flow depth in the depressed gutter. Also, an additional term, C, was introduced to account for the increased inlet capacity due to the depression. Hence, Equation 2.33 became

$$\frac{Q}{Ly\sqrt{gy}} = K + C \tag{2.39}$$

The parameter K retains the same values for depressed inlets as for undepressed inlets (see Section 2.1.2.1). By dimensional analysis, Li et al. found that C was a function of the following

dimensionless terms: $\frac{V_L^2}{gy}, \frac{L}{a}, \theta, \frac{L_2}{a}$, and $\frac{Q_{co}}{Q_a}$, where L_2 is the length of the downstream depression transition and Q_{co} is the carryover flow rate. Based on comparison with experimental data, it was found that

$$C = \frac{0.45}{1.12^M} \tag{2.40}$$

where M is given by the following equation:

$$M = \frac{L \frac{V_L^2}{gy}}{a \tan\theta} \tag{2.41}$$

As with all empirical equations, the range of applicability of Equations 2.40 and 2.41 is limited to the conditions for which they were developed and tested. The equations were tested for supercritical approach flows only, with longitudinal roadway slopes ranging from 0.005 to 0.08. The article states that Equation 2.40 was developed for K = 0.23, implying that the equation was valid only for a transverse roadway slope of 0.0833; however, the equation was apparently tested for transverse slopes of both 0.0833 and 0.0417.

The inlets used in Li et al.'s study had a downstream transition length L_2 equal to four times the depth of depression, a. For inlets which do not meet this constraint, the depression a in Equation 2.41 was replaced by an equivalent depression, a' , a' is the depth of depression which, with a downstream depression of length 4a' gives a transition with the same vertical rise as that of the original depression. The value of a' is calculated by

$$a' = \frac{a - L_2 S}{1 - 4S} \tag{2.42}$$

No experimental tests of the method for different inlet geometries were mentioned by Li et al. Therefore, the applicability of the method using Equation 2.42 is unknown.

Li et al.'s article included data from experiments conducted on 1/3 scale inlets with a prototype depression 0.105 m deep and 0.838 m wide. Inlet lengths varied from 0.91 m to 2.74 m. The transverse pavement slope was 0.0833. The data indicated good agreement of both

100% efficiency and less than 100% efficiency experimental results with the predictions of Equations 2.39-2.41, as shown in Figure 2.11.

2.1.3 Comparison of Izzard's and Li's Analyses

A comparison of Izzard's and Li's analyses reveals the effects of the different assumptions and inlet geometries for which the equations were developed. For undepressed curb inlets, the two analyses are fairly similar. For depressed curb inlets, the effects of the different depression geometries of the inlets tested are apparent.

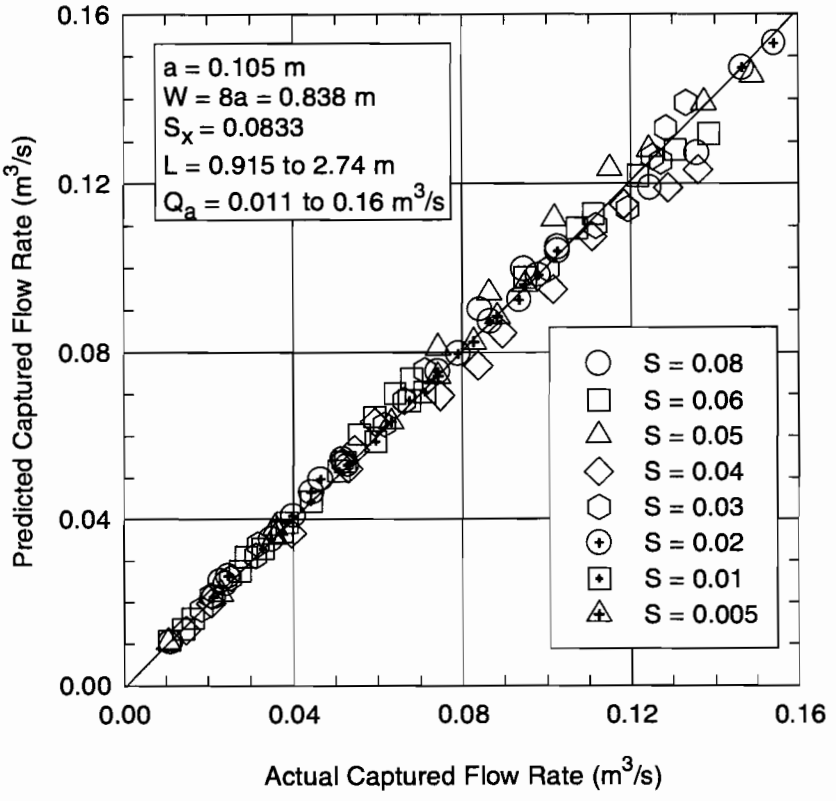

Figure 2.11 Comparison of Equations 2.39-2.41 with Data Published in Li et al. (1951b) for Depressed Curb Inlets

2.1.3.1 Undepressed Curb Inlets

Izzard's and Li's empirical 100% efficiency equations for undepressed inlets may be compared directly. Izzard's 100% efficiency equation (Equation 2.16) can be rearranged as

$$\frac{Q_a}{L_r y_n^{3/2}} = 0.39 \tag{2.43}$$

To make Equation 2.43 comparable with Li's equation (Equation 2.33), both sides are divided by $\sqrt{g}$. With g = 9.81 m/s^2, Equation 2.43 becomes

$$\frac{Q_a}{L_r y_n \sqrt{g y_n}} = \frac{0.39}{\sqrt{g}}$$
$$\frac{Q_a}{L_r y_n \sqrt{g y_n}} = 0.12 \tag{2.44}$$

The left-hand side of Equation 2.44 is identical to Li's 100% efficiency equation (Equation 2.33), but the value of the constant on the right hand side is different. In Li's equation, K = 0.20 to 0.23, compared to a value of 0.12 for Izzard's equation. Thus, for a given approach flow rate and upstream calculated normal depth, Li's equation predicts that an inlet would capture at least two-thirds more flow than is predicted by Izzard's equation. However, the difference between the two equations is actually greater than the difference indicated by the numerical coefficient, because the calculated normal depth used by Izzard is slightly less than the calculated normal depth used by Li as a result of the two different forms of Manning's equation used in the developments (Equations 2.4 and 2.28).

Another way to compare the equations is shown in Figure 2.12. The figure is a plot of the calculated length required to capture 100% of the approach flow for various approach flow rates. The longer the inlet length required for 100% interception, the less the inlet capacity. The calculations for Figure 2.12 were performed for a longitudinal slope of 0.02 and a transverse slope of 0.0417, which is within the range of applicability for both methods. For these conditions, Figure 2.12 shows that Li's equation (Equation 2.33) predicts almost twice the inlet capacity predicted by Izzard's equation (Equation 2.16) for a given length L_r.

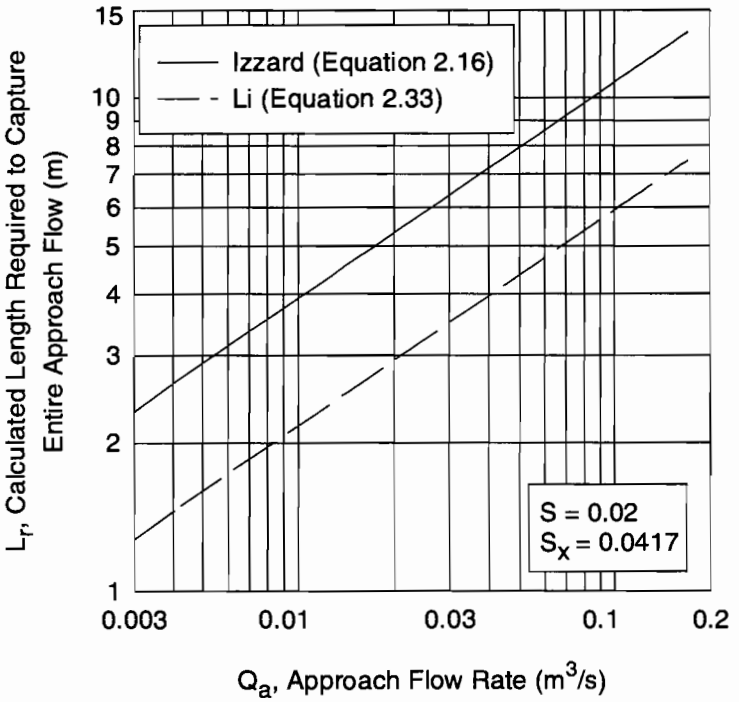

Figure 2.12 Comparison of Izzard's and Li's 100% Efficiency Equations for Undepressed Curb Inlets

Figure 2.13 is a comparison of Izzard's and Li's 100% efficiency equations for undepressed curb inlets (Equations 2.16 and 2.33, respectively) with experimental data from the 100% efficiency tests conducted on undepressed curb inlets in this research project (Section 4.3.2). The figure is plotted in terms of q_L, the captured flow per unit of inlet length. Figure 2.13 shows that Li's equation gave fairly accurate predictions for the 100% efficiency capacity of the inlets, while Izzard's equation underestimated the capacity of the inlets.

Figure 2.14 is a comparison plot of Li's and Izzard's less than 100% efficiency equations for undepressed curb inlets. The figure shows that for a given approach flow rate, Izzard's equation (Equation 2.15) predicts the inlet will capture a greater percentage of the approach flow than is predicted by Li's equation (Equation 2.36). It is interesting that Li's 100% efficiency equation predicts higher inlet capacities than Izzard's 100% efficiency equation, while the opposite is true for the less than 100% efficiency equations.

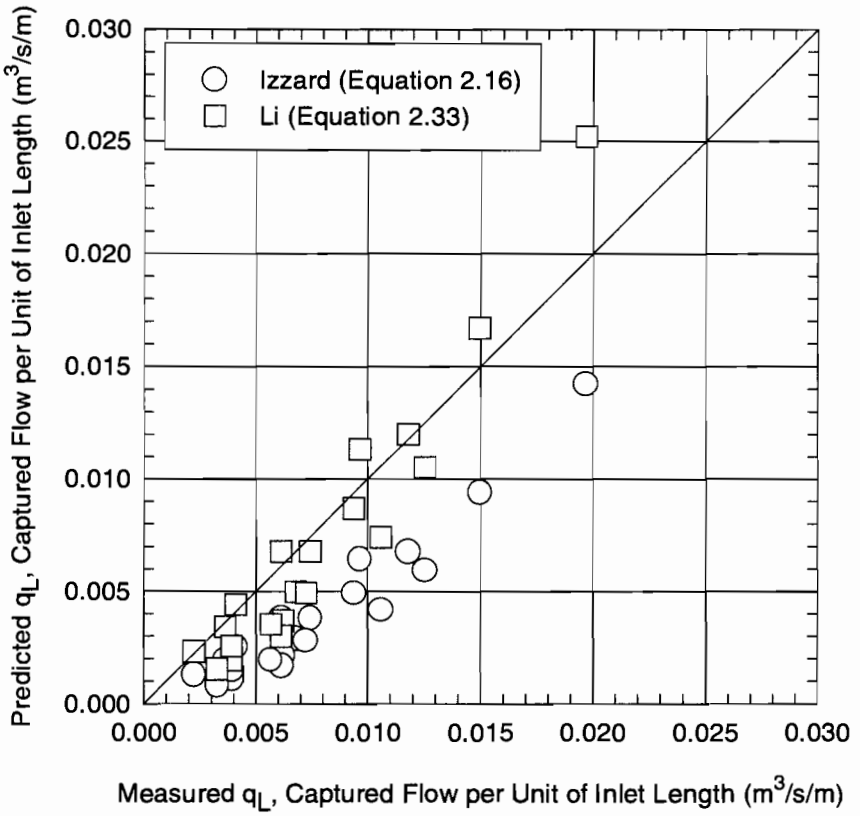

Figure 2.13 Comparison of Izzard's and Li's 100% Efficiency Equations for Undepressed Curb Inlets with Experimental Data

Figure 2.15 is a comparison of Izzard's and Li's less than 100% efficiency equations for undepressed curb inlets with experimental data from this research project (Section 4.3.2). As shown in the figure, both Izzard's and Li's design methods underestimated the capacity of the inlets, but Izzard's equations gave more accurate results than Li's equations. Both Izzard's and Li's less than 100% efficiency methods require the use of their corresponding 100% efficiency equation to calculate L_r, the required length to capture 100% of the approach flow. The fact that Li's design equations gave acceptable results for 100% efficiency implies that the poor results for less than 100% efficiency can be attributed to his less than 100% efficiency equation (Equation 2.36). Izzard's 100% efficiency equation (Equation 2.16) was a poor predictor of the capacity of

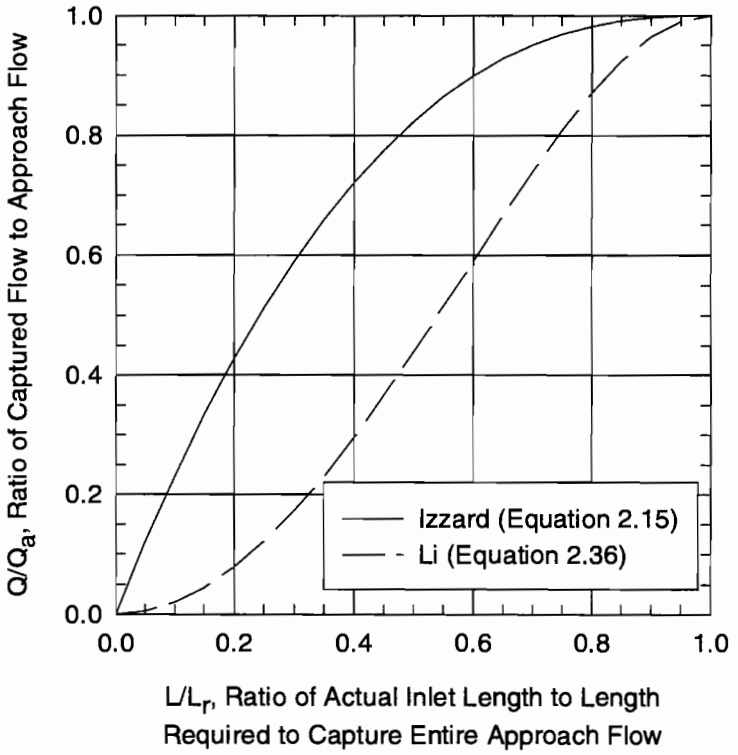

Figure 2.14 Comparison of Izzard's and Li's Less than 100% Efficiency Equations for Undepressed Curb Inlets

the undepressed curb inlets tested in this research project, yet when Equations 2.15 and 2.16 were used together to predict the less than 100% efficiency capacity of the inlets, the overall results were much better (Figure 2.15).

2.1.3.2 Depressed Curb Inlets

The comparison of Izzard's and Li et al.'s equations for depressed curb inlets is not as straightforward as for undepressed inlets because the equations take different forms. Furthermore, the limited applicability of Li et al.'s equations requires that the comparison be restricted to the specific inlet geometry tested in Li et al.'s development. All of the comparison calculations were performed for an inlet with a depression 0.105 m deep and 0.838 m wide, with a downstream depression transition 0.421 m long. This geometry is consistent with Li et al.'s development, but is not representative of TxDOT curb inlets.

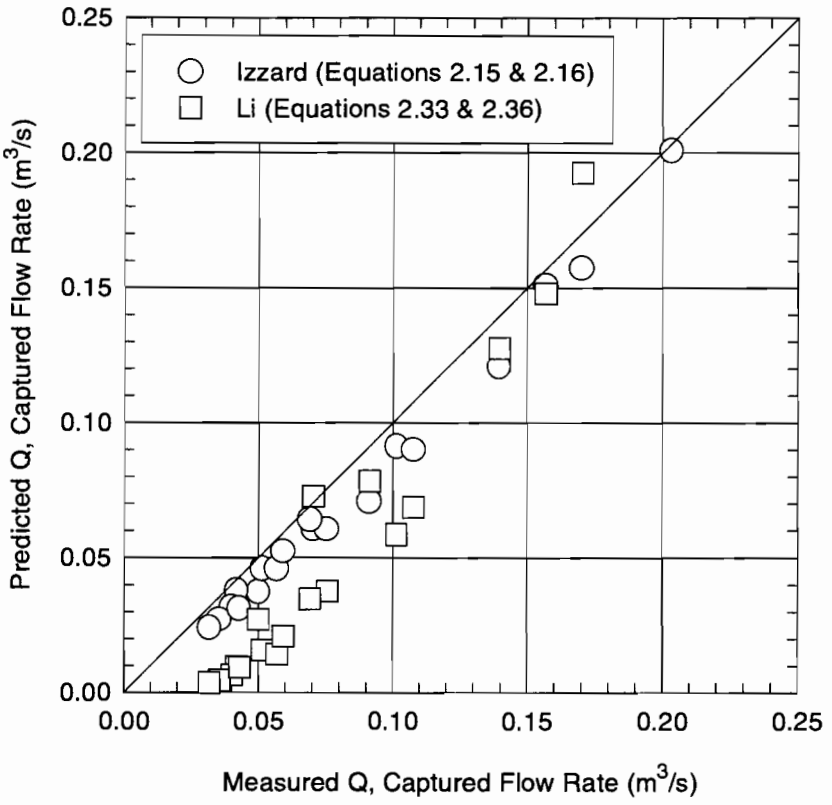

Figure 2.15 Comparison of Izzard's and Li's Less than 100% Efficiency Equations for Undepressed Curb Inlets with Experimental Data

For 100% efficiency, a convenient way to compare the two methods is by examining the calculated length required to intercept 100% of the approach flow rate for various flow rates. Figure 2.16 shows a plot of L_r as a function of Q_a as calculated by Izzard's and Li et al.'s 100% efficiency equations for depressed inlets. For lower approach flow rates, Li et al.'s equation (Equation 2.39) predicts significantly greater required lengths than those predicted by Izzard's equation (Equation 2.21). For higher flow rates, the trend is reversed, with Izzard's equation predicting greater required lengths. Because Figure 2.16 was calculated for a different inlet geometry than was tested in this research project, it is not possible to compare the values shown in the figure with the results of this research project.

For higher flow rates, the trend of Li et al.'s equation does not agree with the observed behavior of the TxDOT Type C and Type D inlets tested in this project (Section 4.3.2). As

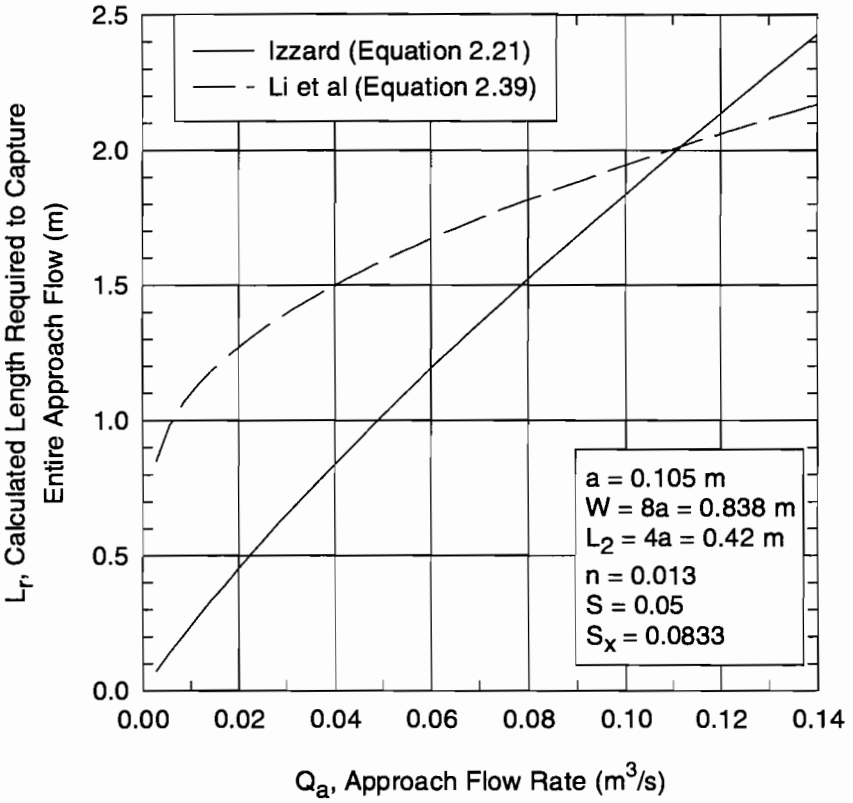

Figure 2.16 Comparison of Izzard's and Li et al.'s Equations for the 100% Efficiency Capacity of Depressed Curb Inlets

shown in the figure, Li et al.'s equation increases sharply for lower flow rates, but the rate of increase decreases as the approach flow rate increases. As discussed in Chapter 4, the principle of diminishing returns seems to apply to the length of TxDOT depressed curb inlets required for 100% efficiency because most of the captured flow is intercepted by the first part of inlet. Therefore, the first part of the inlet is much more efficient than the rest of the inlet because the roadway geometry and the depression transition upstream of the inlet help to concentrate water against the curb. This concentration of flow is quickly removed by the inlet at its upstream end. The remaining length of the inlet is capturing water which must make its way to the curb from farther out in the roadway, where a smaller percentage of the flow exists. Therefore, beyond a certain approach flow rate, adding length to the curb inlet does little to increase the 100% efficiency capacity of the inlet. Figure 2.16 shows that this trend is not represented by Izzard's

equation either, but Izzard's equation is more nearly representative of the behavior observed for the TxDOT inlets, especially for higher approach flow rates.

In contrast with the behavior observed for the TxDOT inlets, there is an explanation for the trend of Li et al.'s equation. The unique geometry of the inlets tested by Li et al. obviously caused the inlets to behave differently from the TxDOT inlets. Li et al. tested inlets with a 0.838 - m wide depression, which is much wider than the 0.457 m depression of the TxDOT inlets. This wide depression allowed the entire approach flow rate to be contained within the depressed gutter. Therefore, the entire flow was concentrated close to the curb. For Li et al.'s experiments, the ponded width just upstream of the inlet never exceeded 0.838 m; for the experiments on the TxDOT inlets, ponded widths were up to 4.27 m (prototype) for some of the tests. Li et al.'s depression geometry allowed the inlets to be considerably more efficient than the TxDOT inlets. Because Li et al.'s inlets were so efficient, the length required for 100% efficiency increased at a decreasing rate as the approach flow rate was increased. Of course, the efficiency of Li et al.'s inlets would be at least partially offset by the nuisance to motorists caused by a 0.838-m wide depression in the traffic lane.

Curiously, Li et al.'s less than 100% efficiency equation for depressed curb inlets predicts lower captured flow rates than Izzard's equation. However, both equations share a similar trend, as shown in Figure 2.17. As for the 100% efficiency results, this behavior can be attributed to the different inlet geometries for which the equations were developed. Evidently, Li et al.'s inlets were near their ultimate interception capacity at 100% efficiency. The depression geometry of Li et al.'s inlets created a more uniform efficiency along the length of the inlet than is possible for other curb inlets at 100% efficiency. For inlets such as the TxDOT inlets tested in this project, significantly higher flow rates can be captured by allowing some water to bypass the inlet. As the head on the downstream portion of the inlet increases with increasing flow rate, the efficiency of the downstream portion of the inlet is significantly increased. This behavior helps to explain why most highway curb inlets are designed to allow some carryover flow.

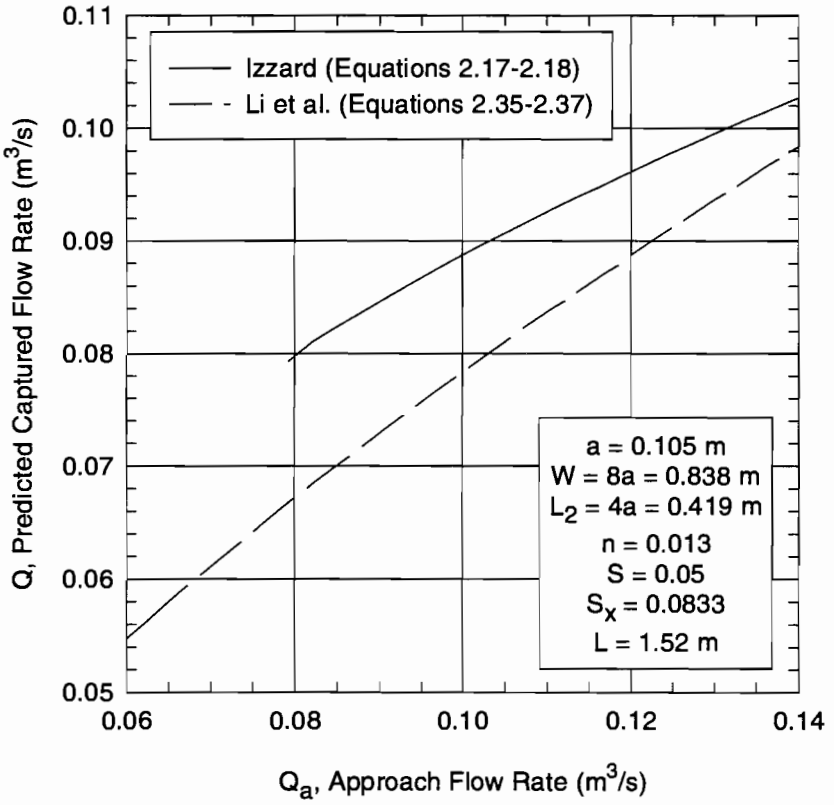

Figure 2.17 Comparison of Izzard's and Li et al.'s Equations for the Less than 100% Efficiency Capacity of Depressed Curb Inlets

2.1.4 Other Investigations

The references described in the following sections had some application to the TxDOT curb inlets tested in this project, but did not provide as much useful background information as Izzard's and Li's articles.

2.1.4.1 HEC-12 (1984)

Johnson and Chang were the authors of the Federal Highway Administration's (FHWA) Hydraulic Engineering Circular No. 12 (HEC-12). HEC-12 contains the FHWA's guidelines and recommended design procedures for the drainage of highway pavements. Consequently, the equations and procedures presented in HEC-12 are widely used in highway drainage design.

A design procedure is presented in HEC-12 for undepressed curb inlets, with an extension of the procedure developed for depressed curb inlets and curb inlets on streets with composite transverse slopes. For undepressed curb inlets, the HEC-12 equation for the length required to intercept 100% of the approach flow is

$$L_T = 0.82\, Q_a^{0.42} S^{0.3} \left(\frac{1}{nS_x}\right)^{0.6} \tag{2.45}$$

Equation 2.45 is similar to Izzard's empirical 100% efficiency equation for undepressed curb inlets (Equation 2.16). If Izzard's modified Manning's equation (Equation 2.4) is substituted into Equation 2.16 for the normal depth y_n, Equation 2.16 becomes

$$L_T = 1.51 Q_a^{0.44} S^{0.28} \left(\frac{1}{nS_x}\right)^{0.56} \tag{2.46}$$

The similarities between Equation 2.46 and Equation 2.45 are obvious. When experimental data from 100% efficiency tests conducted on undepressed curb inlets for this research project were compared with the predictions of Equation 2.46 (Equation 2.16), Equation 2.46 overestimated the inlet length required to capture 100% of the approach flow. Because Equation 2.45 has a smaller numerical coefficient than Equation 2.46, the predictions of Equation 2.45 are closer to the undepressed curb inlet behavior observed in this project that those of Equation 2.46; that is, for a given flow rate and roadway geometry, Equation 2.45 predicts a shorter length required for 100% efficiency than does Equation 2.46. However, the HEC-12 equation (Equation 2.45) still underestimated the capacity of the undepressed curb inlets tested in this project (Section 4.3.2), as shown in Figure 2.18.

The HEC-12 equation for the interception efficiency (Q/Q_a) of undepressed curb inlets shorter than the length required for 100% efficiency is

$$\frac{Q}{Q_a} = 1 - \left(1 - \frac{L}{L_T}\right)^{1.8} \tag{2.47}$$

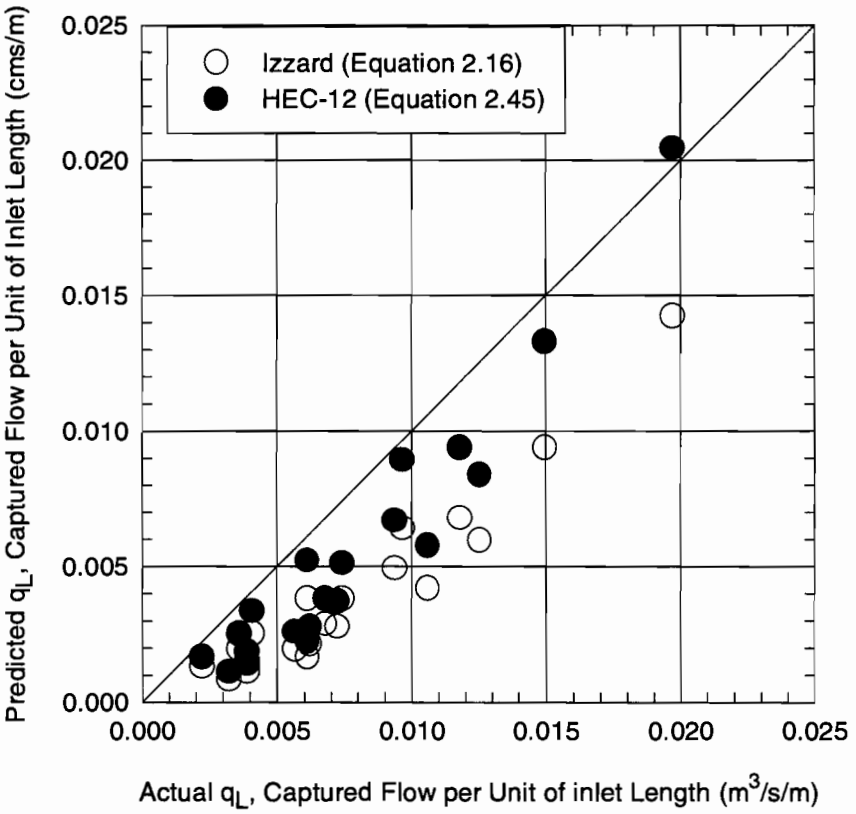

Figure 2.18 Comparison of Izzard's and HEC-12's 100% Efficiency Equations for Undepressed Curb Inlets with Experimental Data

Equation 2.47 is identical to Izzard's equation for the less than 100% efficiency capacity of undepressed curb inlets (Equation 2.15) except for the value of the exponent. Figure 2.19 shows a comparison of the HEC-12 equations and Izzard's equations with experimental data from this research project for undepressed curb inlets. As shown in Figure 2.19, Izzard's equations (Equation 2.15 with L_r calculated by Equation 2.16) just slightly underestimated the less than 100% efficiency capacity of the undepressed curb inlets tested in this project. However, the predictions of the HEC-12 equations (Equation 2.47 with L_r calculated from Equation 2.45) are even closer to the experimental data. Figure 2.19 shows that the HEC-12 equations gave acceptably accurate predictions of the less than 100% efficiency capacity of the undepressed curb inlets tested in this research project (Section 4.3.2).

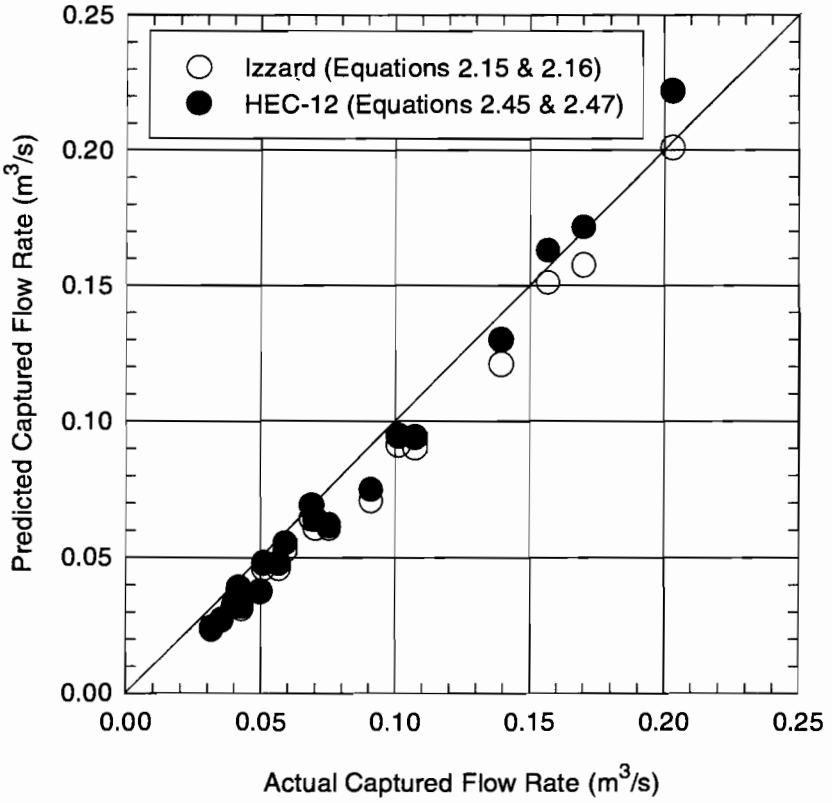

Figure 2.19 Comparison of Izzard's and HEC-12's Less than 100% Efficiency Equations with Experimental Data for Undepressed Curb Inlets

According to Johnson and Chang, Equation 2.46 is valid for both depressed and undepressed curb inlets. For depressed curb inlets, Equation 2.45 is modified by replacing S_x in the equation with an equivalent cross slope, S_e, given by

$$S_e = S_x + S_w E_o \tag{2.48}$$

S_w is the transverse slope of the gutter measured in relation to the transverse slope of the pavement (Figure 2.20). S_w is given by

$$S_w = \frac{a}{W} \tag{2.49}$$

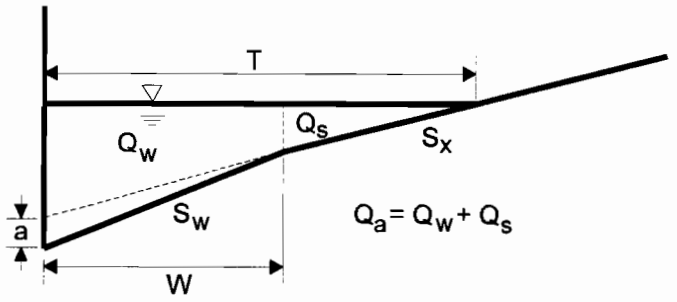

Figure 2.20 Cross-Section of Flow Just Upstream of a Depressed Curb Inlet

E_o is the ratio of flow in the depressed section to the total gutter flow (Figure 2.20) and is given by

$$E_o = \frac{Q_w}{Q} = 1 - \frac{Q_s}{Q} \tag{2.50}$$

where Q_w is the flow rate contained in the depressed section of width W and Q_s is the flow rate outside of the depressed section (Figure 2.20). Unfortunately, E_o is difficult to calculate because the ponded width in the depressed section is unknown. A nomograph is provided in HEC-12 for the purpose of calculating the ponded width in the depressed section, but the assumptions and equations used to construct the nomograph are not provided. Repetitive use of a graphical solution such as the one presented in HEC-12 is inconvenient. The most likely way to determine the ponded width in the depressed section for a given approach flow rate and for supercritical gutter flow is to calculate the uniform flow depth in the undepressed section upstream of the depressed section, and then to calculate the flow depth in the depressed section by specific energy considerations. Once the flow depth in the depressed section is known, the ponded width can be calculated.

The experimental data from the TxDOT curb inlets tested in this research project (Section 4.3.2) were compared with the predictions of the HEC-12 equations. In most cases, the HEC-12 equations gave better agreement with experimental data than Izzard's equations, but still were

not acceptably accurate. The HEC-12 equations are completely incompatible with the effective length concept developed for predicting the capacity of the TxDOT inlets (see Chapter 4).

2.1.4.2 Bauer and Woo (1964)

Bauer and Woo (1964) performed experiments on depressed curb inlets at Colorado State University. The primary purpose of their research project was to develop design information for depressed curb inlets. The modeling experiments were performed at full scale on a roadway model 25.6 m long and 3.66 m wide. The model had adjustable longitudinal and transverse slopes. During the tests, the longitudinal slope was varied from 0.002 to 0.04 and the transverse slope was varied from 0.015 to 0.06. The inlet opening length was varied from 1.52 m to 10.67 m in 1.52-m increments. The initial experiments of the research project were conducted to determine the optimum upstream and downstream depression transition geometry. Various configurations were tested, and it was found that a depression of width W = 12a with transition sections of length W gave the greatest inlet capacity. However, no tests were performed with transitions of length greater than W, so no conclusions about the effects of longer upstream and downstream transitions can be drawn from these results.

Once the inlet depression geometry was finalized, the remaining experiments were conducted with W = 0.61 m and a = 0.051 m. Inlet design curves were developed based on the experimental results. Design curves were also developed for geometrically similar inlets using Froude's law of similitude relationships. The design curve parameters were the ponded width upstream of the inlet (T), the transverse slope (S_x), the longitudinal slope (S), and the inlet length (L). According to Bauer and Woo, the roadway roughness was relatively insignificant and was thus not used as a design parameter. Once the design parameters are known or estimated, the design curves may be consulted to determine the inlet capacity.

It is not readily apparent how Bauer and Woo's design curves were developed. A plot of Q/Q_a as a function L/F_wT was shown in the report, where F_w is the Froude number of the approach flow at a point at a distance W away from the curb, but it is unclear how the plot relates to the design curves. The authors recommended against extending the method to inlets with different geometries than those tested. No data or plots were presented in the report to indicate

how the predictions of the design curves agree with the author's experimental data. The authors did apply Izzard's equations (Section 2.1.1) to their experimental data and concluded that Izzard's equations substantially underestimated the capacity of inlets with a depression wider than 0.3 m. In contrast with Bauer and Woo's findings, Izzard's equations overestimated the capacity of the TxDOT depressed inlets tested in this research project (see Chapter 4).

2.1.4.3 Izzard (1977)

In a 1977 paper, Izzard re-analyzed the data from which Bauer and Woo's (1964) design charts were developed. Izzard used Bauer and Woo's plot of Q/Q_a as a function of L/F_wT to describe the performance of depressed curb inlets. Izzard showed that the function was piecewise continuous, with the behavior of the function governed by reference inlet lengths he designated L_1, L_2, and L_3. Equations were developed for calculating these lengths. L_3 in Izzard's analysis was analogous to L_r as previously defined in this report; that is, L_3 = the inlet length required to intercept 100% of the approach flow. L_1 and L_2 have no corresponding physical meaning, but rather define points on Izzard's plot of Q/Q_a as a function of L/F_wT. For inlet lengths between 0 and L_2, the interception efficiency Q/Q_a was a function of the inlet length and L_1. For inlet lengths between L_2 and L_3, the interception efficiency was a function of the Inlet length and L_3.

Izzard compared the predictions of his equations with the experimental data used in Bauer and Woo's analysis. While most of the data fit the equations quite well, there were a significant number of data points which exhibited large errors. Izzard gave no explanation for this behavior except to note that these data departed from the norm and were not used in his analysis. However, the extraneous data did seem to follow a fairly consistent trend and further analysis of their deviation perhaps could have revealed shortcomings of the testing procedure or the prediction equations.

Izzard stated that his design method was applicable for any transverse pavement slope, any longitudinal slope, any width of depression, any ponded width upstream of the inlet, and any pavement roughness. However, since Izzard's method was based on Bauer and Woo's data, a

specific inlet geometry with a depression of width 12a and upstream and downstream depression transitions of length W was used. The experiments were conducted for longitudinal slopes of 0.01 and 0.04, transverse slopes of 0.015 and 0.06, Manning's n of 0.01 and 0.016, ponded widths of 1.52 m and 3.05 m, and a depression of width 0.61 m with upstream and downstream transitions of length 0.61 m. Furthermore, the experiments were limited to supercritical flow.

Izzard's revised design method was compared to data from the Type D curb inlet experiments performed in this research project (Section 4.3.2). Izzard's equations underestimated the capacity of the inlets by up to 50% for lower flow rates, but results were better for higher flow rates. A possible reason for this underestimation is the different depression geometry (longer upstream and downstream transitions) of the TxDOT inlets.

2.1.4.4 Uyumaz (1992)

Uyumaz (1992) presented another design method based on Bauer and Woo's basic analysis. Again, a plot of Q/Q_a as a function of L/F_wT was used to develop design equations. The equations were developed from data from experiments conducted at 1/4 scale, with longitudinal slopes between 0 and 0.06 and transverse slopes between 0.02 and 0.06. The roughness of the pavement surface was not stated. The inlet geometry used in the experiments was similar to Bauer and Woo's inlets except Uyumaz's approach gutter had a composite cross slope. Model inlet lengths of 0.38 m, 0.76 m, and 1.14 m were tested. These are presumably scale values of 1.52-m, 3.05-m, and 4.57-m prototype inlets.

Uyumaz's analysis resulted in two regression equations for the interception efficiency (Q/Q_a) as a function of L/F_wT: a linear equation for $Q/Q_a \leq 0.6$ and a quadratic equation for $Q/Q_a \geq 0.6$. Uyumaz presented a separate set of regression coefficients for each set of longitudinal and transverse slopes he tested. A plot shown in the article exhibits acceptable agreement between the regression equations and experimental data; Uyumaz stated that the errors between predicted and measured captured flow rates were all less than 10%. The main drawbacks of this method are its restriction to the specific inlet geometry tested and the fact that a separate equation is required for each set of longitudinal and transverse slopes.

2.1.4.5 Forbes (1976)

Forbes (1976) presented an interesting numerical procedure to calculate the flow into both depressed and undepressed curb inlets. Assuming steady flow, he divided the flow field into a number of intermediate cross-sections and studied the flow over a succession of short intervals for which the flow conditions could be assumed to remain constant. At the end of each time step, the quantity, direction, and velocity of the flow at each cross-section were re-computed. In this way, he was able to calculate the amount of water which flowed over the inlet lip between cross-sections. Of course, many simplifying assumptions were made in his analysis, and Forbes pointed out that he did not intend his method to be a rigorous theoretical study of curb inlet hydrodynamics.

Forbes compared his method with the equations and design curves published by Johns Hopkins University (1956) and with the unpublished experimental data of Zwamborn and of Goldfinch. He found that applying an empirical coefficient of 0.48 to the gravitational acceleration in his calculations gave reasonable agreement with the Johns Hopkins equations and with Zwamborn's data, but the empirical coefficient had to be reduced to 0.3 to match Goldfinch's data.

One of the most interesting aspects of Forbes' analysis was his numerical study of the effect of the length of the upstream depression transition on the capacity of curb inlets. His model predicted that substantially shorter inlet lengths could be used provided that the length of the upstream transition was increased accordingly. These results were confirmed by Goldfinch's model tests. Forbes' results offer at least partial confirmation that inlet capacity can be increased by using longer depression transitions rather than the relatively short transitions tested by Bauer and Woo (1964) and others.

2.1.4.6 Wasley (1960, 1961)

In his Ph.D. dissertation (1960) and in a subsequent journal article (1961), Wasley presented a complex theoretical method for analyzing the flow into undepressed curb inlets. He proposed that the flow field could be represented as a main flow along the length of the roadway combined with a cross flow toward the curb inlet. He modeled this behavior as a cross flow

superposed onto a steady open channel flow with the velocity varying with distance from the curb. Wasley modeled the cross flow as the instantaneous failure of a dam retaining a triangular reservoir. His theoretical work was supported by a comprehensive series of laboratory experiments.

Wasley's research was aimed more at analyzing the flow dynamics and determining velocity distributions as the flow turns to enter the inlets than developing a discharge relationship. Consequently, Wasley's method is not well suited for design because of its complexity. Furthermore, while the restriction to undepressed curb inlets was necessary from a theoretical standpoint, it is a major shortcoming from a design standpoint.

2.1.4.7 Holley et al. (1992)

Holley et al. (1992) conducted tests on TxDOT recessed curb inlets at the University of Texas. Inlets were tested with both linear and reverse curve transitions upstream and downstream of the inlet opening. In addition, tests were performed to evaluate the effect of the slope of the recessed portion of the inlet between the curb line and the actual inlet opening. This research is not particularly applicable to the research performed for this project except that it introduced the concept of an effective inlet length. That is, Holley et al. found that the recessed curb inlets tested in their research behaved similarly to flush undepressed curb inlets of greater length. Thus, the effects of the recessed transitions upstream and downstream of the inlet and the recessed slope are similar to increasing the inlet opening length of a flush undepressed inlet. This concept is used in Chapter 4 of this report to describe the effect of the depression transitions upstream and downstream of the TxDOT Type C and Type D curb inlets.

2.2 BRIDGE DECK DRAINS

In the literature search performed for this project, few references were found which related specifically to bridge deck drains. Many of the available references on grated inlets referred to street drains, whose hydraulic characteristics for higher flow rates are significantly different from bridge deck drains. The primary difference is that bridge grates are followed by a drain pan and a subsequent piping system that are dissimilar in size and geometry to the inlet

boxes and piping used with street drains. Consequently, the design methods developed for street drains are not fully applicable to bridge deck drains.

The primary reference which relates to the inlets tested in this research project is Holley et al. (1992). Holley et al. tested the same bridge deck drain tested in this research project, except the orientation of the drain was reversed (see Section 5.1.1 and Figure 5.1-5.2). The research of Holley et al. is briefly described in Section 2.2.1. Several other references on grated inlets are described in Sections 2.2.2-2.2.5, and are included primarily to show how other authors conducted research on grated inlets and how their results were presented.

2.2.1 Holley et al. (1992)

Holley et al. (1992) performed extensive testing of the same TxDOT bridge deck drain tested in this research project. As discussed in Chapter 5, the drain was designated "Drain 2" in Holley et al.'s experiments and was called "Drain 2B" in the current research project. The only difference between Drain 2 and Drain 2B was the orientation of the drain. Both drains were oriented normal to the curb face. However, the drain pan outlet pipe for Drain 2 was placed next to the curb. While the outlet pipe for Drain 2B was away from the curb. Both drains had a 0.152 m diameter outlet pipe. A comparison of the hydraulic performance of Drain 2 and Drain 2B is given in Chapter 5.

One of the most important aspects of Holley et al.'s research was the classification of the drain behavior as "low flow" or "weir/orifice control," in which the capacity of the inlet is controlled by weir control as the water flows through the grate or orifice control as the water leaves the drain pan and enters the piping system, and "high flow" or "piping system control," in which the capacity of the inlet is controlled by back-pressure in the piping system. Holley et al. showed that there is a significant difference in the hydraulic capacity of the inlet under these two types of control. The experiments revealed that the efficiency of the inlet was greater for weir/orifice control than for piping system control. Thus, for a given set of longitudinal and transverse slopes, increasing the flow rate in the weir/orifice control regime caused an increase in captured flow, while the same increase in approach flow in the piping system control regime

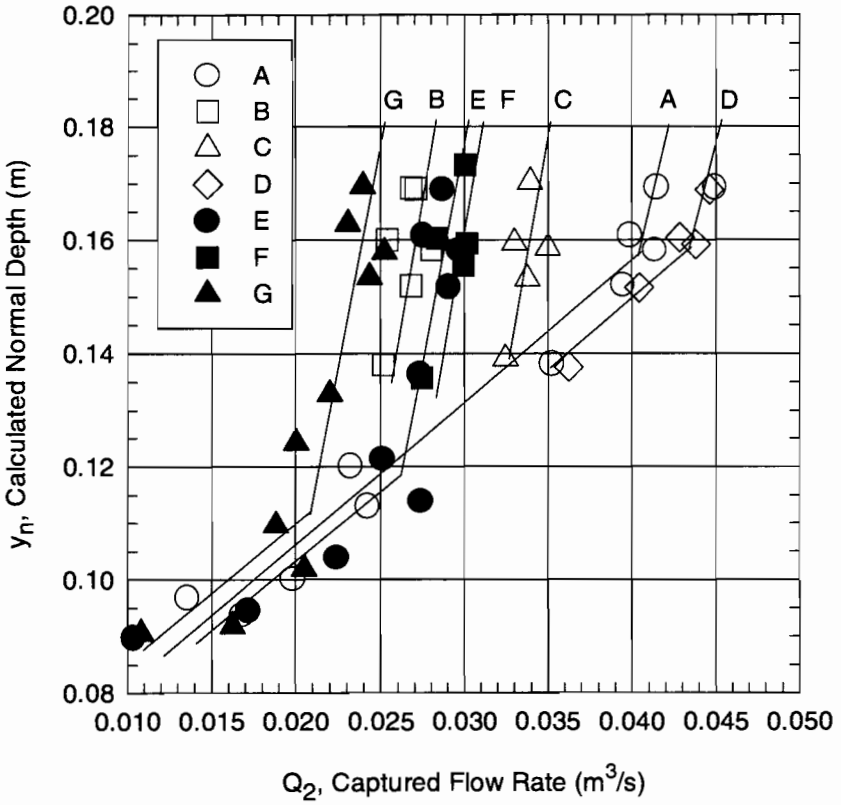

Figure 2.21 Effects of Piping System on the Hydraulic Performance of Drain 2

caused a much smaller increase in captured flow. This behavior is illustrated in Figure 2.21, which is a plot of the inlet captured flow rate as a function of the calculated normal depth upstream of the inlet. The data in the figure are for S = 0.001 and S_x = 0.06 and 0.08 only. The letters A-G in Figure 2.21 represent different drain piping configurations. For each configuration, the relationship between y_n and Q_2 begins with one slope for the lower values of y_n and Q_2 and then, at some point which varies with the piping configuration, there is a definite break in slope, with the subsequent slope being much steeper. The flatter slopes of the data correspond to weir/orifice control for the smaller Q_2 values, while the steeper slopes correspond to piping system control.

Subsequent research and re-analysis of Holley et al.'s data by Smith and Holley (1995) has shown that the flow regimes are more appropriately classified "weir control" and "orifice

control." The weir control regime exists when water is able to fall freely into the drain pan. Orifice control exists when the drain pan is full and the capacity of the drain is controlled by the orifice at the outlet of the drain pan. Smith and Holley's research has led to a new understanding of the transition between flow regimes, as discussed in Section 5.1.3.

Holley et al. tested several different piping systems in order to determine the effects of back-pressure in the piping on the capacity of Drain 2. The main differences in the piping configurations were the number of 90° elbows in the system, the location of the first elbow relative to the outlet of the drain, and the total lengths of vertical pipe and horizontal pipe. The tests revealed that the vertical distance to the first elbow in the system was the most important factor in controlling the hydraulics of the inlet, with greater vertical drop before the first elbow resulting in greater inlet capacity. Holley et al. found that the most critical configuration (the one with the least capacity) was the one in which an elbow was placed directly on the drain pan downspout, giving essentially no vertical drop before the elbow. This piping system was referred to in Holley et al.'s report as "Configuration G." For Configuration G, the transition between weir control and piping system control occurred at about 0.02 m^3/s.

The remainder of Holley et al.'s tests were directed at predicting the capacity of Drain 2 for low flow conditions. A number of additional tests were conducted, and a regression analysis was performed on the resulting data. The best regression equation found was

$$Q_2 = 11.2\, y_n^{2.49} \left(\frac{S}{S_x^2} \right)^{0.44} \tag{2.51}$$

where Q_2 is the flow rate captured by Drain 2, S is the longitudinal roadway slope, and S_x is the transverse roadway slope. The limits of applicability of Equation 2.51 were given as the more restrictive of $Q_2 < 0.023$ m^3/s or

$$y_n = 0.09 \frac{S_x^{0.39}}{S^{0.18}} \tag{2.52}$$

Equation 2.52 was developed by observing the flow conditions in the inlet box and noting the flow depth for each set of slopes at which piping system control was first observed.

None of the drain piping configurations tested in Holley et al.'s experiments was representative of actual TxDOT bridge deck drain installations. In actual installations, a gap is provided in the downspout piping to allow small shifts of the drain pan outlet with respect to the piping system due to expansion/contraction of the bridge deck (see Figure 5.10). The presence of this gap would not have affected Holley et al.'s results for low flow conditions.

2.2.2 Larson (1948)

Larson (1948) conducted hydraulic capacity tests and debris tests on several grated inlets. He tested conventional grates with both parallel and transverse bars, and also experimented with grates with transverse bars angled at 45° to the curb. The intended purpose of the angled bars was to develop a component of velocity along the transverse bars to aid in removing debris from the bars. Debris tests performed as part of Larson's research project showed that the inclined bars were not particularly effective in removing debris from the grate or preventing the grate from capturing debris. Rating curves and a design method were developed for the inlets tested; however, because Larson was not able to vary the transverse slope in his experiments, the curves and design method were limited to grates on a transverse slope of 0.0485.

Two important conclusions were developed as a result Larson's work. First, Larson recognized that allowing some carryover flow increased the capacity of the inlet per unit of inlet length. Thus, up to a limiting value of the carryover flow rate, the inlet capacity increases with the carryover flow. Larson illustrated the benefit of this behavior by proving (with his design method) that the number of inlets in series required to drain a street for a given design storm could be reduced by allowing some carryover flow early in the series of inlets. Second, Larson found that both the hydraulic capacity and the debris-handling characteristics of the grates could be significantly improved by rounding the tops of the transverse bars to conform approximately to the contour a free overfall from the leading edge of the bar. This idea was developed and tested further in the curved-vane inlets of Burgi and Gober (1978) (see Section 2.2.4).

2.2.3 Li et al. (1951a)

Li et al. presented the results of hydraulic model studies performed on longitudinal-bar grates in a 1951 journal article. The bars of the grate were 0.076 m deep and 3.18 cm wide, with rounded tops. The hydraulic tests were conducted at 1/2 scale on a model 6.10 m long and 0.91 m wide. The longitudinal slopes ranged from 0.005 to 0.06, and the transverse slopes varied from 0.0417 to 0.0833. Manning's n for the model was not given.

Li et al. used dimensional analysis to identify the variables which influenced the grate capacity. Then hydraulic tests were conducted to determine the effect of each of the identified variables on the capacity of the inlet. The carryover flow past an inlet was divided into the following three categories:

- flow that passes between the curb and the first opening in the grate,
- flow that passes outside of the last opening in the grate, and
- flow that passes over the grate itself.

Because the first category of flow is negligible for most grates, Li et al. recommended only the latter two categories be considered in the inlet design. Separate empirical expressions were developed for the length of grate required to capture all of the flow that passes outside the grate opening and the length of grate required to capture all of the flow which passes over the grate. In design, these two lengths are calculated and the greater length is used. Also, an expression was derived for the carryover flow passing outside of the grate if the grate length is less that the length required for 100% efficiency, but no corresponding expression was given for the carryover flow passing over the inlet.

The applicability of Li et al.'s equations is limited because only longitudinal-bar grates were tested. Li et al. estimated that the presence of transverse bars at the quarter points of the grates would increase the length required to capture all of the flow that passes over the grate by a factor of two; however, this assumption was never tested. The only possible application of Li et al.'s equations to bridge deck drains would be for conditions in which the grate controls the capacity of the drain (see Section 2.2.1).

2.2.4 Burgi and Gober (1978)

In an abridged 1978 report, Burgi and Gober summarized a study of several types of grates on the basis of structural integrity, bicycle safety, debris handling, and hydraulic efficiency. Hydraulic tests on the grates were performed in a flume 2.44 m wide and 18.3 m long. The longitudinal slopes varied from 0.005 to 0.013 and the transverse slopes ranged from 0.0208 to 0.0625. Manning's n of the model surface was between 0.016 and 0.017. Only the grates themselves were tested; no inlet box or piping system was used. Apparently the hydraulic tests of the inlets were conducted by Burgi (Chang et al., 1981). The design methods for grate inlets in FHWA HEC-12 (1984) are based on Burgi's data.

The basic grate designs which were tested included a grate with longitudinal bars only, a longitudinal-bar grate with transverse rods, several grates with inclined transverse bars and longitudinal rods, a grate with curved transverse vanes and longitudinal rods, and a reticuline ("honeycomb" pattern) grate. None of the grates was similar to Drain 2B; however, the inclined-bar grates were similar to the grate of Drain 4 (see Figure 5.10).

Burgi and Gober found that the hydraulic efficiency of all the grates improved as the longitudinal slopes increased. The reason they gave for this behavior was that at steeper longitudinal slopes, a given gutter flow occupies a smaller cross-sectional area; thus, a greater percentage of the flow passes over the inlet grate. This conclusion implies that the transverse slope should also be important, since steeper transverse slopes would concentrate more flow over the inlet opening. However, this possibility is not mentioned in Burgi and Gober's report.

Another key finding of Burgi and Gober's study was that the transverse components of the inlets had a large effect on hydraulic efficiency. Above a limiting longitudinal slope for a given flow rate, a given transverse slope, and given grate dimensions, it was found that excessive splashing caused by high-velocity flow striking the transverse bars of the grates severely limited the capacity of the grate. The one exception to this finding was the inlet with curved transverse vanes, for which splashing was minimized. However, Burgi and Gober noted the necessity of the transverse bars or rods to provide bicycle safety.

No design equations or rating curves were presented in Burgi and Gober's abridged report. The design information developed for the grates is found in HEC-12 (1984). However,

the grates were categorized based on their relative hydraulic efficiencies. It was found that the most efficient grates were the grate with longitudinal bars only and the grate with curved transverse vanes. The longitudinal-bar grate was not bicycle safe. Except for the reticuline grate, the remaining grates had very similar hydraulic efficiency. The reticuline grate was found to be subject to excessive splashing at higher longitudinal slopes, yet was as efficient as any other grate for longitudinal slopes less than 0.03.

2.2.5 HEC-12 (1984)

FHWA HEC-12 (1984) presented design equations and curves for grate inlets developed from Burgi's experimental data. The first step in the design method is to compute the percentage of the approach flow which is frontal flow; the remaining flow passes to the side of the grate. Then empirical design equations or charts are used to calculate the percentage of the frontal flow and side flow intercepted by the grate. These percentages depend on the flow characteristics, roadway geometry, and the grate's size and interception characteristics.

HEC-12 is probably the most widely-used reference for the design of grate inlets. TxDOT uses the HEC-12 design method to design its grate inlets, including bridge deck drains. However, it cannot be overemphasized that the design information in HEC-12 and most other sources is for grates only, and may not adequately predict the performance of inlets in which the drain pan or the subsequent piping system affects the flow.

2.3 SUMMARY

The preparation of this literature review revealed several knowledge gaps which this research project helped to fill. Although many different design methods for depressed curb inlets were located, most of these methods were developed to be applicable for a variety of inlet geometries, and thus might be less accurate for a particular inlet geometry. Comparison of the design methods located in the literature review with data from the experiments performed on the TxDOT inlets showed that none of the methods were acceptably accurate for the design of the inlets. Therefore, the literature review revealed that a new empirical design method was required for the specific geometry of the TxDOT inlets.

One of the primary concerns with the hydraulic characteristics of the TxDOT curb inlets was that backwater effects could be caused by the close proximity of the inlet lip to the back wall of the inlet box. For the TxDOT inlets tested in this research project, the distance from the inlet lip to the back of the inlet box was only 0.152 m, while for most other types of curb inlets, the distance is 0.46 m to 0.61 m. Figure 2.22 is a plan view of the TxDOT inlets, showing the short distance between the inlet lip and the back of the inlet box. It was believed that the water passing over the inlet lip might not have enough room to fall freely into the inlet box, but would strike the back wall of the inlet box and cause water to back out into the street. None of the references, discovered in the literature review addressed this particular type of backwater effect. Therefore, experiments were required to determine if the backwater effect existed, and if so, to identify its influence on the capacity of the inlets.

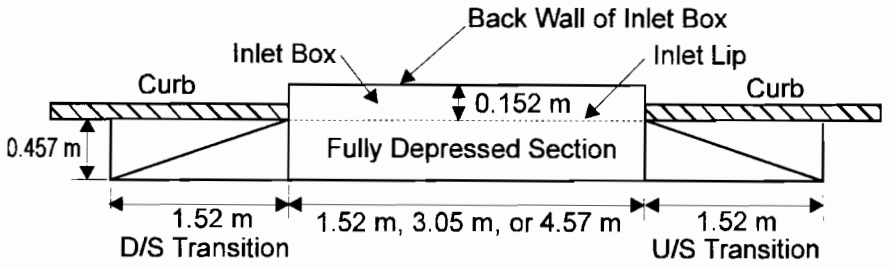

Figure 2.22 Plan View of TxDOT Type C and Type D Curb Inlets

The only reference identified during the literature review which dealt specifically with bridge deck drains (rather than grated street inlets) was Holley et al. (1992). As mentioned in Section 2.2, the hydraulic characteristics of bridge deck drains are significantly different than those of grated street inlets, because bridge deck drains are followed by a drain pan and piping system that is dissimilar in size and geometry to the inlet boxes and piping used with street drains. Holley et al. tested and developed design equations for one of the same bridge deck drains tested in this project (Drain 2 in Holley et al.'s project, Drain 2B in this research project). The only difference between Drain 2 and Drain 2B was the orientation of the drain (see Section 5.1 and Figures 5.1-5.2). The orientation of the drain pan has a significant affect on the capacity

of the inlet. Because the drain is usually installed in bridges in the same orientation as Drain 2B, design equations were needed for the drain in this orientation.

The literature review revealed that, in general, there is a lack of knowledge of the hydraulic characteristics of bridge deck drains. The bridge deck drain research described in this report focused primarily on developing design equations for bridge deck drains. Furthermore, bridge deck drains represent only a portion of the research project described in this report, with the remainder of the research devoted to flush depressed curb inlets. Additional research work on Drain 2B was performed by another researcher as part of the same TxDOT research project (Smith and Holley, 1995). Smith and Holley's research is distinguished from the research presented in this report because his work focused exclusively on describing the hydraulic characteristics of Drain 2B, including the effects of the piping system below the drain. The results of Smith and Holley's research are presented in a separate report (Smith and Holley, 1995). Smith and Holley's work resulted in a more complete description of the flow patterns in the drain pan and outlet piping as the transition from the weir control regime to the orifice control regime occurs. Smith and Holley tested many different piping configurations with Drain 2B to determine the effect of outlet piping on the drain's capacity. He also studied the effects of vortices in the drain pan and outlet piping on the capacity of the drain. Smith and Holley's work led to a much clearer understanding of the hydraulic characteristics of Drain 2B and of bridge deck drains in general.

3. EXPERIMENTAL METHODS

All of the hydraulic testing described in this report was conducted on a large physical roadway model located in the hydraulics laboratory of the Center for Research in Water Resources (CRWR) of the University of Texas at Austin. The model is a 3/4-scale representation of one lane of a roadway. The model lane is 18.9 m long and 3.2 m wide, which is the model width of a 4.27-m roadway lane. The model has adjustable slopes in both the longitudinal and transverse directions. The model can be sloped to either its right or left side. (In open-channel hydraulics, it is customary to define right and left looking downstream, and this convention is used throughout this report.) Curb inlets were installed on the right side of the model and bridge deck drains were installed on the left side. The design and construction of the model will be fully explained later in this chapter.

The model used in this project was designed and constructed during 1990-1991 as part of a previous project (Holley et al., 1992). The model was designed to meet a number of different objectives. First, the model had to accommodate prototype flow rates of up to 0.3 m^3/s. Second, longitudinal and transverse pavement slopes of up to 10% had to be available to represent a wide range of highway geometric conditions. Third, the model had to allow easy installation of various drainage inlets. Finally, structural criteria such as overall strength, rigidity, and maximum allowable deflection had to be met. All of these objectives were satisfied in the design of the model.

3.1 MODEL LENGTH SCALE

One of the most important considerations in the original design of the model was the length scale ratio. The length scale ratio is defined as the ratio of length in the model to length in the prototype. Several factors which needed to be considered in choosing the length scale included establishment of uniform flow upstream of the inlet opening, available pump capacity, available space in the laboratory, construction constraints, cost, and avoidance of surface tension and Reynolds number effects at small scales.

The model and the prototype must have equal Froude numbers in order to obtain hydraulic similitude. This condition is met by the relationships (Roberson, Cassidy, and Chaudhry, 1988):

$$V_r = \Lambda_r^{1/2} \tag{3.1}$$

and

$$Q_r = \Lambda_r^{5/2} \tag{3.2}$$

where Λ_r = length scale ratio, V_r = velocity ratio, and Q_r = discharge ratio. Each ratio is defined as the model value divided by the corresponding prototype value.

With all the constraints considered, a length scale of 3/4 was chosen, i.e., the model size was 3/4 of the prototype size. At 3/4 scale, a depth of 0.15 m in the prototype is 0.11 m in the model, and a prototype flow rate of 0.3 m^3/s is 5.2 m^3/s in the model.

3.2 ORIGINAL MODEL CONSTRUCTION

The roadway model consists of a wooden deck supported by a steel structure. All of the dimensions in this section are model dimensions.

The steel support structure was constructed to allow both the longitudinal and transverse slopes of the roadway to be varied. Figure 3.1 shows the key elements of the steel structure. Two longitudinal beams 18.3 m long are used to support the wooden roadway channel. The beams are placed parallel to each other at a spacing of six feet, centered laterally under the roadway deck which was added later. The longitudinal beams are supported by cross beams welded perpendicular to and underneath the longitudinal beams at a distance of 4.2 m from the each end of the longitudinal beams. The location of the cross beams was chosen so that the deflections at the two ends of the channel and at the point half way along the length between the two cross beams would be equal for a uniformly distributed load. The upstream cross beam is suspended with two 5-ton manual chain hoists from a portal frame. The hoists are attached from near each end of the top beam of the portal frame to the top of the cross beam. On the right side

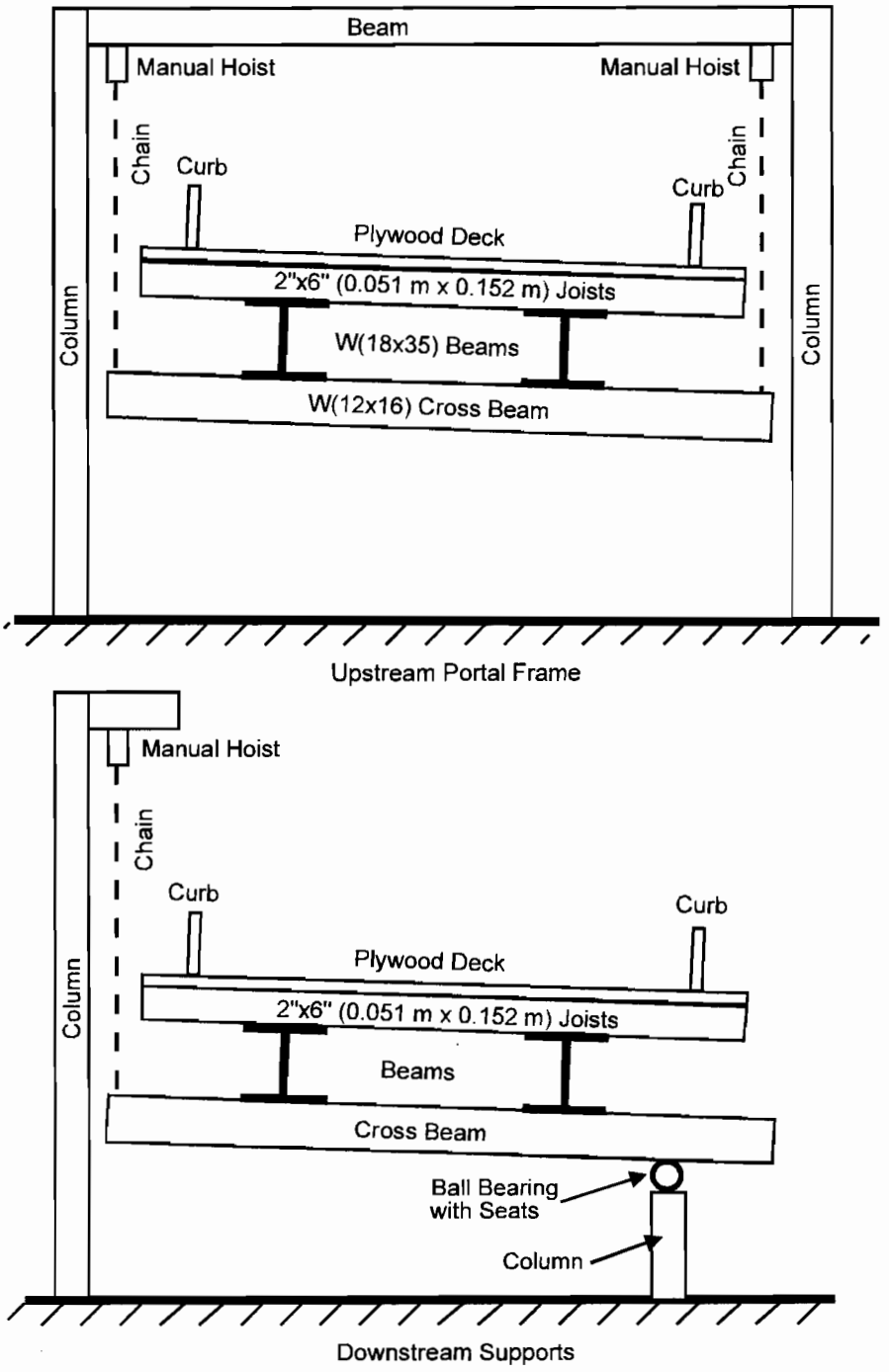

Figure 3.1 Cross-Sectional Diagram of Primary Structural Components of Model (Looking Downstream)

of the downstream cross beam, the support is a pivot consisting of a 0.05-m ball bearing in seats on top of a short column (Figure 3.1). A taller column with a third chain hoist is used to support the left side of the downstream cross beam. With the use of the frames, pivot, and manual chain hoists, the longitudinal gutter and transverse pavement slopes can be changed easily.

The structure is designed to allow no more than a 0.003-m deflection at any location along the roadway for the dead load plus the live load (water and personnel). This constraint was imposed to ensure that neither the hydraulics of the flow nor the measurements would be severely affected by deflections or changes in deflections as the amount of water or other loads on the structure changed.

The wooden roadway deck was placed on top of the longitudinal steel beams. The wooden support structure consists of 2″x6″ (0.051 m x 0.152 m) floor joists bolted to clip angles welded to the tops of the longitudinal beams at 0.61-m intervals. The pavement surface of the model consists of a 0.0191-m tongue-and-groove plywood deck installed on the joists (Figure 3.1). The plywood surface was waterproofed with asphalt/aluminum roof sealant, then textured to represent the hydraulic roughness of pavement by incorporating sand grains into several coats of acrylic roof sealant. The total wood structure was 4.27 m wide and 19.5 m long. The curbs are placed on both sides of the model roadway at a spacing of 3.20 m, which is the model width of a 4.27 m lane. The curbs for the roadway are constructed of pressure-treated 2″x6″ (0.051 m x 0.152 m) timbers. The roadway deck is wide enough to allow walkways approximately 0.5 m wide on each side of the roadway.

3.3 MODEL RECONSTRUCTION

The construction described in the previous section took place in 1990-1991. Experiments for the previous project were conducted during 1991-1992. The project described in this report began in the fall of 1993. During the time between projects, the model was used primarily for demonstrations.

During model inspections performed before experimental work on this project began, it was observed that the model surface had begun to deteriorate. Cracks in the surface texture had developed at numerous joints between the plywood sheets which formed the roadway deck.

These cracks allowed water to penetrate into the plywood, causing rotting and warping of the sheets.

It was originally thought that the damage to the model surface could be corrected by a series of repair operations. The surface texture was removed from each joint between plywood sheets, then the joints were re-caulked to prevent leakage. The entire model surface was re-textured with sand grains incorporated into several coats of epoxy paint. A thick layer of texture was applied in low spots in an attempt to level the model surface. It was hoped that the epoxy paint would provide a waterproof seal for the deck and a durable model surface.

These repairs were successful in curtailing leakage from the plywood deck, but they did not provide a level model surface. A series of initial tests and a full topographic survey of the model showed that the surface was too uneven for reliable, accurate measurements to be made. In order to ascertain the true condition of the plywood, the texture was removed from some of the most badly damaged sheets. Inspection of these sheets revealed that the deterioration of the plywood was worse than was initially suspected. Because it was apparent that the plywood was too badly damaged to last for the full duration of the project, it was decided to replace the entire plywood deck.

It was also suspected that warping of the 2″x6″ (0.051 m x 0.152 m) joists contributed to the distortion of the model surface. Water damage was evident on many of the 2″x6″ (0.051 m x 0.152 m) members. After the original plywood deck was removed, an elevation survey was taken of each joist to determine the straightness of the member. Any joist exhibiting elevation variations greater than 0.0016 m was replaced. These surveys indicated that many of the existing joists were badly warped.

In an effort to systematically eliminate all possible sources of structural distortion in the new construction, an elevation survey was taken of the longitudinal steel beams. The surveys revealed elevation variations in both beams. One of the beams had an arched profile, with elevation variations of up to 0.013 m from the low points at the end of the beam to the high point at the center. Yield strength calculations confirmed that these variations were not caused by permanent deflections from the imposed loads. Further study revealed that the profiles of the beams were within allowable specifications for steel beams published by the American Institute

of Steel Construction (AISC, 1986). However, the variations were judged too large for the purposes of this project.

Rather than replacing the steel beams, it was decided to compensate for their profiles by inserting steel shims under the 2″x6″ (0.051 m x 0.152 m) joists, requiring precision surveying of both the steel beams and the wooden joists. Once the new joists were shimmed and in place, a final survey was performed to ensure the entire wooden substructure met the criterion of a maximum of 0.0016 m elevation variation.

A 0.0191-m tongue-and-groove plywood deck was then placed on the joists. Figure C.1 in Appendix C is a photograph of the new wooden deck under construction. Once the deck was in place, a topographic survey was performed to verify that the deck was plane. The extreme care that was used in the reconstruction resulted in a very even deck surface. After the deck was in place, the underside of the deck and the entire substructure was coated with an epoxy sealer to deter water damage and rust.

A few minor modifications to the original structural design were incorporated into the reconstruction. The upstream and downstream overhangs were shortened from 0.61 m to 0.30 m on each end and the overhanging supporting wooden structural members were doubled to lessen the possibility of deflection in these cantilevered sections. Also, the channel location on the plywood surface had to be shifted slightly to the right to accommodate one of the drains to be tested during the project.

In the original construction, pointer mechanisms had been affixed to both the upstream and downstream cross beams. The pointers were used with scales mounted on the columns of the upstream frame and downstream column. The longitudinal and transverse model slopes were set by manipulating the chain hoists until the pointers registered the proper readings on all the scales. In the new construction, the pointer assemblies were re-designed to pivot in both the horizontal and vertical planes so that the pointer rod could always be horizontal when reading the scale. A miniature bubble level was installed on each pointer rod to indicate when the rod was level. This design reduced the complexity of the geometry involved in the pointer scale calculations and improved the accuracy with which the slopes could be set. Figure C.2 in Appendix C is a photograph of the new pointer mechanism.

The model road surface was waterproofed by applying two layers of fiberglass fabric and resin to the plywood. The hydraulic roughness of pavement material was simulated by incorporating sand grains into the final coat of fiberglass resin. The surface texture of the model will be described in more detail in Section 3.5.

3.4 MODEL LAYOUT

A plan view of the physical model is shown in Figure 3.2. Water is pumped from a half-million gallon reservoir to the headbox. Immediately downstream of the headbox is a series of baffles to dampen the flow disturbances in the model. For supercritical flow, the distance from the headbox to the inlet being tested was usually long enough to allow the water to reach uniform flow prior to entering the inlet section.

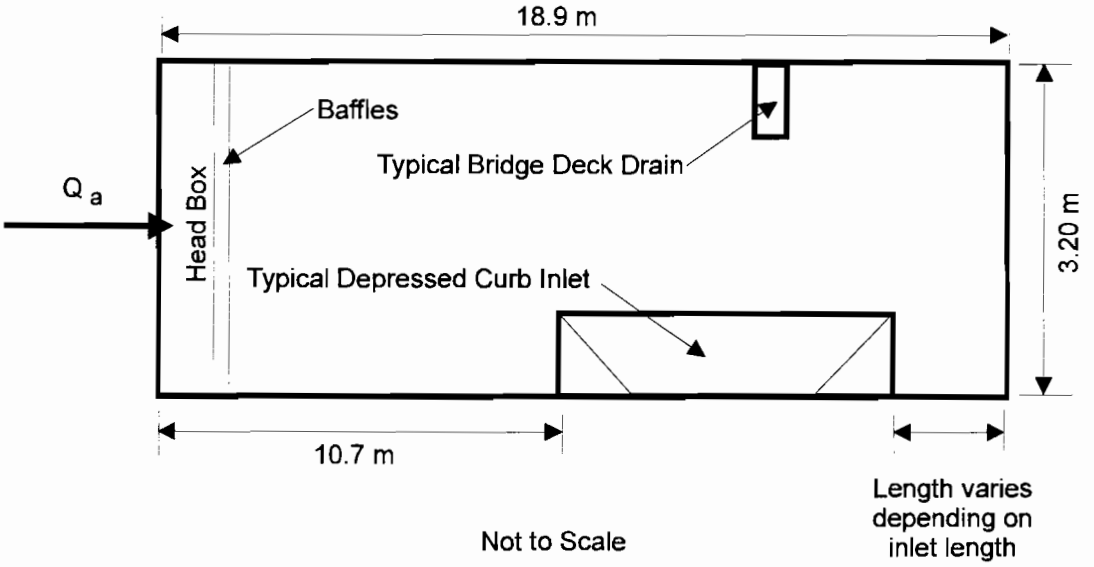

Figure 3.2 Plan View of Roadway Model (Model Dimensions)

The model was designed to test curb inlets and bridge deck drains. Curb inlets were installed on the right side of the model, while bridge deck drains were installed on the left side of the model. The model is designed so that the deck can slope to either the right or the left. Typically, inlets were installed on both sides of the model at once. The model was wide enough

so that there was no hydraulic interference between inlets on opposite sides of the model during inlet tests.

The bridge deck drains were installed in pre-cut holes in the model surface. A rim was provided below the top of the hole to allow the top of the drain to lie flush with the model surface. The edges around the drain were caulked to prevent leakage and to protect the wooden deck.

Curb inlets were constructed to fit in a cutaway section along the right side of the model. The inlets utilized modular construction consisting of upstream and downstream transition pieces and up to three inlet pieces. In order to change the inlet length, the downstream transition piece was moved to its new location and inlet pieces were either added or removed to form an inlet of the proper length. The upstream transition piece remained fixed for the duration of the tests. This modular design allowed inlet length and geometry to be changed easily. Figure C.3 in Appendix C is a photograph of the curb inlet pieces under construction.

The space beneath the model was subdivided into two large tanks which were used to separate the flow captured by the inlet from the carryover flow. The tanks were formed of cinder block walls waterproofed with cement grout. The water exiting each tank flowed over a V-notch weir which was used to measure the flows. Then the captured flow and carryover flow mixed back together in the reservoir return channel and flowed over an additional V-notch weir placed outside the laboratory before entering the reservoir.

3.5 MODEL SURFACE

As mentioned in Section 3.1, hydraulic similitude requires that prototype and model Froude numbers are equal. This requirement and Manning's equation lead to (Henderson, 1966)

$$n_r = \Lambda_r^{1/6} \tag{3.3}$$

where n_r = ratio of Manning's roughness coefficient for the model to that for the prototype. Manning's n is defined by Manning's equation:

$$V = \frac{1}{n} R_h^{2/3} S_f^{1/2} \tag{3.4}$$

where V = mean flow velocity, R_h = hydraulic radius of flow in the roadway = cross-sectional area of flow (A) divided by wetted perimeter (P_w), and S_f = friction slope.

In order to model typical pavement surfaces, the model had to have an equivalent prototype n value between 0.015 and 0.020. For the original model construction, it was attempted to represent a prototype Manning's n of 0.015 (Holley et al., 1992). The corresponding model n using Equation 3.3 and $\Lambda_r = 3/4$ is 0.0143. Since there is a known relationship between the size of sand grains on a surface and n for plane sand bed channels, it was decided to roughen the roadway surface with sand grains to produce the desired n value.

The size of sand grains to be used also had to be decided. Henderson (1966) gives the relationship between median sand grain size (d_{50}) and Manning's roughness coefficient (n) as

$$n = 0.041 d_{50}^{1/6} \tag{3.5}$$

with d_{50} in m. For n = 0.0143, this equation gives d_{50} = 1.7 millimeters. The closest available grain size for presorted sand was 2 mm. Assuming that the nominal size is the median grain size, the corresponding model n value from Equation 3.5 is 0.0147.

During the previous project, experiments conducted to quantify the roughness of the surface revealed that n was 0.019 for the model or 0.020 for the prototype. This n value was confirmed by many measurements made during the tests in the previous project. It is not known for certain why the actual Manning's roughness was greater than what was calculated from Equation 3.5. However, the most likely reason is that the sand grains were not as close together as would be the case for a sand bed channel.

In the original construction of the model, the surface was textured by incorporating sand grains into several coats of acrylic roof coating. However, it was later apparent that the roof coating did not provide adequate waterproofing for the plywood deck and contributed to the deck's premature deterioration. For the model reconstruction, a more durable medium was sought for waterproofing the deck and bonding the sand grains to the surface.

Several different methods for texturing the surface were examined. After consulting with experts in sealant technology, the choices were narrowed to the use of epoxy concrete sealant or fiberglass. After experimenting with both materials, it was decided to texture the surface by applying two layers of fiberglass mat and several coats of fiberglass resin, incorporating the sand grains into the final coat of resin. Although both materials produced extremely durable surfaces, fiberglass was chosen over epoxy concrete sealant because it was felt that the fiberglass surface would be easier to cut and repair when new holes in the model surface were required for inlet testing.

The fiberglass was applied to the deck by first coating the plywood with resin, laying the fiberglass fabric mat into the resin with 0.075 to 0.1 m of overlap between strips of fabric, then soaking the mat with additional resin applied from the top. The second layer of mat was applied after the first layer had completely cured. Longitudinal seams in the layers of the fabric were staggered to minimize ridges in the model surface. After the second layer of fiberglass had completely cured, irregularities in the surface were corrected by grinding and/or removing and patching the fiberglass. The curbs were fiberglassed in a similar manner, being careful to overlap the fiberglass at the base of the curb to prevent water from reaching the wooden curb.

Based on the experience gained in the previous project, it was decided to use smaller sand grains in the surface of the new construction to obtain an n value closer to the center of the allowable range for n. The next smallest available grain size had a mean diameter of approximately 1.3 mm. The corresponding n value from Equation 3.5 for this grain size is 0.0137. However, it was not expected that the actual n value would be this low. The sand grains were bonded to the surface by incorporating them into the final coat of fiberglass resin.

Experiments were conducted to quantify the resulting roughness. The tests were conducted at various flow rates for longitudinal slopes of 0.001, 0.003, 0.02, and 0.04. The transverse slope for all tests was zero. The water depths were measured at several cross-sections along the length of the model. The standard step method (Henderson, 1966) was used to calculate n. A spreadsheet was used to generate calculated water surface profiles for trial values of n. The correct n value for a run was the value which caused the calculated profile to agree most closely with the measured profile. Both subcritical and supercritical profiles were

calculated. Figure 3.3 shows a typical subcritical profile, with Q_a = 0.091 m^3/s and S = 0.002. The value of Manning's n for the profile shown in Figure 3.3 was 0.0175. A typical supercritical profile is shown in Figure 3.4, with Q_a = 0.085 m^3/s and S = 0.02. The calculated value of Manning's n for the profile shown in Figure 3.4 was 0.0175. Like Figure 3.4, all of the supercritical profiles in the Manning's n tests were uniform flow. Ten profiles were calculated in this manner, with an average value of Manning's n of 0.017 for the model, or 0.018 for the prototype.

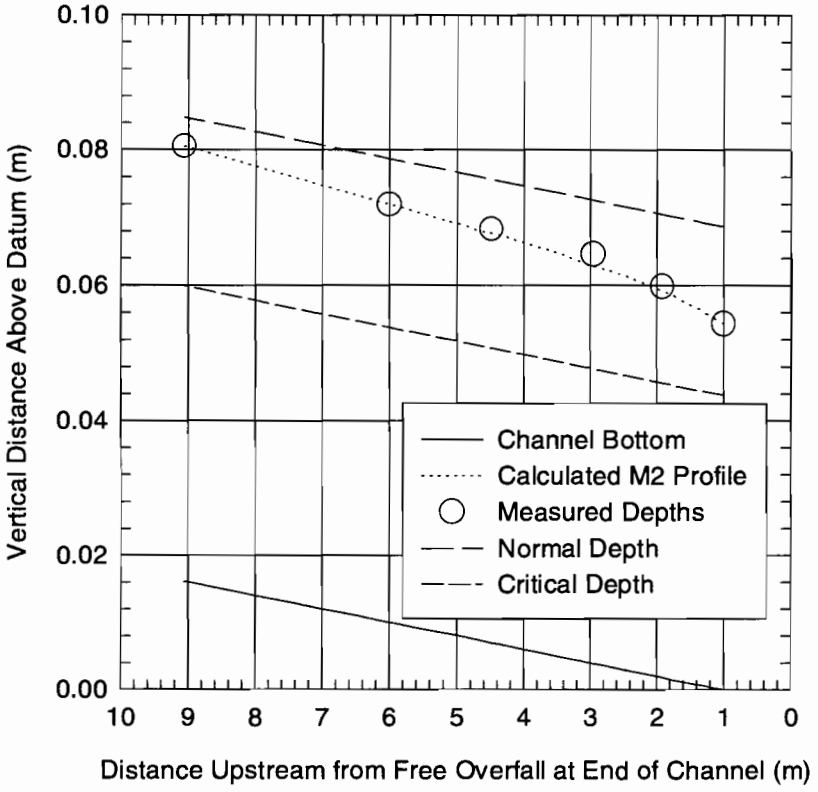

Figure 3.3 Typical Subcritical Profile Calculated for Manning's n Tests

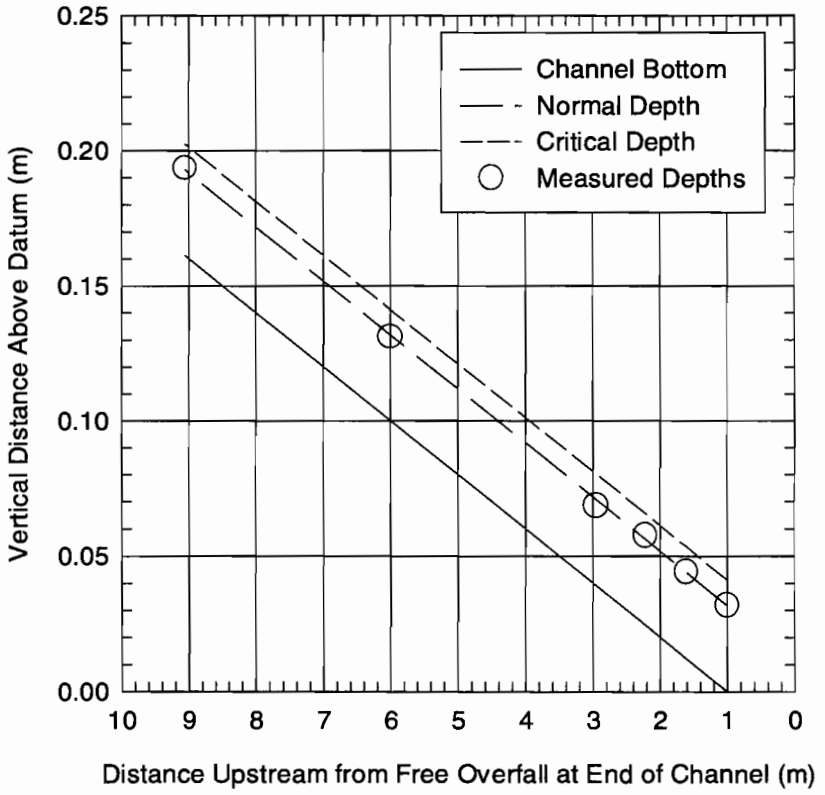

Figure 3.4 Typical Supercritical Profile for Manning's n Tests

The value of Manning's n was confirmed by many measurements made during the inlet tests. Figure 3.5 shows a comparison of the calculated normal depth and measured depth upstream of the inlet for all of the curb inlet tests and most of the bridge deck drain tests performed for this project. The points at which the upstream normal depth was measured varied depending on which type of inlet was being tested. Although considerable scatter is evident in Figure 3.5, the agreement is acceptable considering that not all flows reached uniform flow. The tests indicated that there is no significant change in n with changing depths for the range of depths encountered in these experiments.

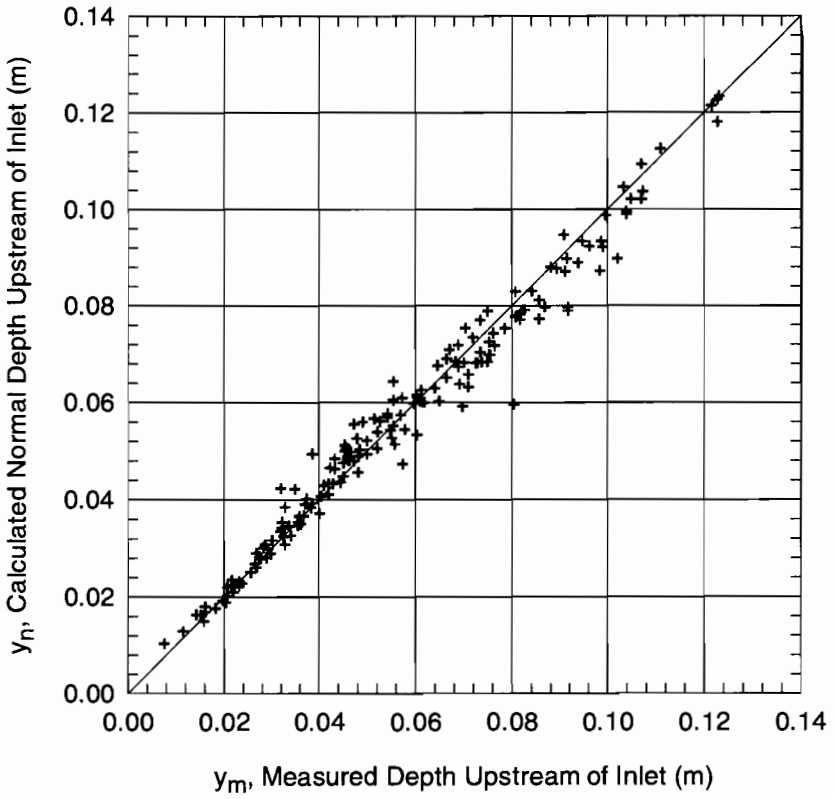

Figure 3.5 Comparison of Calculated and Measured Depths for Inlet Tests

3.6 MEASUREMENTS

During the experimentation, the following variables were typically measured for a given inlet: the flow rate into the model, the flow rate captured by the inlet being tested, the flow rate passing the inlet (the carryover), and water depths and ponded widths on the roadway surface.

Figure 3.6 is a schematic diagram of the system by which the water is pumped into the model from a 2000 m^3 reservoir outside the laboratory. Two vertical turbine pumps (designated north and south) pump from the reservoir into the two ends of an overhead 0.305-m diameter steel pipe loop in the laboratory. The pumps can be operated separately or simultaneously. For the placement of this model, each pump separately can discharge up to 0.1 m^3/s.

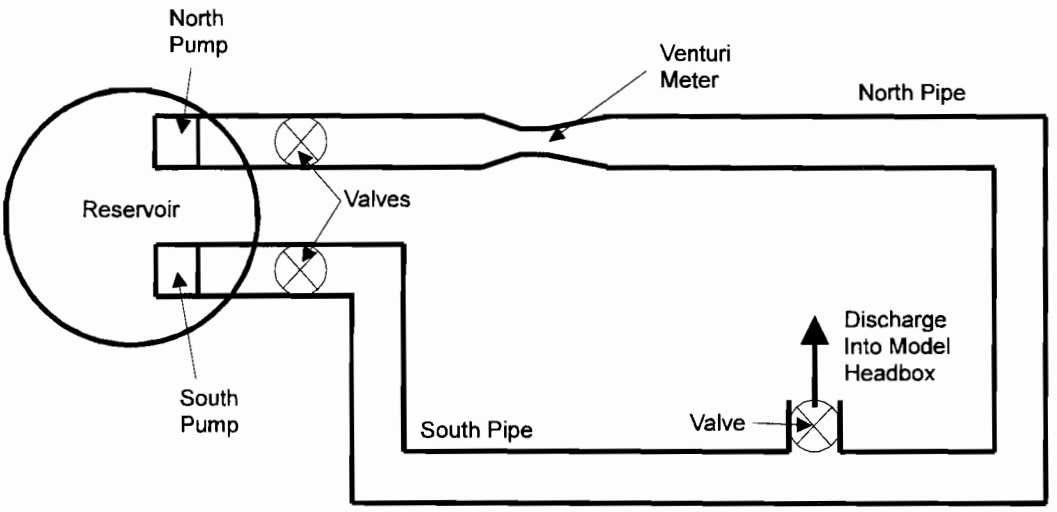

Figure 3.6 Schematic Diagram of Piping System

With both pumps operating in parallel, the total flow is 0.2 m^3/s. (These maximum flow rates are much less than for some other operations in the laboratory because the roadway model is elevated above the laboratory floor. The end of the pipe delivering flow to the model is about 3.7-m above the laboratory floor, thus increasing the heads against which the pumps have to operate.) The discharge into the model is controlled by a 0.305-m diameter butterfly valve just prior to the headbox.

The total flow was measured by either a venturi meter or a 90° V-notch weir. Separate V-notch weirs were used to measure the captured flow and the carryover of each inlet. Both the captured flow weir and carryover weir were designed with interchangeable plates with different notch angles for more precise measurement of a wide range of flow rates. All of the flow measurement devices were calibrated at the start of the project, and the calibrations were checked periodically during the project to ensure accuracy of the flow measurements.

3.6.1 Venturi Meter

Flow from the north pump into the model was measured by a venturi meter in the north line of the system. The north pump was able to produce all but the highest flow rates required

during the model studies. The standard equation for discharge through a venturi meter (Streeter and Wylie, 1985) is

$$Q=\frac{C_d A_2\sqrt{2g\Delta h}}{\sqrt{1-\left(\frac{A_2}{A_1}\right)^2}} \tag{3.6}$$

where Q = discharge, C_d = discharge coefficient, A_1 = area of approach pipe, A_2 = area of venturi meter throat, Δh = difference in piezometric head between the entrance and throat of the venturi meter, and g = acceleration of gravity.

For a given venturi meter, A_1 and A_2 are constants. For a well-made venturi, the discharge coefficient will be constant for throat Reynolds numbers above about $2x10^5$ (Streeter and Wylie, 1985). The pipe Reynolds number (Re) is defined as

$$Re = \frac{VD}{\upsilon} \tag{3.7}$$

where V = mean flow velocity, D = diameter, and υ = kinematic viscosity. Since D and υ are constant (except for small changes in υ due to temperature changes), the discharge coefficient should be constant for all velocities greater than a certain value, or equivalently, for all discharges greater than a certain value.

The venturi meter in the north pipe had an approach diameter of 0.305 m and a throat diameter of 0.152 m. For a venturi meter of this size, the discharge coefficient should be constant for throat velocities greater than 1.5 m/s in the venturi meter throat (0.037 m/s in the 0.305-m approach pipe) or for discharges greater than 0.028 m^3/s. Accordingly, Equation 3.6 can be simplified to

$$Q = K\Delta h^{0.5} \tag{3.8}$$

where

$$K = C_d A_2 \sqrt{\frac{2g}{\left[1 - \left(\frac{A_2}{A_1}\right)^2\right]}} \tag{3.9}$$

K should be constant for discharges greater than 0.028 m^3/s.

The venturi meter was calibrated volumetrically using part of the return floor channel as a volumetric tank. The available volume for calibration was 58.4 m^3. Figure 3.7 shows the calibration data. The piezometric head difference (Δh) was measured with either or both an air-water manometer and a water-mercury manometer. Both manometers were connected to the

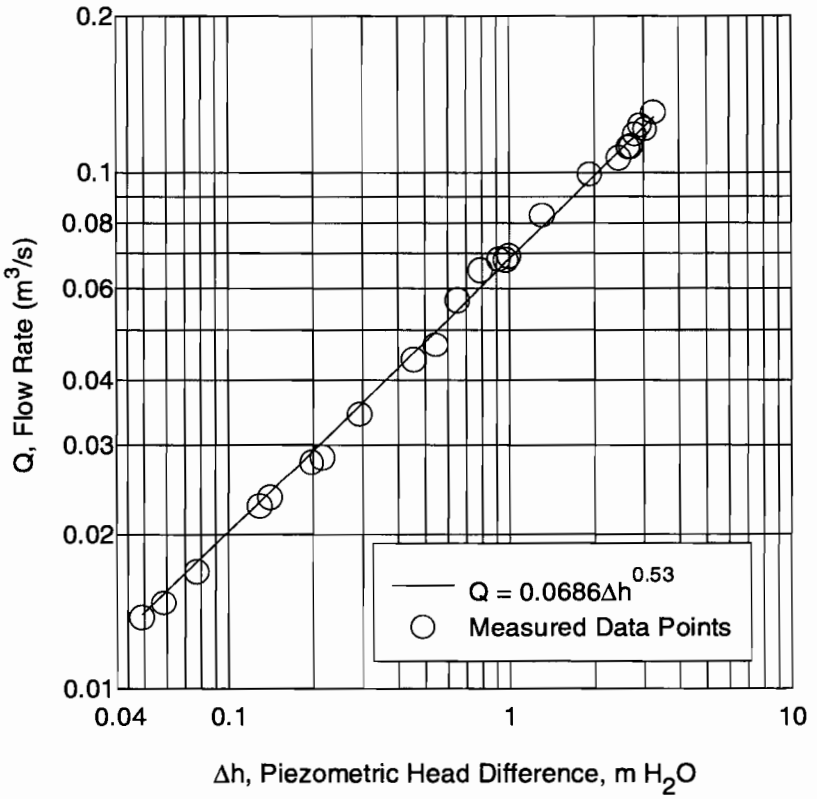

Figure 3.7 Calibration of Venturi Meter

venturi meter at all times. Because the specific gravity of water is much less than that of mercury, the air-water manometer is more accurate for measuring small flow rates than the mercury-water manometer. However, the capacity of the air-water manometer was not great enough to measure all of the flow rates required in this project. Typically, the water-mercury manometer had to be used to measure flow rates greater than about 0.043 m^3/s.

The data obtained from the venturi meter calibration tests did not give an acceptable fit in the form of Equation 3.8. The best curve fit found for the data was

$$Q = 0.0686\,\Delta h^{0.53} \tag{3.10}$$

The least-squares correlation coefficient (R^2) of the line was 0.998, with a standard error of 0.083 cfs. This calibration was continually proved to be reliable and accurate throughout the course of the project.

The fact that the exponent on Δh in the calibration was 0.53 rather than 0.5 as in Equation 3.8 indicates that the discharge coefficient for the venturi meter was not constant over the range of flows for which it was used. The larger exponent for Δh in the calibration equation implies that the discharge coefficient is increasing with increasing Reynolds number, which is typical for venturi meters. Figure 3.8 shows a plot of the discharge coefficient as a function of the venturi meter throat Reynolds number. Although some scatter is apparent in the figure, the data do show a trend of increasing discharge coefficient with increasing venturi throat Reynolds numbers up to a value of $Re = 4x10^5$. For Reynolds numbers greater than $4x10^5$, the average value of the discharge coefficient is 0.842. For a well-streamlined venturi meter, the discharge coefficient should be constant for throat Reynolds numbers greater than $2x10^5$ (Streeter and Wylie, 1985). The fact that the discharge coefficient values for this venturi meter are about 0.84 implies that this venturi meter is not well streamlined.

The overall trend in Figure 3.8 is typical of venturi meters; however, the range of discharge coefficient values obtained in this calibration was considerably lower than is typical for a well-made venturi meter. Typical venturi meter discharge coefficients are between 0.94 and

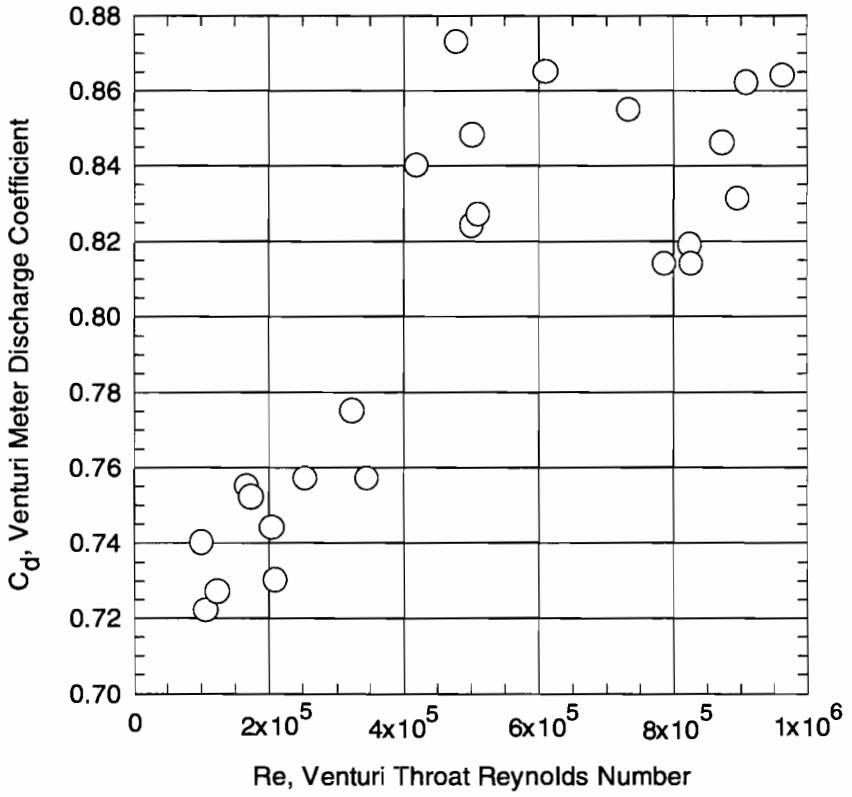

Figure 3.8 Venturi Meter Discharge Coefficient as a Function of Approach Pipe Reynolds Number

0.99 (Streeter and Wylie, 1985). The most probable reason for the lower discharge coefficients obtained in this calibration is that the contraction section of this venturi meter is a normal pipe contraction and is thus not very well streamlined. The discharge coefficients obtained in this calibration are consistent with those obtained in previous calibrations of the same venturi meter (Holley et al., 1992).

3.6.2 V-Notch Weir for Total Flow Rate

The total flow rate into the model was usually measured with the venturi meter. However, the venturi meter was capable of measuring flow from the north pump only. When higher flow rates were required and both pumps were used, the total outflow from the model was measured by a 90° V-notch weir placed outdoors in the return channel to the outside reservoir. The head-discharge equation for a V-notch sharp-crested weir (Bos, 1989) is

$$Q = C_{ev} \frac{8}{15} \sqrt{2g} \tan\left(\frac{\theta}{2}\right) h_1^{2.5} \tag{3.11}$$

where C_{ev} = effective discharge coefficient, θ = angle included between the sides of the notch, and h_1 = head on the weir.

To apply this equation to both fully and partially contracted sharp-crested weirs, it was modified to a form proposed by Kindsvater and Carter (1957), namely

$$Q = C_{ev} \frac{8}{15} \sqrt{2g} \tan\left(\frac{\theta}{2}\right) h_e^{2.5} \tag{3.12}$$

where h_e = effective head on the weir. The effective head is $(h_1 + K_h)$, where K_h represents the combined effects of surface tension and viscosity. Values of K_h have been determined empirically as a function of the notch angle. This particular V-notch weir had a notch angle of 90°, giving a value of K_h of approximately 0.001 m (Bos, 1989).

For water at temperatures between 5°C and 30°C, C_{ev} for a V-notch sharp-crested weir can be a function of the following three variables: h_1/P, P/B and θ. P is defined as the height of the bottom of the weir notch above the invert of the channel in which the weir is placed and B is defined as the width of the approach channel. For this weir, P = 0.305 m, B = 1.52 m, and θ = 90°. The weir functioned as a partially contracted weir over the range of flow rates used in this project. Since P, B, and θ were constants, C_{ev} for this application should be a function of only h_1/P.

In accordance with the guidelines in Bos (1989), measurement of h_1 was made upstream of the weir at a distance of 3 to 4 times the maximum possible value of h_1. A bubbler and a gas-water manometer were used to measure the head upstream of the weir accurately. The source of the gas for the bubbler was bottled oxygen with a constant outlet pressure of almost zero so that the bubbling rate was very low. The low flow rate was to ensure that negligible head loss occurred between the bubbler tip and the manometer.

Calibration tests were conducted to determine Q as a function of h_e and C_{ev} as a function of h_1/P. The calibrated venturi meter was used to determine the flow rate over the V-notch weir, and h_1 was measured as described above. Measured values of Q as a function of h_e are plotted in Figure 3.9. The calibration data did not fit the form of Equation 3.12. The best fit which could be found for the data was

$$Q = 1.28\, h_e^{2.53} \tag{3.13}$$

The least-squares correlation coefficient for this calibration line was $R^2 = 0.998$, with a standard error of 0.0014 m^3/s.

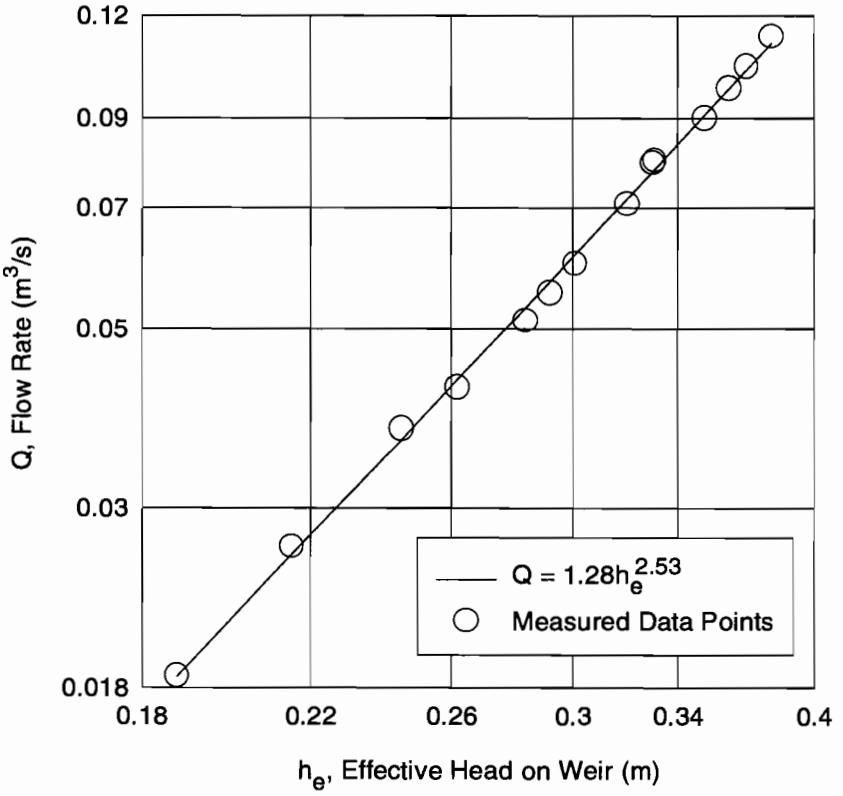

Figure 3.9 Calibration of 90° V-Notch Total Flow Weir

The fact that the exponent on h_e in the calibration equation was 2.53, rather than 2.5 as in Equation 3.12, implies that the discharge coefficient for the weir was not constant, but was

increasing with h_1, or since P is constant, with h_1/P. C_{ev} was calculated from Equation 3.12 and plotted in Figure 3.10 as a function of h_1/P. The mean of the C_{ev} values was 0.52, with a standard deviation of 0.012. In spite of the implication of the calibration equation, the discharge coefficients in Figure 3.10 appear to be randomly scattered. It is unknown why the best-fit line for the data did not fit the form of Equation 3.12, but the calibration was proved to be reliable and accurate throughout the project.

The calculated discharge coefficients for this weir were lower than the range of values presented by Bos (1989) for a partially contracted 90° V-notch weir with a constant P/B value of 0.2. According to Bos, the discharge coefficients should be between 0.58 and 0.60. However,

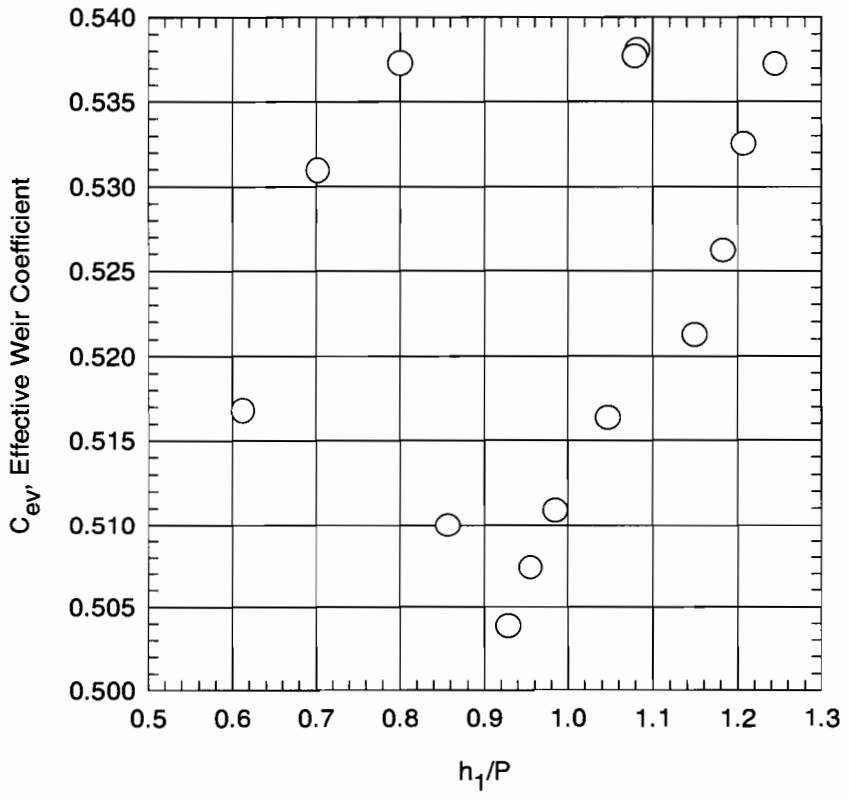

Figure 3.10 Discharge Coefficients for 90° V-Notch Total Flow Weir

these values are for comparison to a supposedly standard weir, and the calibration itself was much more accurate than the comparison with a standard weir.

3.6.3 V-Notch Weirs for the Carryover

A V-notch weir with two interchangeable weir plates was used to measure the carryover flow from inlets on the model. The interchangeable plates allowed the use of different notch angles for different ranges of flow rates. The two notch angles used were 90° and 135°. The 90° notch angle weir was used only for flows less than 0.028 m^3/s. The 90° weir was more accurate for lower flow rates because the smaller notch angle made small changes in flow rate produce greater changes in h_1 compared to the 135° weir.

Equation 3.12 was used to calibrate both weirs. The value of K_h for both weirs was approximately 0.001 m (Bos, 1989). Because θ, P, and B were constants for both weirs, C_{ev} was a function of h_1/P only. A bubbler connected to a gas-water manometer was used for accurate measurement of h_1. Baffles were placed upstream of the measurement section to tranquilize the flow. The calibrated venturi meter was used to measure the flow rate over the weirs. Both weir calibrations were checked periodically throughout the project. The measured flow rates for the weirs always agreed with the venturi meter measurements within 5% after the initial calibration.

3.6.3.1 90° V-Notch Carryover Weir

For the 90° carryover weir, P = 0.372 m and B = 1.68 m. These values classified the weir as partially contracted over the range of flow rates for which it was used. Calibration tests were conducted to determine Q as a function of h_e and C_{ev} as a function of h_1/P. Measured values of Q as a function of h_e are plotted in Figure 3.11. The best-fit equation for the data was

$$Q = 1.19\, h_e^{2.5} \tag{3.14}$$

R^2 for the calibration line was 0.999, with a standard error of 0.00045 m^3/s.

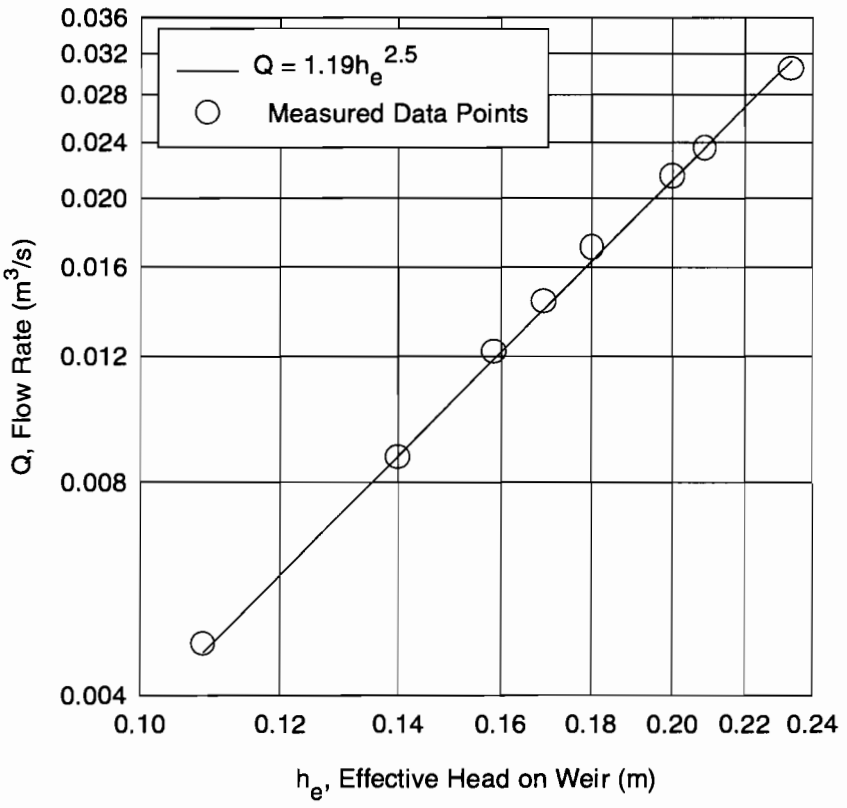

Figure 3.11 Calibration of 90° V-Notch Carryover Weir

Discharge coefficients were calculated from Equation 3.12 and plotted in Figure 3.12 as a function h_1/P. The mean of the calculated discharge coefficients is 0.52, with a standard deviation of 0.011. The discharge coefficients in Figure 3.12 are lower than the range of 0.58 to 0.60 given by Bos (1989) for a partially-contracted 90° V-notch sharp-crested weir with a constant P/B value of 0.22. However, these values are for a supposedly standard weir. The weir calibration shown in Equation 3.14 and Figure 3.11 was continually proved to be accurate and reliable throughout the project.

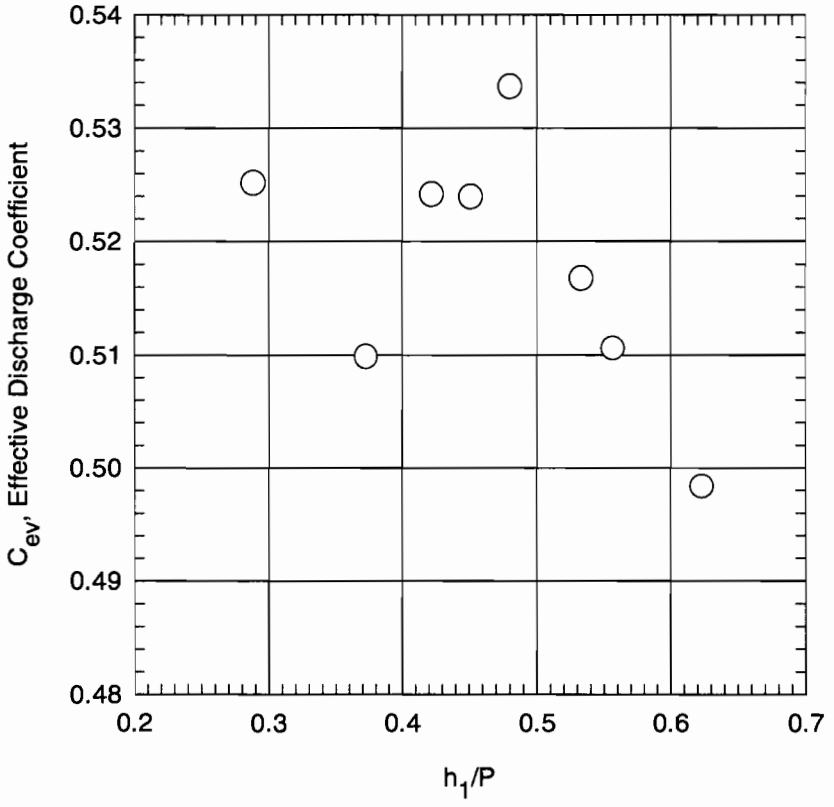

Figure 3.12 Discharge Coefficients for 90° V-Notch Carryover Weir

3.6.3.2 135° V-Notch Carryover Weir

The measurements of the 135° V-notch carryover weir were P = 0.311 m and B = 1.68 m. Calibration tests were performed to determine Q as a function of h_e and C_{ev} as a function of h_1/P. The best-fit equation for the calibration data was

$$Q = 3.04\, h_e^{2.5} \tag{3.15}$$

The calibration line is shown in Figure 3.13. R^2 for this calibration was 0.999, with a standard error of 0.0013 m^3/s.

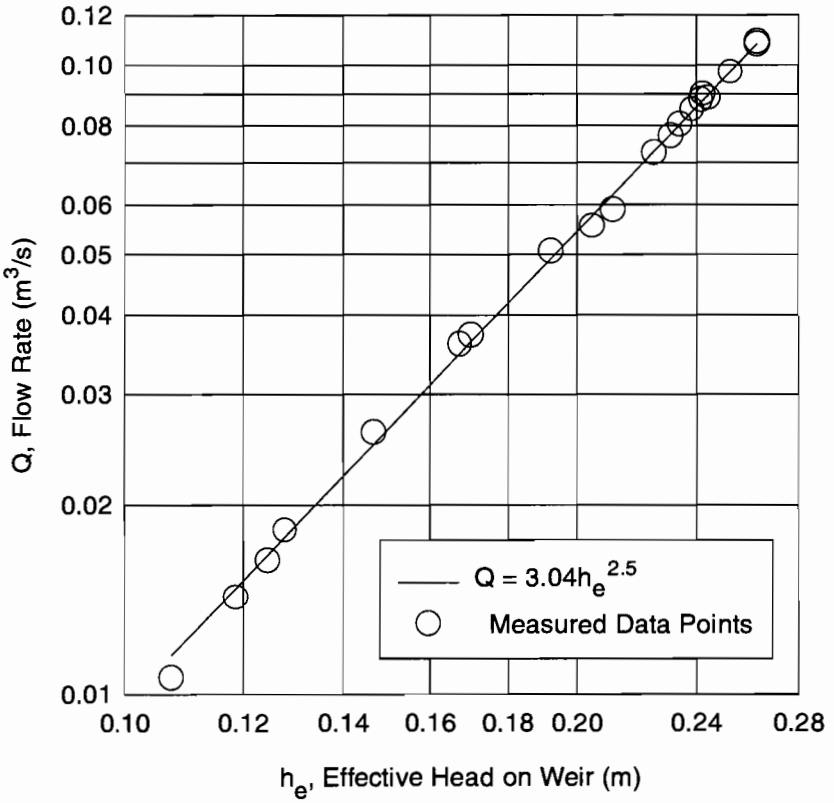

Figure 3.13 Calibration of 135° V-Notch Carryover Weir

Calculated values of C_{ev} are plotted as a function of h_1/P in Figure 3.14. The mean of the calculated discharge coefficients is 0.53, with a standard deviation of 0.016. After a thorough literature search, no data were found for $\theta = 135°$ to compare with these C_{ev} values.

3.6.4 V-Notch Weirs for the Captured Flow

An interchangeable-plate weir similar to the carryover weir was used to measure the flow captured by the inlets. Again, both 90° and 135° V-notch weir plates were available. As for the previous weirs, K_h was approximately 0.001 m, and C_{ev} was a function of h_1/P only. The head on the weir was measured with a gas-water manometer connected to a bubbler, with baffles

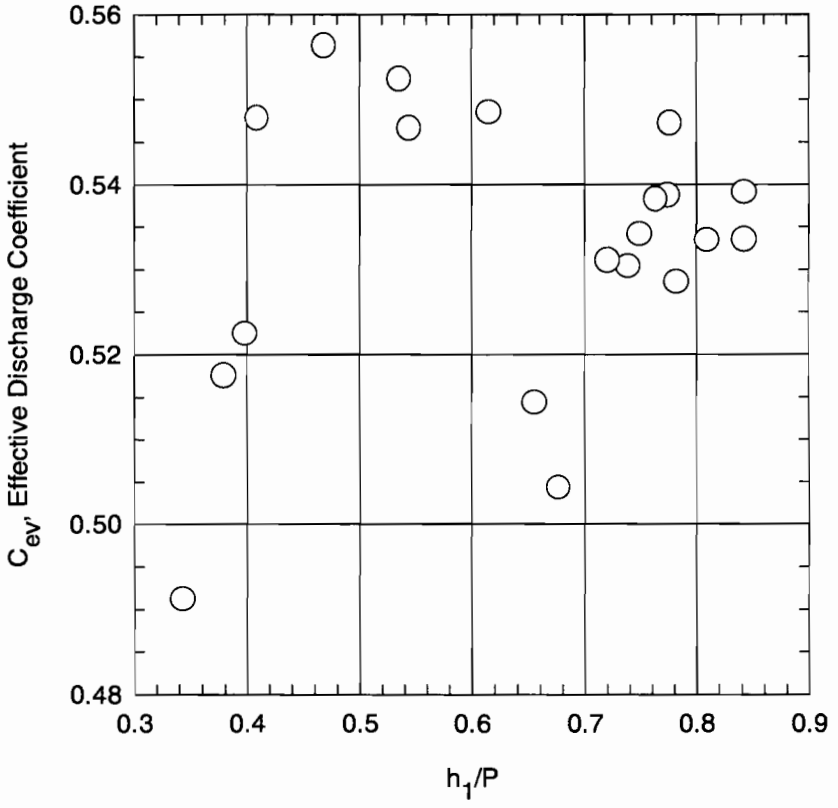

Figure 3.14 Discharge Coefficients for 135° V-Notch Carryover Weir

placed upstream of the measurement section to dampen disturbances in the flow. During calibration, flow rates over the weirs were measured with the venturi meter. The captured-flow weir calibrations were checked periodically throughout the project and were always found to agree with the venturi meter measurements within 5% after the initial calibration.

3.6.4.1 90° V-Notch Captured Flow Weir

The measurements of the 90° V-notch captured flow weir were P = 0.381 m and B = 1.83 m. Experiments were conducted to determine a calibration line for Q as a function of h_e. The best-fit equation for the data was

$$Q = 1.21 h_e^{2.5} - 0.0054 \tag{3.16}$$

for 0.12 m $\leq h_e \leq$ 0.23 m. Q is plotted as a function of h_e in Figure 3.15. The least-squares correlation coefficient for the calibration line was 0.999, with a standard error of only 0.0001 m^3/s.

The discharge coefficients for the calibration experiments are plotted as a function of h_1/P in Figure 3.16. The mean of the discharge coefficients is 0.49, with a standard deviation of 0.017. As with the previous 90° weirs discussed, the discharge coefficients were lower than the typical range for a standard partially contracted 90° V-notch weir.

3.6.4.2 135° V-Notch Captured Flow Weir

For the 135° V-notch captured flow weir, P = 0.302 m and B = 1.83 m. The data from calibration tests on this weir were used to fit an equation for Q as a function of h_1. The best curve fit found for the data was

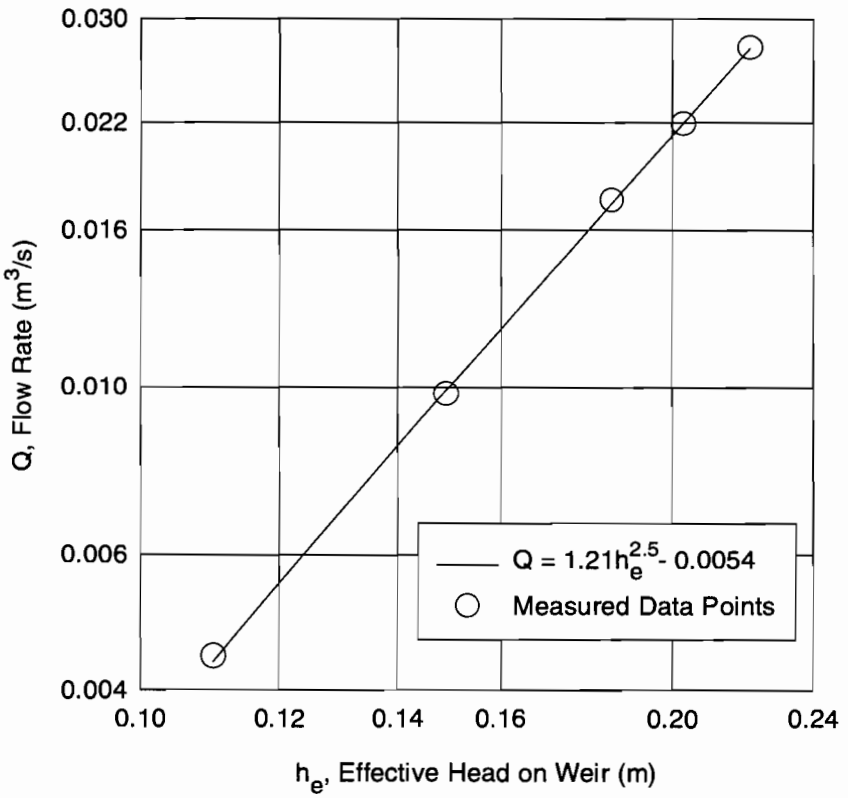

Figure 3.15 Calibration of 90° V-Notch Captured Flow Weir

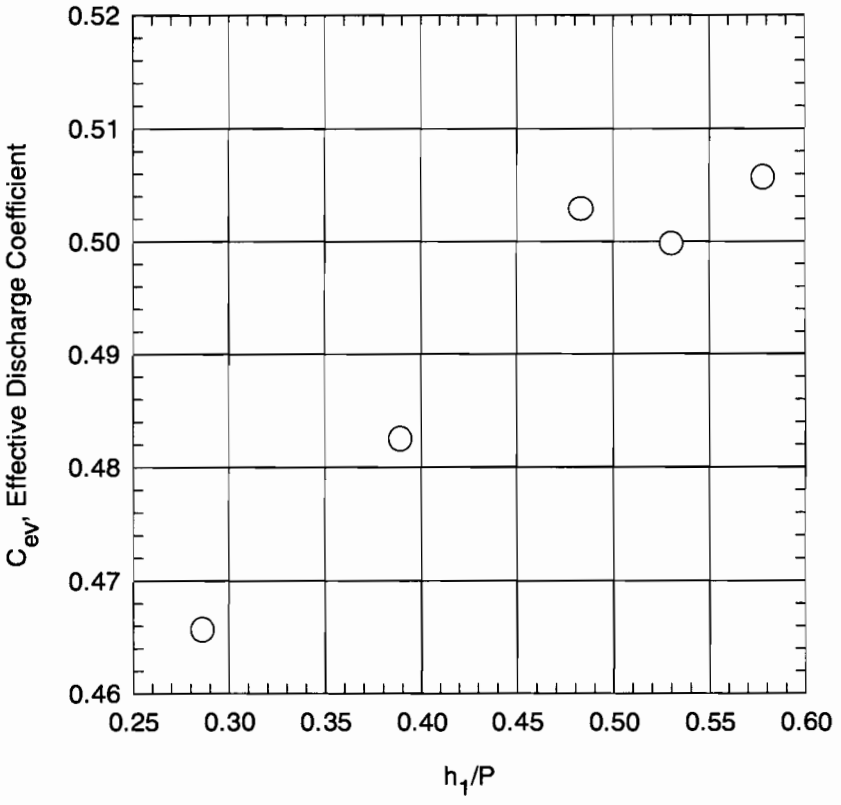

Figure 3.16 Discharge Coefficients for 90° V-Notch Captured Flow Weir

$$Q = 3.74\, h_1^{2.69} \tag{3.17}$$

Because h_1 and h_e differ only by the constant value of K_h, this equation can be expressed equivalently as

$$Q = 3.76\, h_e^{2.70} \tag{3.18}$$

Equation 3.17 was the form of the calibration used during the project. R^2 for the calibration was 0.997, with a standard error of 0.0015 m^3/s. Q is plotted as a function of h_1 in Fig. 3.17.

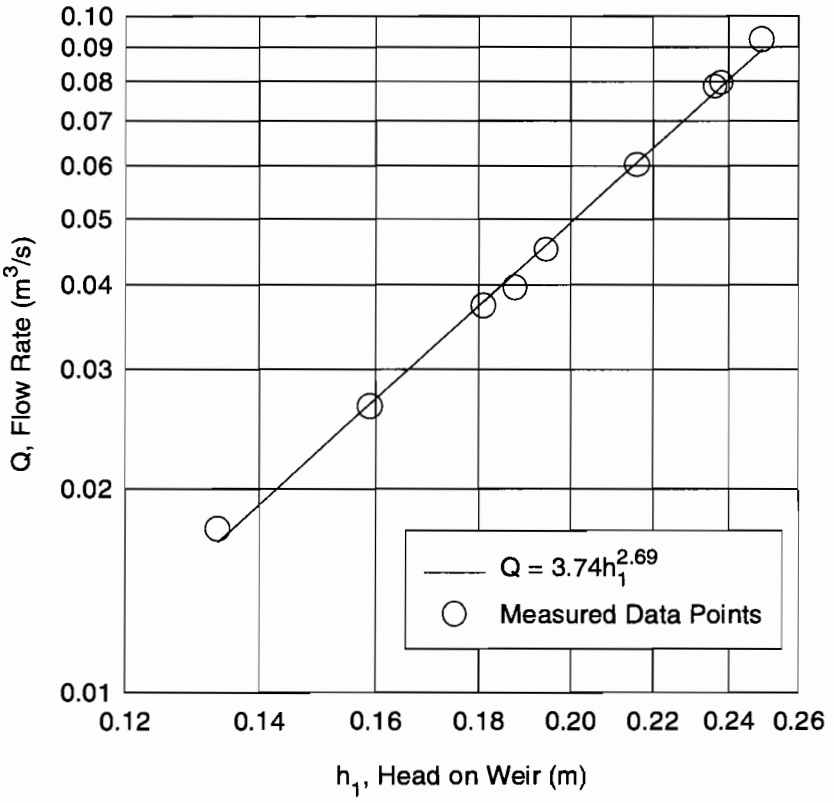

Figure 3.17 Calibration of 135°V-Notch Captured Flow Weir

The exponent on h_e in Equation 3.18 is significantly greater than 2.5 in the standard V-notch weir equation (Equation 3.12). This difference indicates that the weir discharge coefficient is increasing with increasing values of h_1/P. This trend is apparent in Figure 3.18, which is a plot of C_{ev} as a function of h_1/P. The mean of the C_{ev} values is 0.43, with a standard deviation of 0.022.

One possible explanation for the increasing discharge coefficient is that the air pocket beneath the weir nappe was not adequately aerated. The weir nappe constantly entrains air from the air pocket as it flows over the weir. If the water does not spring forth completely from the weir crest and clings to the face of the weir, a vacuum can develop beneath the nappe.

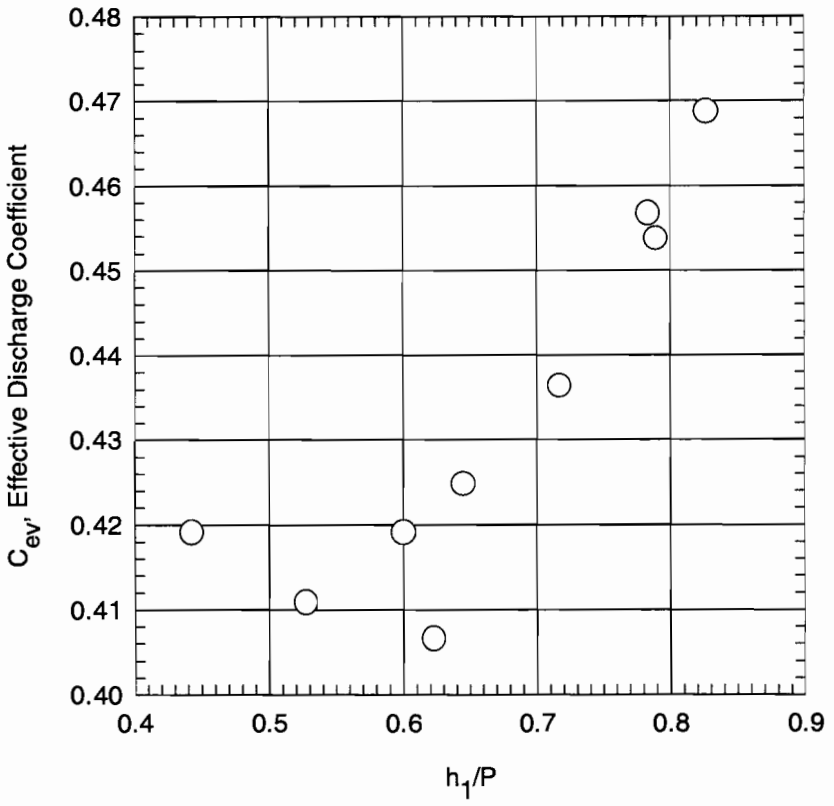

Figure 3.18 Discharge Coefficients for 135° V-Notch Captured Flow Weir

The vacuum causes an additional force which tends to pull the water over the weir, thus increasing the discharge coefficient (Bos, 1989). Although this phenomenon is more common with rectangular-notch weirs, it is believed that the 135° notch angle of this weir is wide enough to cause this behavior. During the calibration and the subsequent inlet tests, water was routinely observed clinging to the face of the weir. To help counteract this effect, a ventilation pipe was installed on the carryover weir, but no ventilation pipe was installed on this captured flow weir. This may explain why the behavior of the 135° V-notch weirs for the carryover and captured flow exhibited substantially different calibrations despite very similar designs.

3.6.5 Water Surface Elevation Measurement

Measurements were made of the water surface elevation in the gutter of the roadway at several cross sections upstream and one downstream of each inlet. For curb inlet tests, the gutter depths just upstream and downstream of the inlet opening were measured. The majority of the water surface elevation measurements were made using point gauges. The water surface elevations just before and after the curb inlet opening were measured by mounting a tape measure to the depressed transition and visually reading the depth on the tape. At times, the water surfaces on the roadway were too rough for direct measurement, so cylindrical stilling wells were used for measuring the depths. A static tube was placed with one of its ends just flush with the inside of the curb so as not to interfere with flow next to the curb. The other end of the static tube was connected to the stilling well just outside the curb on the walkway. With the use of the stilling well, the water depths could be measured more accurately than was possible for the gutter flow itself. The point gauges used for the water surface measurements were graduated at 0.01 ft (0.003 m) intervals, with a vernier calibrated to 0.001 ft (0.0003 m). Typically, water surface elevation measurements were repeatable to a tolerance of $\pm$ 0.001 m.

Two personnel walkways and two instrument carriages were used to span the model. The walkways and the instrument carriages could be moved longitudinally along almost the entire length of the roadway. One carriage was placed upstream of the inlet and the other downstream. A horizontal instrument bar equipped with a linear bearing was mounted on the instrument carriage. A point gauge was mounted on the linear bearing. Since the linear bearing could be moved laterally along the instrument carriage, it was possible to move the point gauge across the full width of the roadway.

Measurement tapes were mounted on the curbs so that the point gauge carriage could be accurately positioned along the roadway. Another tape was placed along the instrument bar so that the point gauge could be accurately positioned laterally.

4. EXPERIMENTAL RESULTS FOR FLUSH DEPRESSED CURB INLETS

The primary objectives of the experimental work on curb inlets were to determine if backwater effects existed for the inlets due to the close proximity of the inlet lip and the back of the inlet box and to develop a design discharge relationship for the inlets. The results of the experiments are presented in this chapter. As discussed in Section 4.3.2, the experimental results led to a broader investigation of the design relationships to be used for these inlets. Backwater effects are discussed in Section 4.3.1. For the discharge relationship, Izzard's method for the design of depressed curb inlets was modified with an empirical equation for the 100% efficiency capacity of the inlets using the effective inlet length concept. The design approach is developed and presented in Section 4.3.2.

4.1 GEOMETRY AND DESCRIPTION

Two types of TxDOT flush depressed curb inlets were tested. The inlets were designated by TxDOT as Type C and Type D inlets. The only difference between Type C and Type D inlets is the depth of the depressed section; Type C inlets have a 0.10-m depression while Type D inlets have a 0.076-m depression. Figure 4.1 shows plan and perspective views of typical Type C and Type D inlets. The inlets consist of a depressed section and inlet opening 1.52, 3.05, or 4.57 m long, with upstream and downstream depression transitions 1.52 m long. The transition sections change gradually from the undepressed gutter into the fully depressed inlet section over their 1.52 m length. The flow captured by the inlet spills over the inlet lip into an inlet box where it enters the storm sewer system. Figure C.4 in Appendix C is a photograph of a field installation of a 4.57-m Type D curb inlet.

Type C and Type D inlets are unique because of the relatively short distance from the inlet lip to the back wall of the inlet box. For Type C and Type D inlets, this distance is only 0.15 m, while for most other types of curb inlets, the distance is 0.457 to 0.610 m. Consequently, it was believed that a backwater effect might be caused by the water flowing over the inlet lip

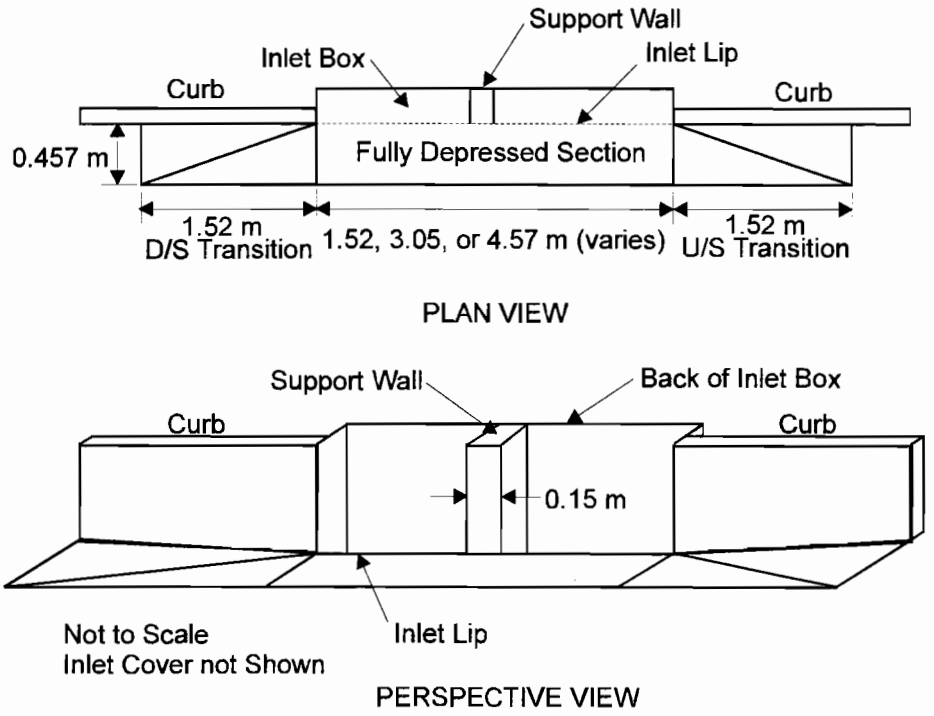

Figure 4.1 TxDOT Type C and Type D Flush Depressed Curb Inlets

and striking the back of the inlet box. If this backwater effect existed, it could reduce the capacity of the inlet and cause water to back out into the street, creating a potentially hazardous situation for traffic

For inlet lengths longer than 1.52 m, support walls 0.15 m long in the direction of flow are installed between the inlet lip and the back of the inlet box at 1.52 m intervals. The support walls effectively divide longer inlet lengths into successive 1.52 m openings. For example, 4.57-m inlets have two support walls, effectively creating three successive 1.52 m openings.

The cross-section view of Type C and Type D curb inlets shown in Figure 4.2 illustrates the conventions used by TxDOT for the definitions of two key variables in the hydraulics of depressed curb inlets: a, the depth of depressed section, and W, the width of the depressed section. For TxDOT curb inlets, the depth of depression is measured not at the inlet lip, but at

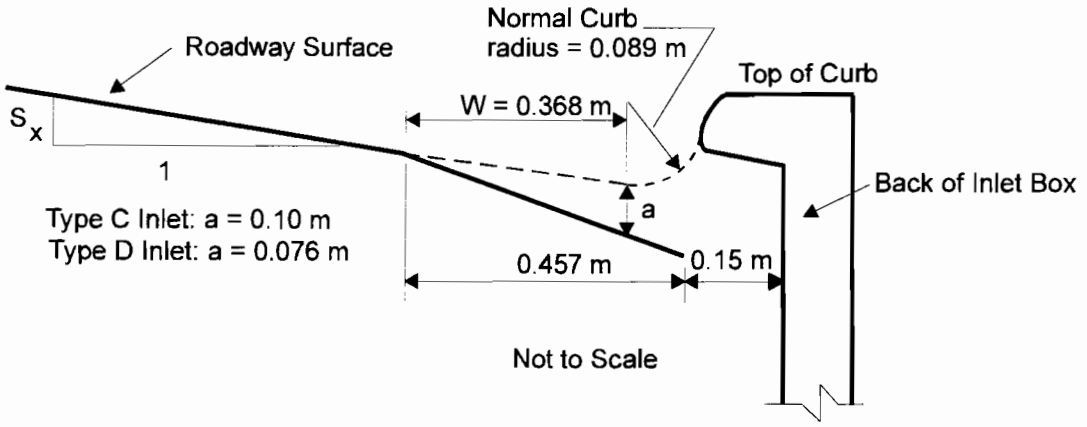

Figure 4.2 Cross-Section View of TxDOT Type C and Type D Inlets

the point where the radius at the bottom of the normal curb face would start (Figure 4.2). Consequently, the width of the depressed section is taken not as the entire distance from the beginning of the depression to the inlet lip, but as the distance from the beginning of the depression to the point at which the depression is measured. So, W was taken as 0.368 m for both Type C and Type D curb inlets.

The inlets were tested at 3/4 scale in the model described in Chapter 3. All dimensions and values are for the prototype unless specifically stated otherwise. The inlets were constructed of plywood and were textured using fiberglass and sand grains in the same manner described in Section 3.5 for the roadway model. The inlets were installed in a cutaway section on the right-hand side of the model (Figure 4.3). Modular construction was used for the inlets to allow the inlet opening length to be changed easily. The inlets consisted of two 1.52-m long depression transitions (upstream and downstream) and up to three 1.52-m long depressed inlet sections. To change the length of inlet opening, the downstream depression transition was moved to its new location and inlet sections were either added or removed to create the desired inlet length. The upstream depression transition was never moved, so the distance from the model headbox to the beginning of the inlet was always the same (8.69 m in the model). In addition to the inlet pieces, undepressed sections with curbs were used to fill in the cutaway section for inlet lengths

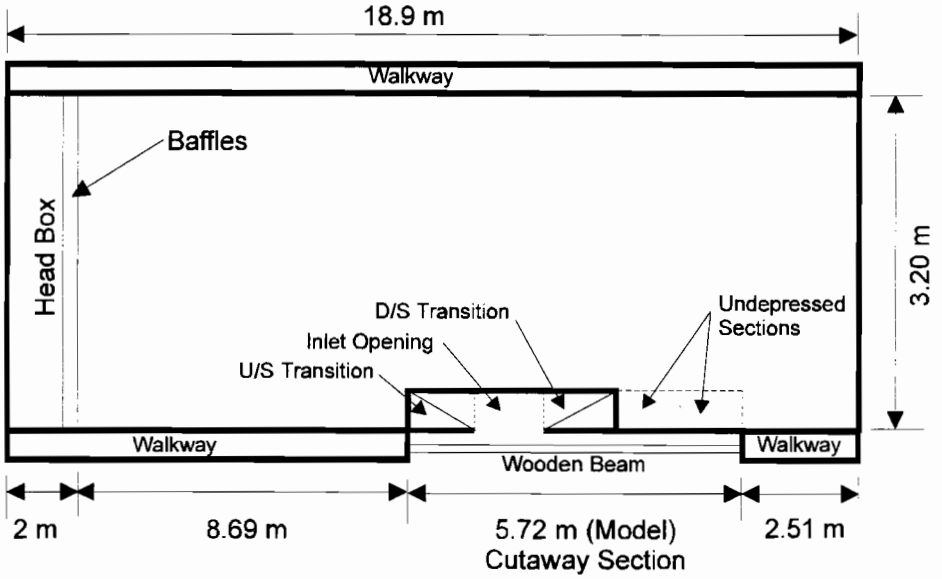

Figure 4.3 Plan View of Model Illustrating Modular Curb Inlet Construction

less than 4.57 m. The back of the inlet box was simulated by mounting a piece of plywood to a wooden beam which spanned the entire length of the cutaway section. Figure 4.3 shows a typical model curb inlet installation with an inlet opening of 1.52 m. The total 1.52 m inlet consists of one inlet section along with the upstream and downstream transition sections.

As discussed in Section 4.3.2, the preliminary analysis of the experimental data from Type C and Type D curb inlets revealed that experimental data from flush undepressed curb inlets were necessary for comparison and for verification of the theory applied to the depressed inlets. To create the undepressed inlets, 0.0095-m thick steel plates were fabricated to fit inside the depressed sections and the depression transitions for the existing modular depressed inlet sections. The plates were supported in the depressed part of the inlet section by wooden blocks. The metal was textured with fiberglass and sand grains using a technique similar to that used for the depressed inlet sections and for the model roadway surface, except no fiberglass mat was applied. Visually and tactually, the steel plates seemed to have the same roughness as the roadway surface. The undepressed inlets created in this manner are designated Type O curb inlets in this report.

4.2 PROCEDURES

One hundred twenty-six tests were conducted on flush curb inlets in the model described in Chapter 3; 52 tests were conducted on Type C inlets, 35 on Type D inlets, and 39 on Type O inlets. For all inlet types, tests were performed at both 100% efficiency and less than 100% efficiency for 1.52-m to 4.57-m inlet openings. These inlet lengths were chosen to represent the extremes of inlet lengths likely to be encountered in practice. The longitudinal slopes used for the inlet tests were 0.004, 0.01, 0.02, 0.04, and 0.06. These slopes were chosen to represent the range of longitudinal slopes allowed by TxDOT. The transverse slopes were 0.0208 (1:48) and 0.0417 (1:24), which are respectively the minimum and maximum transverse slopes allowed by TxDOT.

The procedures used for the tests were as follows:

1. The model was set at the desired longitudinal and transverse slopes.
2. A constant approach flow rate was established into the upstream end of the model. Because the inlets were tested at 3/4 scale, the flow rate from the north pump was sufficient for all tests. Therefore, the venturi meter was used to measure the approach flow rate for all tests. For 100% efficiency tests, the flow rate was adjusted such that the inlet was capturing all of the approach flow except for a very small amount of carryover. This procedure was necessary to ensure that the limit of the inlet's capacity had been reached.
3. The flow depth and ponded width were measured upstream of the inlet. The flow depths were measured with a point gage at two cross-sections where stilling wells were installed. These depth measurements were used to determine if the flow reached uniform depth upstream of the inlet. Also, the flow depths just upstream and downstream of the inlet opening were measured using a measuring tape mounted to the curb face.
4. When the flow over the V-notch weirs reached a steady condition, the captured flow and the carryover flow were measured.

The experimental data for the curb inlet tests are found in Tables B.1-B.3 of Appendix B. A photograph of a typical less than 100% efficiency test is shown in Figure C.5 in Appendix C.

4.3 RESULTS AND ANALYSIS

4.3.1 Backwater Effects

As mentioned in Section 4.1, one of the primary objectives of the curb inlet research performed in this project was to determine if the close proximity of the back wall of the inlet box to the inlet lip of Type C and Type D curb inlets caused a backwater effect which diminished the flow rate captured by the inlet. After performing a few initial experiments to establish the general characteristics of the flow into the inlets, it was apparent that visual observation of the flow conditions during the inlet tests would be sufficient to determine if backwater effects were present. Then, if backwater effects were observed, their influence could be quantified by performing tests with the back of the inlet box removed.

Observation of the flow conditions for the inlet tests revealed that backwater effects did not exist for these inlets. The flow entering the inlet was supercritical for practically all of the inlet tests. Because the flow was supercritical, disturbances occurring in the inlet box could not be transmitted upstream in the flow and out into the street without drowning the supercritical flow and changing it to subcritical. The presence of the upstream transition section and the depressed gutter helped to create supercritical flow into the inlet even for subcritical approach flows.

Usually, the captured flow striking the back of the inlet box created a small roller (up to about 0.1 m in size). The water in the roller simply fell back into the flow passing through the inlet opening and was captured. Of course, increasing the velocity and the amount of flow captured by the inlet increased the size of the roller. Therefore, the roller was more pronounced for higher approach flow rates and steeper transverse slopes, but never became large enough to splash out of the inlet and cause a disturbance in the street flow for any of the flow conditions tested in this project.

Disturbances were also caused by flow striking the downstream end of the inlet box and the 0.15-m support walls installed for inlet lengths longer than 1.52 m (see Figure 4.1). The majority of the part of the flow which struck the downstream end of the inlet box or the support wall was diverted down into the inlet box and was captured. The rest of this part of the flow

splashed out into the gutter flow and was carried past the inlet. For higher flow rates with high velocity (higher longitudinal slopes), splashes 0.15 m to 0.20 m tall were common. However, the amount of flow involved in the splashing, especially the part coming back out of the inlet, was insignificant compared to both the flow captured by the inlet and the carryover flow. Furthermore, this phenomenon would be present for any type of flush curb inlet and would not be limited to the TxDOT curb inlets tested in this project. Also, the presence of a cover on the inlet box (which is installed in the field but was not included in these model studies to aid in observing the flow) would likely curtail the splashing. Figure C.6 in Appendix C is a photograph of a less than 100% efficiency test conducted on a 1.52-m inlet and illustrates the splashing which occurred at the downstream end of the inlet.

For tests performed at less than 100% efficiency with supercritical flow, an oblique standing wave extending into the roadway originated at the downstream end of the inlet opening. The presence of this standing wave has been noted by other researchers, and some have experimented with different geometries at the downstream end of the inlet to help reduce or prevent the occurrence of the wave. These attempts had little success (Hotchkiss et al., 1991). Therefore, the presence of this standing wave is not limited to the TxDOT inlets tested in this research project and does not represent an unusual design problem.

No backwater effects were observed for any of the tests performed on TxDOT Type C and Type D curb inlets. Therefore, no tests were performed with the back of the inlet box removed.

4.3.2 Discharge Capacity

Once it had been established that backwater effects did not exist for the TxDOT inlets, the remainder of the experimental investigation focused on developing design information for the inlets. The data collected from the curb inlet experiments are presented in Tables B.1-B.3 in Appendix B. All of the curb inlet data analysis was performed with Microsoft Excel, including the development of all regression equations. A photograph of a typical less than 100% efficiency test conducted on a 4.57-m inlet is shown in Figure C.5 in Appendix C.

4.3.2.1 Comparison with Izzard's Equations for Depressed Curb Inlets

Since Izzard's (1950) curb inlet equations are used by TxDOT for curb inlet design, the experimental data were compared with the predictions of Izzard's equations. Figure 4.4 shows a comparison of the experimental data for the 100% efficiency tests conducted on Type C and Type D inlets with the predictions of Izzard's 100% efficiency equation for depressed curb inlets

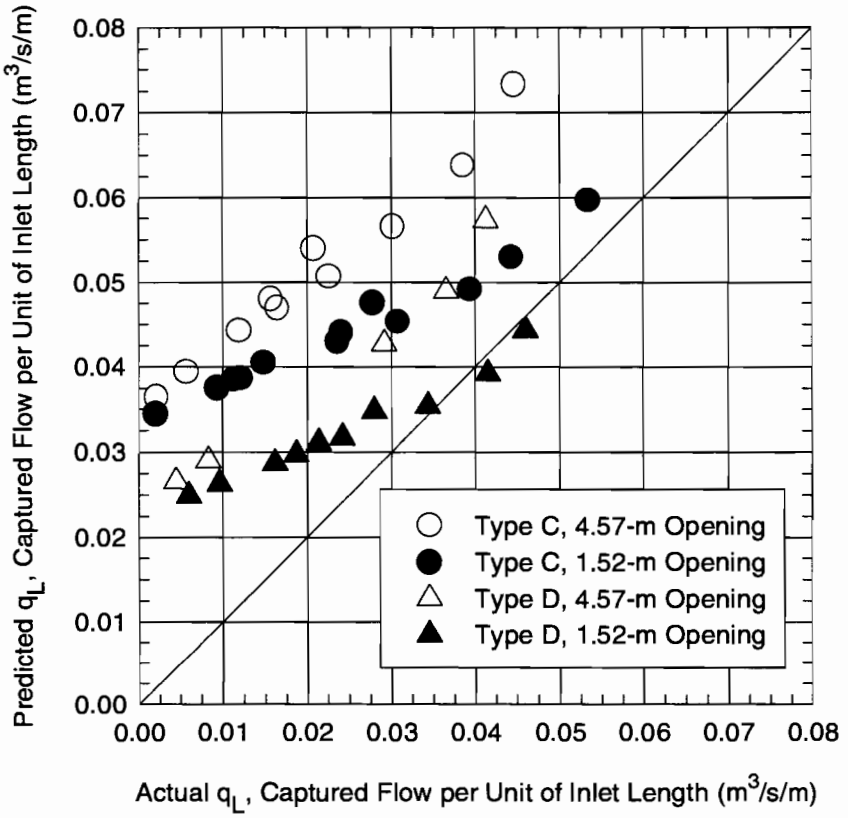

Figure 4.4 Comparison of Izzard's 100% Efficiency Equation for Depressed Curb Inlets (Equation 4.1) with Experimental Data for Type C and Type D Curb Inlets

(Equation 2.21). Figure 4.4 introduces the convention used in this chapter for symbols in the figures pertaining to curb inlets. In all curb inlet figures, hollow symbols denote 4.57-m inlet openings, while filled symbols denote 1.52-m inlet openings. The different inlet types are

distinguished by symbols of different shapes. Equation 2.21 was rearranged to give the following expression for q_L, the flow captured by the inlet per unit of inlet length:

$$q_L = \frac{0.39}{y_n}\left[(a + y_n)^{5/2} - a^{5/2}\right] \tag{4.1}$$

Use of the parameter q_L is a convenient way to compare the 100% capacity of inlets of different lengths.

Figure 4.4 shows that, in general, Izzard's equation overestimates the 100% efficiency capacity of Type C and Type D inlets. The data show that the predictions are less accurate for Type C inlets than for Type D inlets, and also that the predictions are less accurate for 4.57-m inlet lengths than for 1.52-m inlet lengths. These trends imply that the accuracy of the predictions of Izzard's equation decreases with increasing inlet depression and also with increasing inlet length.

The next step in the analysis of the experimental data was the comparison of the data from the less than 100% efficiency tests with Izzard's equation for the less than 100% efficiency capacity of depressed curb inlets (Equation 2.22). The use of Equation 2.22 requires the use of Equation 4.1 to predict the inlet length required to capture 100% of the approach flow (L_r). However, Equation 4.1 had already been proved inadequate for Type C and Type D curb inlets by the comparison with experimental data shown in Figure 4.4. Figure 4.5 shows the comparison of the experimental data from the less than 100% efficiency tests on Type C and Type D curb inlets with the predictions of Equation 2.22, using Equation 4.1 to calculate L_r.

Figure 4.5 shows that Equation 2.22 gave acceptable results for the 1.52-m lengths of Type C and Type D inlets even when Equation 4.1 was used to calculate L_r, but overestimated the capacity of 4.57-m inlet lengths of both Type C and Type D inlets. The combination of the trends of the data in Figures 4.4 and 4.5 led to the hypothesis that Equation 2.18 is a reasonably accurate predictor of the less than 100% efficiency capacity of Type C and Type D curb inlets, as long as a reasonable estimate of L_r is available to use in Equation 2.22. That is, the inlet

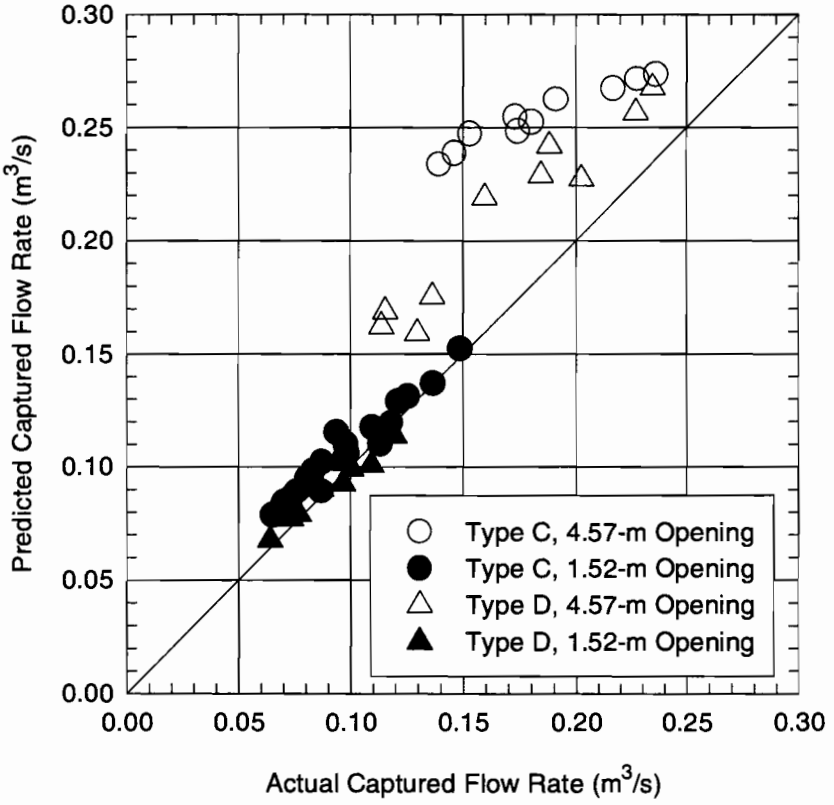

Figure 4.5 Comparison of Izzard's Less than 100% Efficiency Equation for Depressed Curb Inlets (Equation 2.22, Using Equation 4.1 to Calculate L_r) with Experimental Data for Type C and Type D Curb Inlets

configurations which showed the best (though not necessarily acceptable) agreement with Equation 4.1 (1.52-m lengths of Type C and Type D inlets) also showed the best agreement with Equation 2.22.

4.3.2.2 Development of Empirical 100% Efficiency Equations

To test the hypothesis that Equation 2.22 is a good predictor of the less than 100% efficiency performance of Type C and Type D inlets, an empirical equation was sought which would provide more accurate predictions for the 100% efficiency capacity of the inlets than did Equation 4.1. Then the new empirical equation could be used to calculate L_r for use in Equation 2.22 for comparison with experimental data.

In searching for the best empirical equation for the 100% efficiency capacity of Type C and Type D inlets, it was discovered that there was a linear relationship between y_n and q_L for the 100% efficiency data for each inlet length, with insignificant segregation according to the inlet type. Figure 4.6 is a plot of q_L as a function of y_n for the 100% efficiency data. As shown in the figure, there are two separate trends of the data according to the inlet length. Therefore, it was possible to fit two separate linear equations to the data, one for 4.57-m inlet openings and one for 1.52-m inlet openings. The equation developed for 4.57-m openings was

$$q_L = 0.341y_n - 0.0051 \tag{4.2}$$

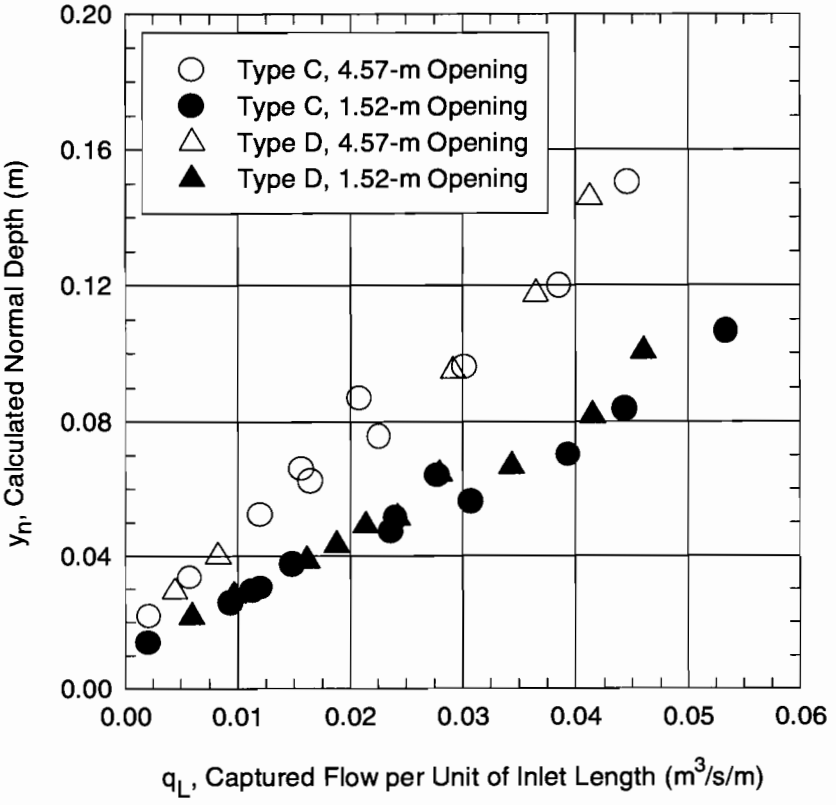

Figure 4.6 Trends of Data from 100% Efficiency Tests Performed on Type C and Type D Inlets

for 0.02 m ≤ y_n ≤ 0.15 m. Equation 4.2 had a correlation coefficient (R^2) of 0.98 and a standard error of 0.0019 $m^3/s/m$. Figure 4.7 shows a comparison of Equation 4.2 with the experimental data for Type C and Type D inlets with 4.57-m openings. The equation developed for 1.52-m inlet openings was

$$q_L = 0.558y_n - 0.0049 \tag{4.3}$$

for 0.015 m ≤ y_n ≤ 0.11 m. The correlation coefficient for Equation 4.3 was 0.97 and the standard error was 0.0023 $m^3/s/m$. A comparison of Equation 4.3 with experimental data for Type C and Type D inlets with 1.52-m openings is shown in Figure 4.8.

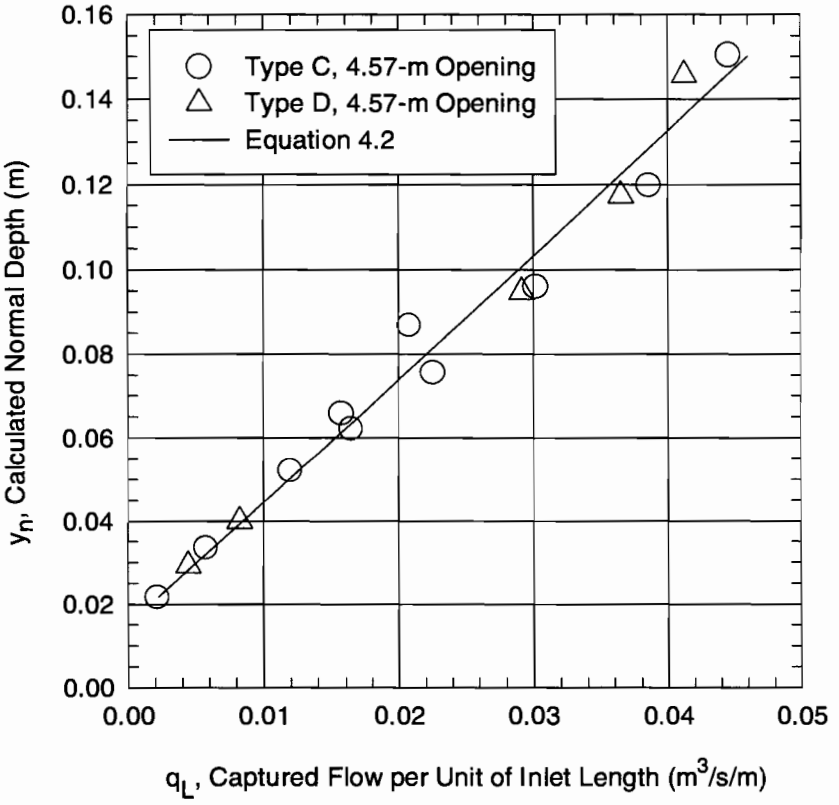

Figure 4.7 Comparison of Equation 4.2 with Experimental Data from 100% Efficiency Tests Performed on 15-ft Lengths of Type C and Type D Curb Inlets

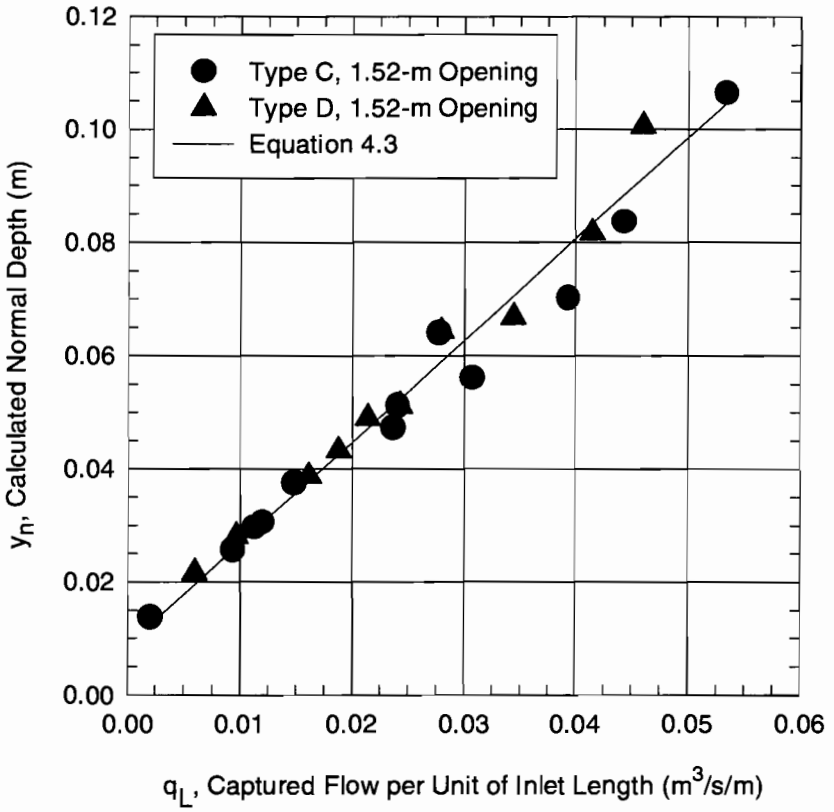

Figure 4.8 Comparison of Equation 4.3 with Experimental Data from 100% Efficiency Tests Performed on 5-ft Lengths of Type C and Type D Curb Inlets

Figure 4.9 shows a comparison of the predictions of Equations 4.2 and 4.3 with experimental data for the 100% efficiency tests on Type C and Type D inlets. The figure illustrates the good agreement between the experimental data and Equations 4.2 and 4.3.

The next step in the analysis of the experimental data was to compare the data from the less than 100% efficiency tests with the predictions of Equation 2.22, using Equations 4.2 and 4.3 to calculate L_r. Figure 4.10 shows this comparison. Although there is obvious segregation for different inlet types because of different ranges of Q/Q_a, the agreement is much better than that shown in Figure 4.5, in which Equation 4.1 was used to calculate L_r. The figure implies that Equation 2.22 is adequate for design purposes, provided that a good estimate of L_r is used in the equation.

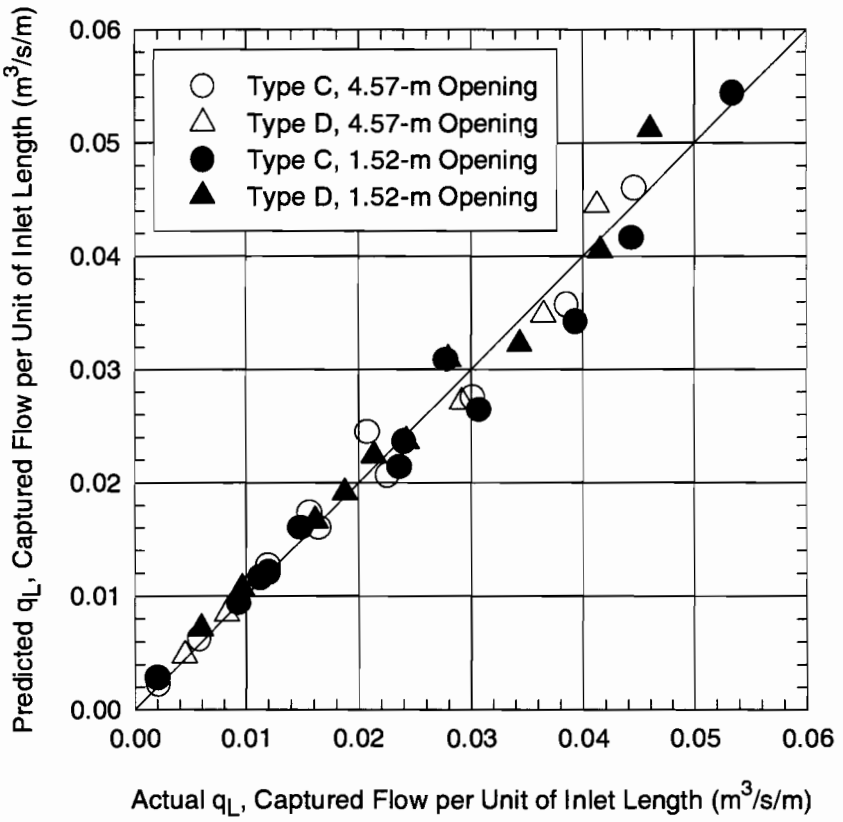

Figure 4.9 Comparison of Equations 4.2 and 4.3 with Experimental Data from 100% Efficiency Tests Performed on Type C and Type D Inlets

Equations 4.2 and 4.3 can be used to predict the 100% efficiency capacity of Type C and Type D curb inlets with 1.52 m and 4.57 m lengths, and Equation 2.22 can be used along with Equations 4.2 and 4.3 to predict the less than 100% efficiency capacity of Type C and Type D curb inlets with 1.52 m and 4.57 m lengths with acceptable accuracy. However, the applicability of this method is severely limited by the requirement of different empirical 100% efficiency equations for each inlet length. Therefore, it was desired to improve the method by developing one 100% efficiency equation which would be applicable for a range of inlet openings.

4.3.2.3 Development of Empirical 100% Efficiency Equation Using the Effective Length Concept

To develop a general equation for the 100% efficiency capacity of the inlets, the use of the effective length concept was explored. The basic premise of the effective length concept is

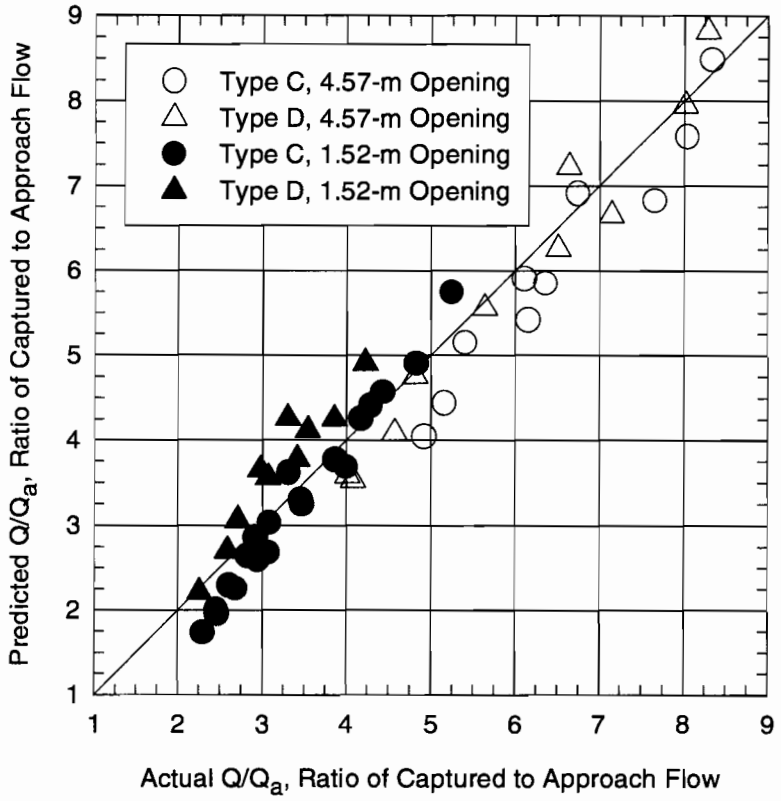

Figure 4.10 Comparison of Izzard's Less than 100% Efficiency Equation for Depressed Curb Inlets (Equation 2.22, Using Equations 4.2 and 4.3 to Calculate L_r) with Experimental Data for Type C and Type D Curb Inlets

that the net effect of the depressed inlet section and the upstream and downstream depression transitions is to make the inlet behave hydraulically as if its length were greater than its physical length. The physical meaning of the effective length is that the upstream transition causes more water to be drawn into the depressed section and eventually over the inlet lip, thus behaving as if it were part of the inlet opening. Similarly, because the downstream depression transition has an adverse slope (depending on the longitudinal slope of the roadway), the water that flows into the downstream depression transition can actually turn around and flow back upstream and into the inlet opening to contribute to the 100% efficiency. Thus, since the presence of the upstream and downstream depression transitions can cause more water to be captured than would be otherwise, the depression transitions behave hydraulically as if they were part of the inlet opening,

increasing the opening's effective length. This concept was used by Holley et al. (1992) to describe the effect of the transition sections on recessed curb inlets (see Section 2.1.4.7).

The application of the effective length concept is apparent in Figure 4.6. Since $q_L = Q/L$ where L = 1.52 m or 4.57 m for Figure 4.6, and both trends of data seem to have a common y-intercept, there is an additional length which could be added to the inlet length L which would collapse the two lines of data into one line. Conceptually, this additional length is the effective length contributed by the presence of the upstream and downstream depression transitions. In order to calculate the effective length, q_L was expressed as $q_L = Q/(L + L_a)$, where L_a = the additional effective length of the inlet contributed by the depression transitions. The total effective length of the inlet (L_{eff}) is $L + L_a$. The equations developed for the data in Figure 4.6 (Equations 4.2 and 4.3) were set equal to each other to be solved for the value of L_a. However, it was not possible to solve the resulting expression algebraically due to the presence of the constants corresponding to the y-intercepts in Equations 4.2 and 4.3. Therefore, new regression equations for the data were developed in which the y-intercept was constrained to be zero. For the 4.57-m inlet length, the following equation analogous to Equation 4.2 was developed:

$$q_L = \frac{Q}{L + L_a} = 0.289 y_n$$
$$Q = 0.289 y_n (L + L_a) \tag{4.4}$$

Of course, Equation 4.4 is not as statistically good as Equation 4.2; the correlation coefficient of Equation 4.4 was 0.95 with a standard error of 0.0032 $m^3/s/m$. Similarly, the following equation was developed for 1.52-m inlet lengths:

$$q_L = \frac{Q}{L + L_a} = 0.482 y_n$$
$$Q = 0.482 y_n (L + L_a) \tag{4.5}$$

Equation 4.5 also had a correlation coefficient of 0.95 with a standard error of 0.0032 $m^3/s/m$. The inlet lengths (L) in Equation 4.4 and Equation 4.5 are 4.57 m and 1.52 m, respectively.

Equations 4.4 and 4.5 were set equal to each other and solved for L_a, revealing that L_a = 3.05 m. Therefore, the 1.52-m and 4.57-m length inlets behaved hydraulically like 4.57-m and 7.62-m inlets, respectively. The fact that L_a = 3.05 m is significant because the total length of transition section was 3.05 m (1.52 m upstream + 1.52 m downstream), which implies that the inlet behaves hydraulically as if the entire lengths of the upstream and downstream depression transitions were part of the inlet opening.

For 100% efficiency, water that flows over any outer edge of the depression will be captured since all parts of the depression slope toward the curb opening for Type C inlets when $S \leq 0.08$ and for Type D inlets when $S \leq 0.06$. For these conditions, the amount of flow captured for 100% efficiency is thus the same for both types of inlets even though they have different depressions. On the other hand, it must be emphasized that the downstream depression transition can be effective for 100% efficiency conditions only for $S \leq 0.08$ for Type C inlets and $S \leq 0.06$ for Type D inlets because the slope of the downstream transition is no longer toward the curb opening at longitudinal slopes greater than these limiting values. Therefore, the value of L_a for the inlets at longitudinal slopes greater than the limiting values would be less than 3.05 m, but no experiments were conducted for either type inlet for $S > 0.06$.

Next, an empirical equation was developed for the flow captured per unit of effective length; this equation is the 100% efficiency equation for the inlets on the basis of their effective lengths. Figure 4.11 shows a plot of flow captured per unit of effective length as a function of the calculated normal depth. The regression equation developed for the 100% efficiency capacity of the inlets on an effective length basis is

$$q_{L,eff} = \frac{Q}{L_{r,eff}} = 0.196y_n - 0.0023 \qquad (4.6)$$

where $q_{L,eff}$ = captured flow per unit of effective inlet length and $L_{r,eff}$ = effective inlet length required to capture 100% of the approach flow rate. The correlation coefficient for Equation 4.6 is 0.98, with a standard error of 0.001 $m^3/s/m$. The standard error of Equation 4.6 is less than the

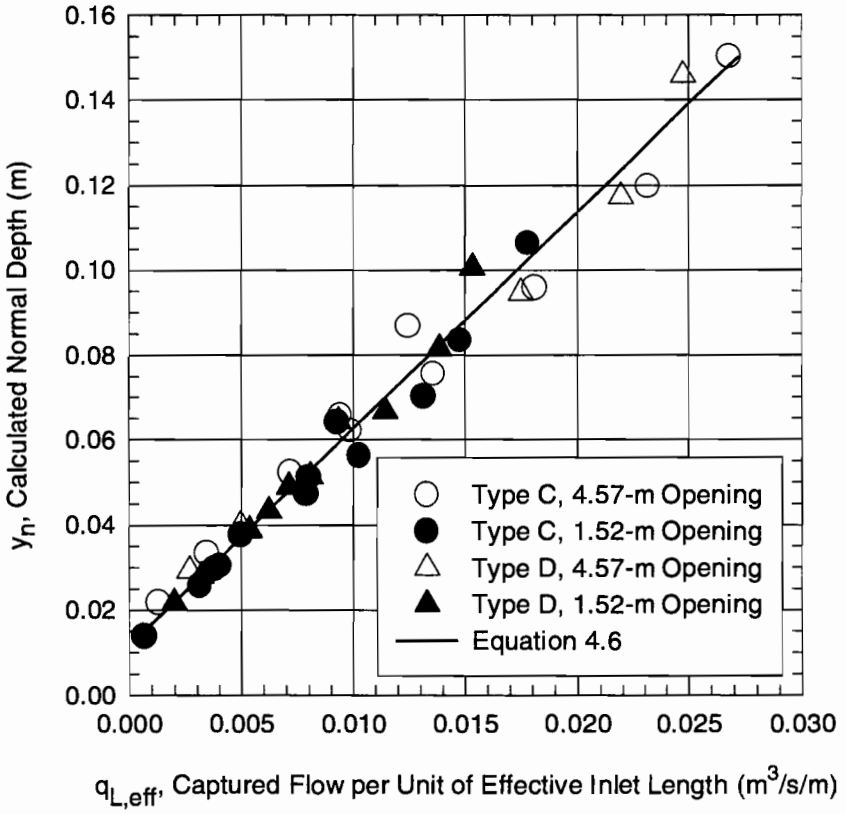

Figure 4.11 Comparison of Equation 4.6 with Experimental Data from 100% Efficiency Tests Performed on Type C and Type D Curb Inlets

standard errors of Equations 4.2 and 4.3 (0.0019 $m^3/s/m$ and 0.0023 $m^3/s/m$, respectively), but the values of $q_{L,eff}$ are less than the values of q_L. Therefore, the standard error of Equation 4.6 should be less than the standard errors of Equations 4.2 and 4.3.

The experimental data for the less than 100% efficiency tests were compared with the predictions of Izzard's less than 100% efficiency equation, using Equation 4.6 to calculate $L_{r,eff}$. Equation 2.22 was modified to be applied on the basis of the effective inlet length:

$$\frac{Q}{Q_a} = \frac{\left(\frac{a}{y_n}+1\right)^{5/2} - \left(\frac{a}{y_n}+1-\frac{L_{eff}}{L_{r,eff}}\right)^{5/2}}{\left(\frac{a}{y_n}+1\right)^{5/2} - \left(\frac{a}{y_n}\right)^{5/2}} \tag{4.7}$$

The results of the comparison of Equation 4.7 with experimental data are shown in Figure 4.12. A comparison of Figures 4.10 and 4.12 shows that the fit obtained using the effective length concept is practically the same as that obtained using Equation 2.22 with the different empirical equations for the 100% efficiency capacity of the inlets (Equations 4.2 and 4.3). Therefore, the accuracy of the effective length method is acceptable. Furthermore, the method is not confined to the use of different empirical equations for each inlet length.

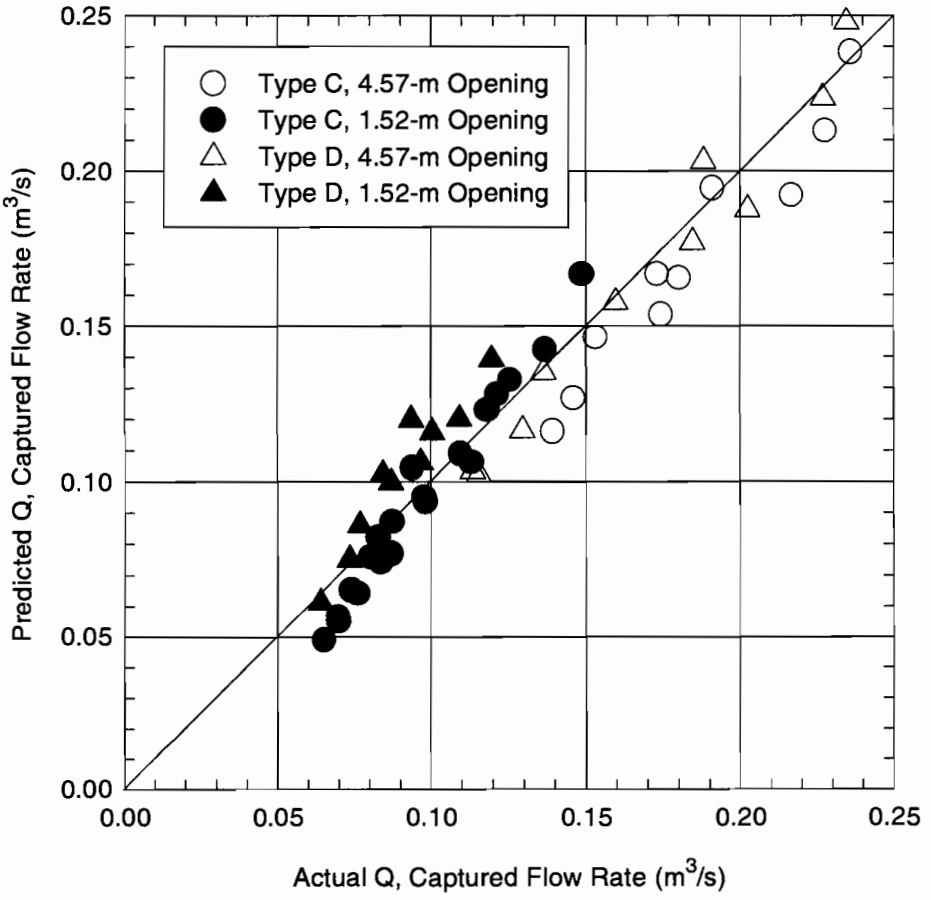

Figure 4.12 Comparison of Izzard's Less than 100% Efficiency Equation for Depressed Curb Inlets (Equation 4.7, Using Equation 4.6 to Calculate L_r) with Experimental Data for Type C and Type D Curb Inlets

4.3.2.4 Verification of Effective Length Concept with Undepressed Inlet Tests

To verify the applicability of the effective length method, it was desired to compare the method with experimental data from tests conducted on inlets with a known effective length. Tests were conducted for both 100% efficiency and less than 100% efficiency for 1.52-m and 4.57-m inlet lengths of flush, undepressed curb inlets (designated Type O inlets in this research project). Because there are no depression transitions associated with undepressed inlets, the effective length of an undepressed inlet is equal to the length of the physical inlet opening. Therefore, if the experimental data from the tests on Type O inlets matched the results of the design method, the applicability of the design method would be proved.

Figure 4.13 shows a plot of captured flow per unit of effective inlet length as a function of the calculated normal depth for 100% efficiency tests conducted on Type C, Type D, and Type O inlets, along with the predictions of Equation 4.6. The figure shows that the data for the 4.57-m opening Type O inlets fall along the line, but the data for the 1.52-m Type O inlets are below the line, indicating that Equation 4.6 underestimated the 100% efficiency capacity of the 1.52-m Type O inlets. Therefore, the 1.52-m length of the undepressed inlet seems to be more efficient per unit of effective length than the other inlets tested in this research project. This behavior illustrates the principle of diminishing returns associated with increasing the length of curb inlets.

As discussed in Section 2.1.3.2, for most curb inlets, the flow entering the first few feet of the inlet opening accounts for the majority of the flow captured by the inlet. Therefore, the first few feet of inlet opening are more efficient than the remainder of the inlet, because the flow captured by the downstream part of the inlet opening typically comes from farther out in the roadway where less of the flow exists. It is believed that this phenomenon explains why the 1.52-m undepressed inlet was more efficient per unit length than the other inlets tested. Because the 1.52-m Type O inlet had the shortest effective length of the inlets tested (1.52-m compared to 4.57-m for the next shortest effective length), a much greater percentage of the inlet length was used to capture the flow concentrated against the curb than is typical for longer curb inlets.

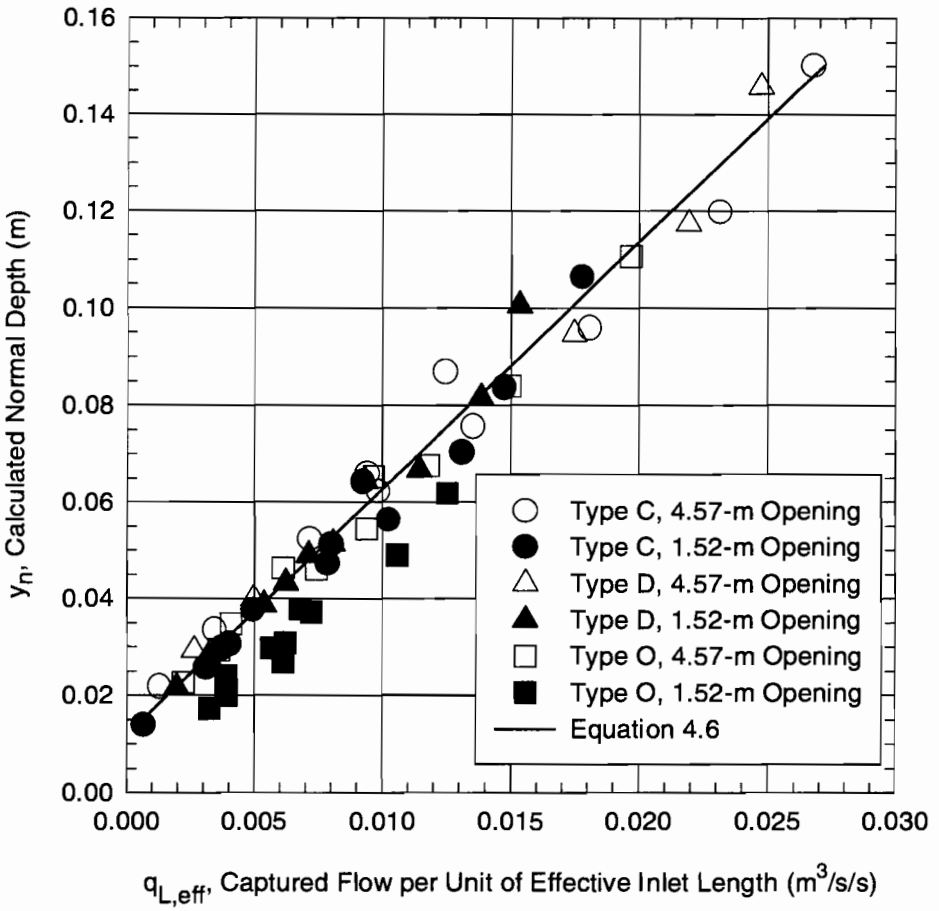

Figure 4.13 Comparison of Equation 4.6 with Experimental Data from 100% Efficiency Tests Performed on Type C, Type D and Type O Curb Inlets

Because the downstream portion of longer curb inlets is capturing water which swings into the inlet from farther out in the roadway, where less flow exists, the downstream part of longer curb inlets is relatively inefficient compared to the upstream part. This condition did not exist for the 1.52-m Type O inlet; therefore, the 1.52-m Type O inlet was more efficient per unit length than the longer inlets tested.

Figure 4.14 is a plot similar to Figure 4.12 showing a comparison of Equation 4.7 used with the effective length 100% efficiency equation (Equation 4.6) with data from less than 100% efficiency experiments conducted for Type C, Type D, and Type O inlets. The figure shows that the data from the Type O inlets do not show significant deviation from the data for Type C and

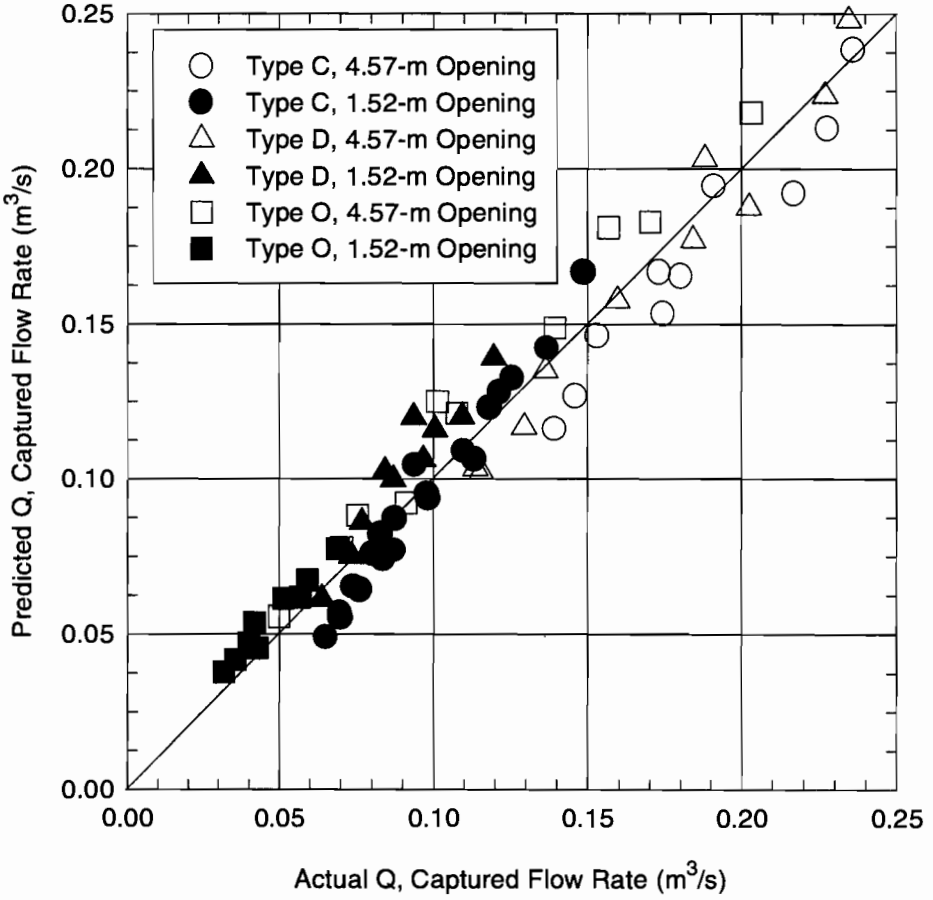

Figure 4.14 Comparison of Izzard's Less than 100% Efficiency Equation for Depressed Curb Inlets (Equation 4.7, Using Equation 4.6 to Calculate L_r) with Experimental Data for Type C, Type D, and Type O Curb Inlets

Type D inlets. In spite of some segregation apparent in the data shown in Figure 4.14, the effective length design method has been shown to be adequate for the design of TxDOT Type C and Type D curb inlets.

4.3.3 Summary of Design Method and Limits of Applicability

The application of the effective length design method developed above is similar to the application of Izzard's original design method described in Section 2.1.1.1. Once the gutter flow rate has been estimated by hydrologic analysis, Equation 4.6 may be used to calculate the effective length required to capture all of the approach flow ($L_{r,eff}$). The physical inlet opening

required (L) is $L_{r,eff}$ - L_a, where L_a = 3.05 m if there are two 1.52-m long depression transitions. If the inlet is being designed for less than 100% efficiency, the desired value of Q/Q_a and the value of $L_{r,eff}$ from Equation 4.6 may be substituted into Equation 4.7 and solved for L_{eff}. Again, the physical length of inlet required is $L = L_{eff} - L_a$. Alternatively, Equation 4.7 may be used to calculate the percentage of the approach flow intercepted by an inlet of a given length.

It is interesting that there is no distinction in the design method between Type C and Type D inlets. As mentioned before, some small segregation is apparent in the experimental data, especially in the comparison of the data with the less than 100% efficiency equations, but the differences were judged to be negligible for the purposes of design. Evidently, the difference in the depression depths of the two inlet types was not great enough to cause much difference in the hydraulic characteristics of inlets.

Equations 4.6 and 4.7 may be used only within the range of conditions for which they were developed and tested. The equations have been tested only for TxDOT Type C and Type D curb inlets. The use of the equations for the design of any other types of curb inlets should be verified by experiments. The equations should be used only for inlet openings from 1.52 m to 4.57 m, for longitudinal slopes between 0.004 and 0.06, for transverse slopes between 0.0208 (1:48) and 0.0417 (1:24), and for approach flow rates up to 0.25 m^3/s. It is essential that these limits be observed because the capacity of the inlets may change relative to Equations 4.6 and 4.7 outside of their range of applicability.

5. EXPERIMENTAL RESULTS FOR BRIDGE DECK DRAINS

The first phase of the experimental work on bridge deck drains was aimed at determining the discharge capacity of Drain 2B (Figure 5.1). Drain 2B was the same drain tested by Holley et al. (1992) in a previous project. The only difference between Drain 2 and Drain 2B was the orientation of the drain. The results of the experimental work on Drain 2B and a comparison of the hydraulic performance of Drain 2 and Drain 2B are presented in Section 5.2.4. The experiments on Drain 2B revealed some limitations of the drain that decreased its hydraulic capacity relative to Drain 2. After the experimental data and discharge relationship for Drain 2B were reviewed by TxDOT hydraulic design personnel, it was decided to construct and test a newly designed inlet. This inlet was designated Drain 4 and is shown in Figures 5.8 and 5.9. The results of tests on Drain 4 and a comparison of the hydraulics of Drain 4 and Drain 2B are presented in Section 5.2.

5.1 DRAIN 2B

5.1.1 Geometry and Description

The bridge deck drain called Drain 2B (Figure 5.1) tested in this research project is the same as Drain 2 tested by Holley et al. (1992) in a previous project. The only difference between Drain 2 and Drain 2B was the orientation of the drain. While both drains were placed perpendicular to the roadway curb, Drain 2 was placed with the outlet of the drain pan next to the curb; Drain 2B was placed with the outlet away from the curb. The difference between Drain 2 and Drain 2B is illustrated in Figure 5.2, where the circle indicates the 0.152-m diameter outlet of the drain pan. As will be shown in subsequent sections, the orientation of the pan had a significant affect on the hydraulic performance of the drain.

Drain 2 and Drain 2B had a grate 0.235 m long (in the flow direction) and 0.927 m wide. The grate was supported by a drain pan. The bottom of the drain pan was inclined towards the entrance to the 0.152-m drain pipe. The orientation of Drain 2 was preferable from a hydraulic

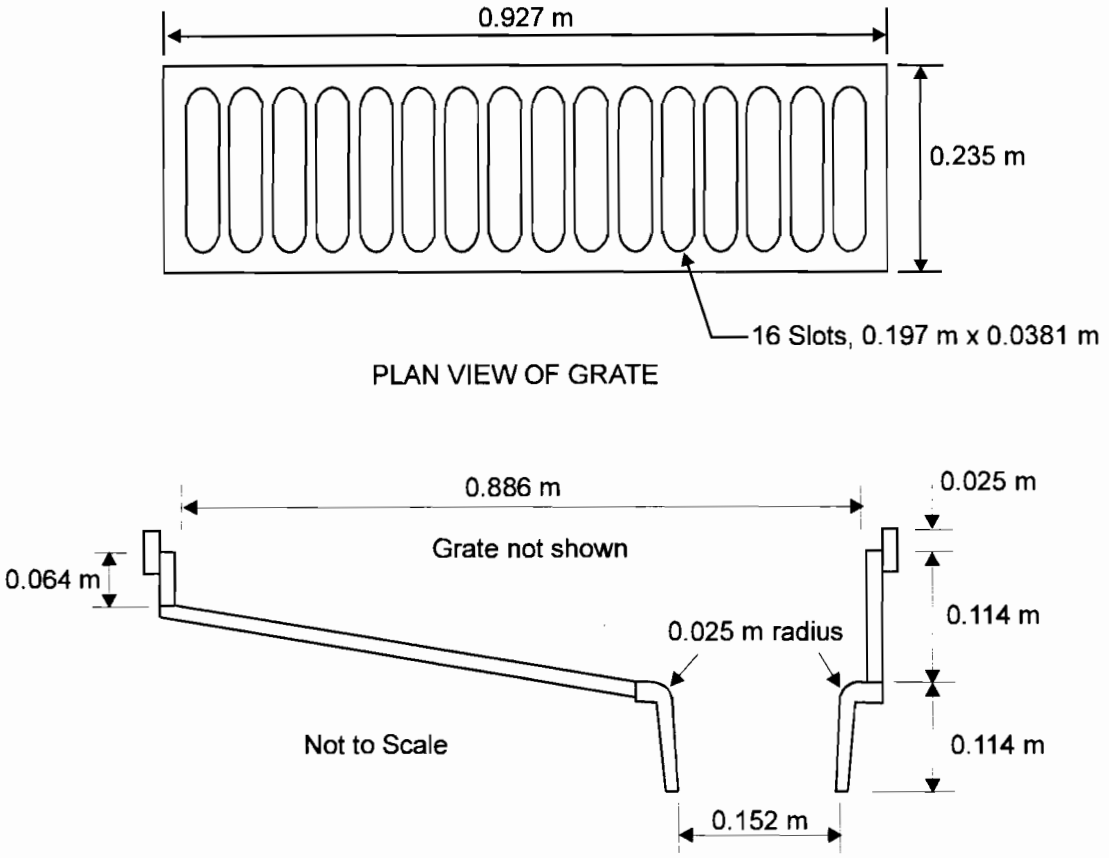

Figure 5.1 Drain 2B

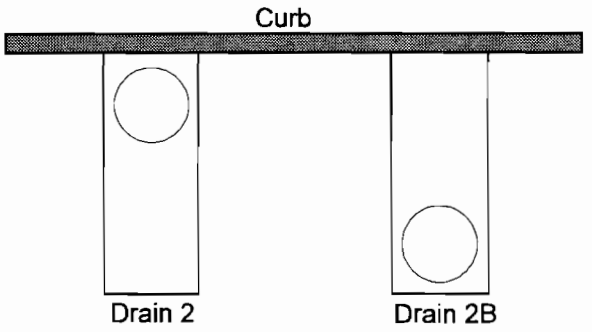

Figure 5.2 Orientation of Drain 2 and Drain 2B

standpoint because the deep part of the pan and the outlet were placed next to the curb where the greatest percentage of the approach flow was concentrated. Thus, when the cross slope of the bridge deck was increased, the slope of the bottom surface of the drain pan was also increased. For Drain 2B, the shallow part of the drain pan was next to the curb, so the part of the drain with the least capacity had the greatest percentage of the frontal flow. Furthermore, when the cross slope of the bride deck was increased, the slope of the bottom surface of the drain pan decreased. The combination of these effects had serious consequences for the hydraulic capacity of the drain. In spite of hydraulic considerations, the drain is normally installed in bridges in the orientation of Drain 2B. Installation of the drain in this manner keeps the downspout piping from interfering with the longitudinal beams which support the bridge. Also, the orientation of Drain 2B allows the piping to be concealed behind the longitudinal beams, improving the aesthetics of the bridge.

The same full-scale inlet model was used for Drain 2 and Drain 2B. The model was constructed entirely of clear plexiglass so that the behavior of the flow inside the drain pan could be observed visually. A photograph of the Drain 2B model is shown in Figure C.7 in Appendix C.

5.1.2 Procedures

Forty-six tests were conducted on Drain 2B. As discussed in Section 2.2.1, the piping system used on the drain was the same as Holley et al.'s (1992) Configuration G, which was a 0.152-m 90° PVC elbow placed on the drain pan outlet pipe. There was essentially no vertical distance between the bottom of the drain pan and the elbow. The longitudinal slopes used in the hydraulic tests were 0.004, 0.01, 0.02, 0.04, and 0.06. These slopes were chosen to represent the range of longitudinal slopes allowed by TxDOT. The transverse slopes used were 0.0208 (1:48) and 0.0417 (1:24), which are TxDOT's minimum and maximum allowable transverse slopes, respectively. The approach flow rates in the tests varied from 0.006 to 0.12 m^3/s.

The procedures used for the tests were as follows:

1. The model was set at the desired longitudinal and transverse slopes.

2. A constant approach flow rate was established into the upstream end of the model using the venturi meter to measure the flow rate.
3. The flow depth and ponded width were measured upstream of the drain. The flow depths were measured with a point gage at two cross sections where stilling wells were installed. These depth measurements were used to determine if the flow reached uniform depth upstream of the drain.
4. When the flow over the V-notch weirs reached a steady condition, the flow captured by the drain and the carryover flow were measured.

Experimental data for bridge deck drains are found in Tables B.4-B.5 of Appendix B. A photograph of a typical test conducted on Drain 2B is shown in Figure C.8 in Appendix C.

5.1.3 Results and Analysis

As discussed in Section 2.2.1 and illustrated in Figure 2.21, Holley et al. (1992) found that the hydraulic behavior of Drain 2 could be separated into different regimes designated weir/orifice control and piping system control in Holley et al.'s report. However, further research and analysis of Holley et al.'s data for Drain 2 revealed that the two regimes are more appropriately designated weir control and orifice control, as discussed in Section 2.2.1 (Smith and Holley, 1995). Consequently, it was expected that similar behavior would be apparent for Drain 2B.

The experimental data for Drain 2B are presented in Figures 5.3 and 5.4. The data are tabulated in Table B.4 of Appendix B. Figure 5.3 is a plot of captured flow as a function of the calculated normal depth of the approach flow for $S_x = 0.0208$. Figure 5.4 is a similar plot for $S_x = 0.0417$. The dashed lines in Figures 5.3 and 5.4 represent the trends of the data for a given longitudinal slope. The information presented in Figures 5.3 and 5.4 for Drain 2B is comparable with that presented in Figure 2.21 for Drain 2. In Figure 5.3, for $Q_{2B} > 0.020$ m^3/s and $S \geq 0.01$, the steep slope of the data trend corresponds to orifice control. Even though the slopes of the data trends increase as Q_{2B} increases in Figure. 5.4, none of the flows have orifice control.

For Drain 2B, the orientation of the drain pan causes a more gradual transition between weir and orifice control than for Drain 2. By definition, weir control exists when the pan is not

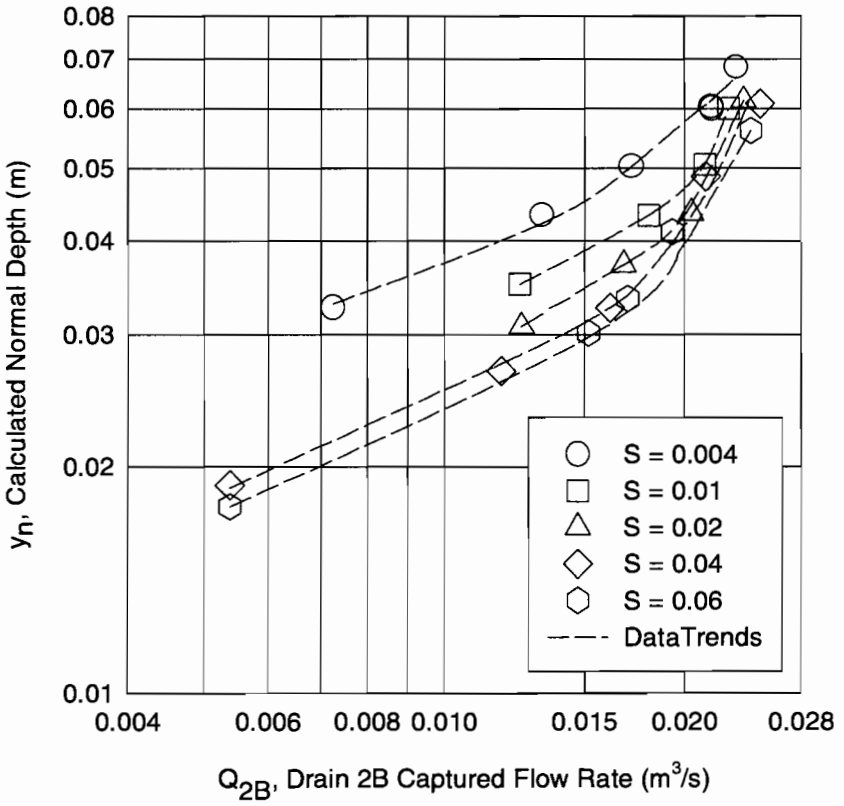

Figure 5.3 Drain 2B Experimental Data for S_x= 0.0208

totally full so that the flow into the drain is controlled by the hydraulics for a hypothetical zero height weir at the upstream edge of the grate. Orifice control exists when the drain pan is completely full and the capacity of the drain is controlled by the orifice at the entrance to the drain pan outlet. Because the shallow part of the drain pan of Drain 2B is located next to the curb, where most of the approach flow is concentrated, the shallow part of the pan fills quickly for even low approach flow rates, causing submerged weir flow through the grate over the shallow part of the pan (Smith and Holley, 1995). Submerged weir flow is still weir-like behavior, except the discharge coefficient for submerged weir flow is lower than for free flow. However, for low flow rates, the grate over the deep part of the pan containing the downspout is still in weir control. As the approach flow rate increases, the portion of the grate that acts as a

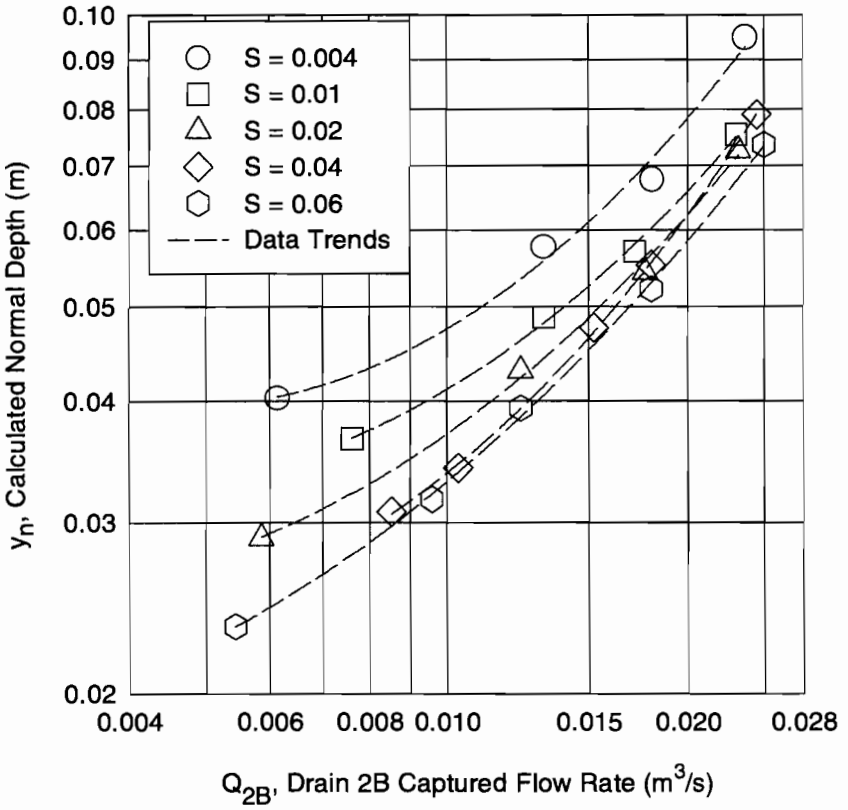

Figure 5.4 Drain 2B Experimental Data for $S_x = 0.0417$

submerged weir gradually increases until the entire drain pan is full. Smith and Holley (1995) showed that the hydraulic behavior of Drain 2B in weir control can be modeled as a weir of decreasing weir length with increasing approach flow rate.

For Drain 2, the transition between weir control and orifice control was apparent from a distinct break in slope in the plot of captured flow as a function of calculated normal depth shown in Figure 2.21. Although the data for Drain 2B exhibited a transition between weir control and orifice control in a manner similar to that which occurred for Drain 2, the transition for Drain 2B was more gradual than for Drain 2. Dye tests during the experimental work showed that the majority of water captured by Drain 2B entered the inlet through the grate over the deep part of the drain pan. A similar situation existed for Drain 2, except that the flow entering the drain through the grate over the deep part of the pan contributed an even greater percentage of

the captured flow for Drain 2 than Drain 2B because the deep part of Drain 2 was located next to the curb. Therefore, the amount of flow captured by Drain 2 was affected mainly by the control regime affecting the deep part of the pan, while the amount of flow captured by Drain 2B was influenced by the control regime affecting both the shallow and deep parts of the pan. For Drain 2, no significant change in behavior occurred when the shallow part of the drain filled with water and the grate over the shallow end of the pan began to act as a submerged weir, because the majority of the captured flow was still entering the drain under weir control over the deep part of the pan. As the flow rate was increased to the point at which the deep part of the pan filled with water and the drain entered the orifice control regime, a sharp change in the hydraulic behavior of the drain occurred. Conversely, for Drain 2B, the effect of the submerged weir behavior at the shallow end of the pan began to be evident before the deep end of the drain pan filled with water, causing a gradual transition in the hydraulics of the drain. Figure C.9 in Appendix C is a photograph of a test performed on Drain 2B under submerged weir conditions.

Before any experiments were performed, it was expected that an equation would be developed for Drain 2B for low flows similar to the one developed by Holley et al. (1992) for Drain 2 (Equation 2.51). However, when the behavior described above was observed and it was apparent that there was no clear break between flow regimes, it was decided to attempt to develop an equation which predicted the capacity of Drain 2B over the entire range of measured flow rates. To develop the equation, a regression analysis was done on the data collected for Drain 2B. Statgraphics, a microcomputer statistical analysis software package, was used to do the regression analysis. The variables used in the regression analysis were

S = longitudinal slope,

S_x = cross slope,

Q_a = approach flow rate (m^3/s),

Q_{2B} = captured flow rate (m^3/s),

y_n = calculated normal depth upstream of the drain (m),

v = average velocity of flow upstream of the drain (m/s), and

T = ponded width of flow upstream of the drain (m).

The best equation obtained from the regression analysis was

$$Q_{2B} = 0.201\, y_n^{1.32} \frac{S^{0.16}}{S_x^{0.60}} \tag{5.1}$$

Equation 5.1 has a correlation coefficient (R^2) of 0.925 and a standard error of 0.0016 m^3/s. Figure 5.5 is a comparison of the predicted captured flow rates from Equation 5.1 with experimental data from Drain 2B. There is a definite pattern to the residuals of Equation 5.1, as evidenced by the upward concavity of the data points in Figure 5.5. In examining the fit of Equation 5.1, it was observed that the pattern of the residuals implied that a quadratic curve would provide a better fit to the data. Equation 5.1 is of the form $Q_{2B} = f(y_n, S, S_x)$. To determine if the fit could be improved, a new function of the form $Q_{2B} = g(f)$ was sought. The

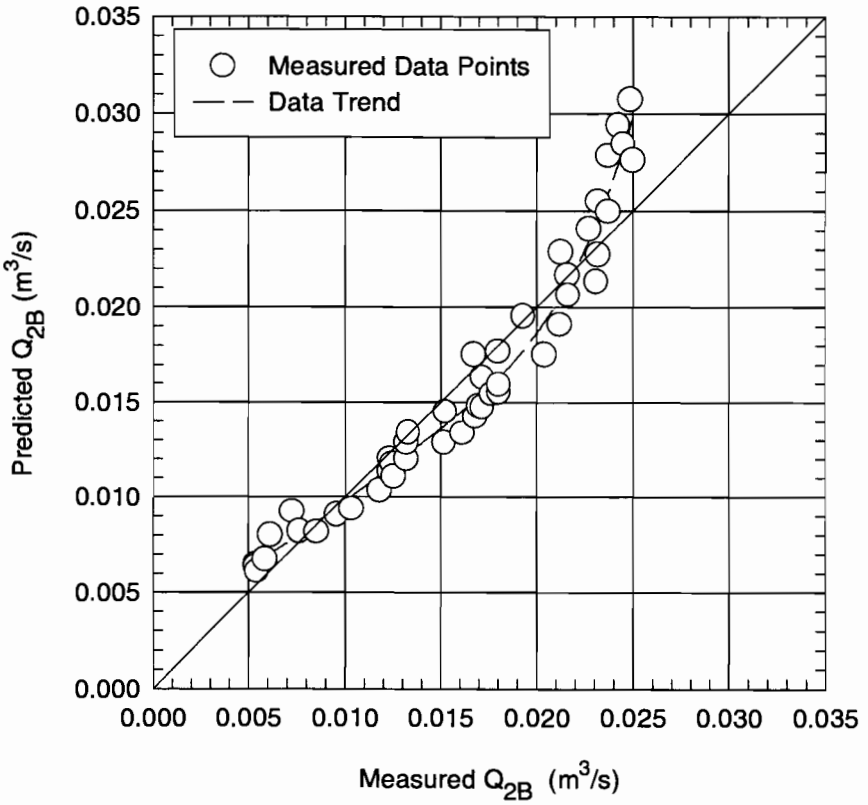

Figure 5.5 Comparison of Equation 5.1 with Experimental Data from Drain 2B

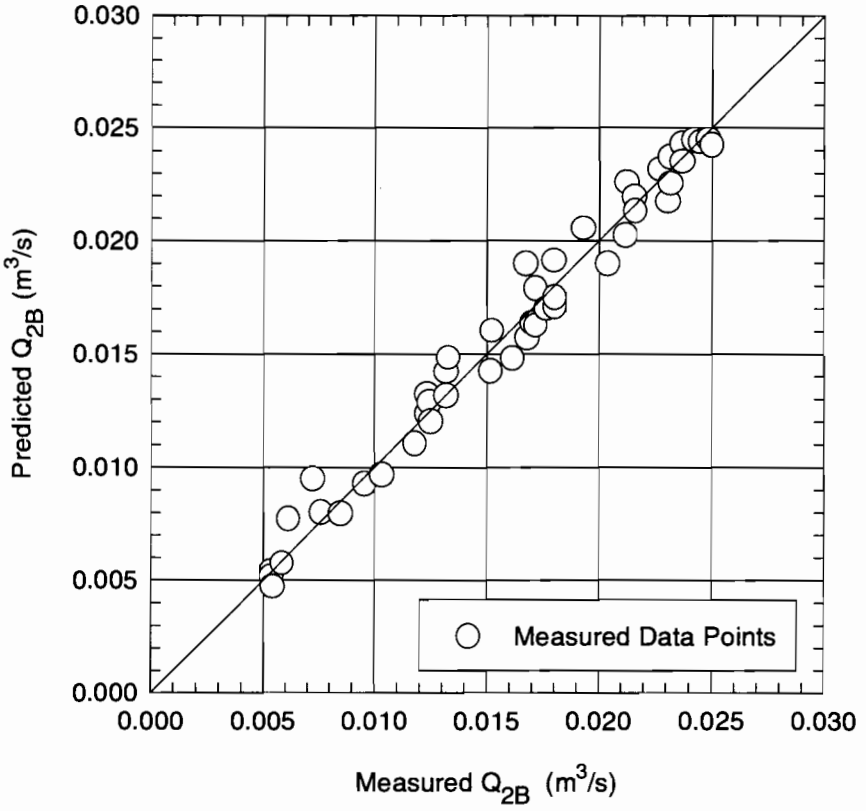

Figure 5.6 Comparison of Equation 5.2 with Experimental Data from Drain 2B

best equation found was

$$Q_{2B} = -0.00646 + 2.04\,f - 33.5\,f^2 \qquad (5.2)$$

where $f = 0.201\,y_n^{1.32}S^{0.16}S_x^{-0.60}$. Figure 5.6 shows a comparison of Equation 5.2 with the experimental data. It is evident from the figure that Equation 5.2 is a better fit to the experimental data than Equation 5.1. The correlation coefficient (R^2) of Equation 5.2 is 0.976. The standard error of Equation 5.2 was 0.00096 m^3/s, compared to 0.0016 m^3/s for Equation 5.1. Therefore, it was possible to fit an equation which was statistically good for the entire range of flow rates tested for Drain 2B. Equation 5.2 may be used for the design of Drain 2B, subject to the limits given in Section 5.1.4.

Based on visual observation of the flow conditions during the experiments and the analysis of the experimental data for Drain 2B, it was concluded that the capacity of the drain could be increased significantly by deepening the drain pan. A deeper drain pan would allow more flow to be captured before the drain pan filled with water, thus increasing the approach flow rate at which the transition from weir control to orifice occurred. This conclusion led to the development by TxDOT personnel of Drain 4, which had a deeper, longer, and wider drain pan than Drain 2B. Also, a new grate design was used with Drain 4 (Section 5.2).

5.1.4 Limits of Applicability

Either Equation 5.1 and 5.2 may be used with acceptable accuracy to predict the capacity of Drain 2B. As with all empirical equations, Equations 5.1 and 5.2 should be applied only for the range of conditions for which they were developed and tested. Equations 5.1 and 5.2 were developed for longitudinal slopes between 0.004 and 0.06, transverse slopes of 0.0208 (1:48) and 0.0417 (1:24), approach flow rates between 0.006 and 0.12 m^3/s, calculated normal depths between 0.018 and 0.09 m, and captured flow rates between 0.005 and 0.025 m^3/s. It is essential that these limits be observed because the capacity of the drain may change relative to Equations 5.1 and 5.2 for conditions outside of their range of applicability.

5.1.5 Comparison of the Hydraulic Performance of Drain 2 and Drain 2B

The comparison of the hydraulic performance of Drain 2 and Drain 2B revealed that the orientation of the drain has a significant affect on its capacity. In general, the hydraulic capacity of Drain 2B was less than that of Drain 2. Even though there were similarities in the hydraulic behavior of Drain 2 and Drain 2B as discussed in Section 5.1.3, the ranges of captured flow rates were different for the two drains. That is, while both drains exhibited the behavior of weir control transitioning to submerged weir control, the transition occurred at lower flow rates for Drain 2B than for Drain 2. The highest flow rate intercepted during the experiments on Drain 2B was about 0.026 m^3/s, which is just greater than the transition from weir flow to orifice flow for Drain 2 at 0.023 m^3/s.

A comparison of the prediction equations for Drain 2 and Drain 2B for a single set of longitudinal and transverse slopes (S = 0.04 and S_x = 0.0417) is shown in Figure 5.7. Figure 5.7 was calculated using Holley et al.'s equation for the low flow capacity of Drain 2 (Equation 2.51) and Equation 5.2 for the capacity of Drain 2B. The equations predict that the capacity of Drain 2B is about the same as that of Drain 2 for lower calculated normal depths or, equivalently, for lower approach flow rates, as would be expected for the region of free-flow weir control. Although the trends shown in Figure 5.7 seem to indicate that Drain 2B is more efficient than Drain 2 for calculated normal depths less than about 0.033 m, the differences between the two equations are small, less than the standard error of either of the equations. (The greatest difference between the predictions of the two equations for low flow rates is about 0.0006 m^3/s,

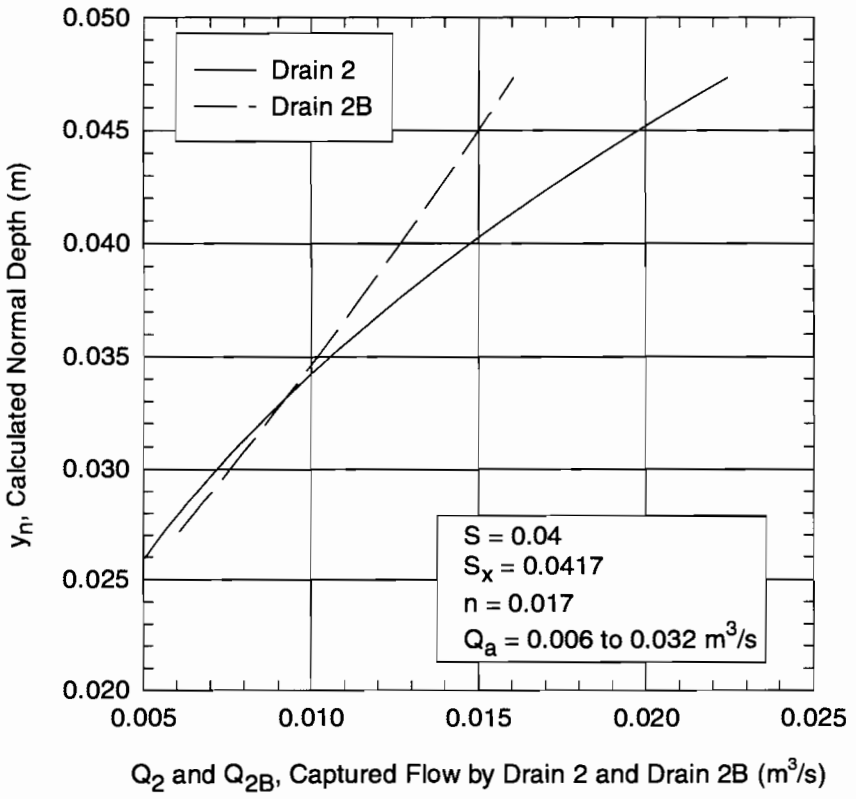

Figure 5.7 Comparison of Design Equation for Drain 2 and Drain 2B

and the standard errors of Equations 5.2 and 2.51 are 0.00096 m^3/s and 0.00085 m^3/s, respectively.) Therefore, the differences between the two equations for low flow rates are not statistically significant. As the calculated normal depth increases, the equations predict that Drain 2 will capture significantly more flow than Drain 2B. It must be emphasized that Equation 2.51 for Drain 2 is applicable for weir control only, while Equation 5.2 for Drain 2B is applicable for both weir control and orifice control.

5.2 DRAIN 4

5.2.1 Geometry and Description

The overall design of the drain pan of Drain 4 (Figure 5.8) was similar to that of Drain 2 and Drain 2B, except that it was longer, wider, and deeper. Most significantly, Drain 4 is 0.041 m deeper than Drain 2B at its shallow end and 0.038 m deeper than Drain 2B at its deep end.

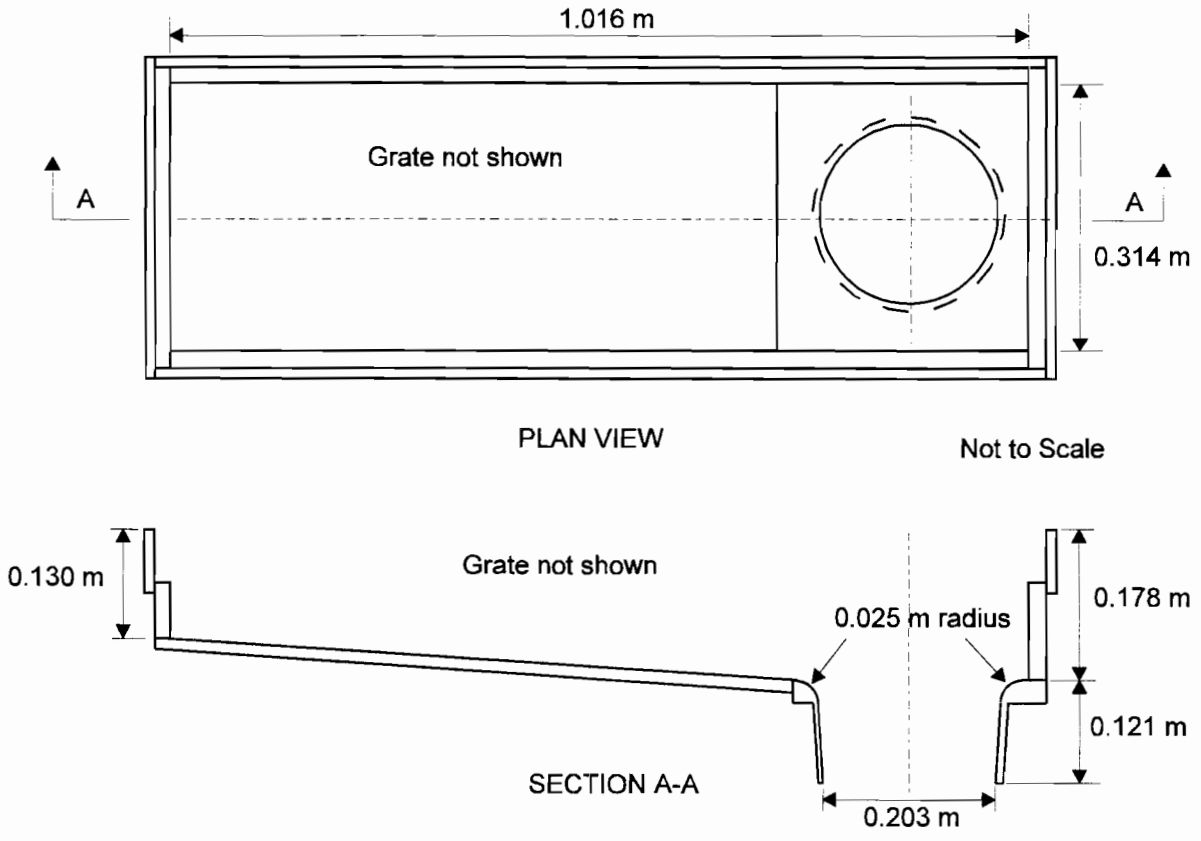

Figure 5.8 Drain 4 Pan

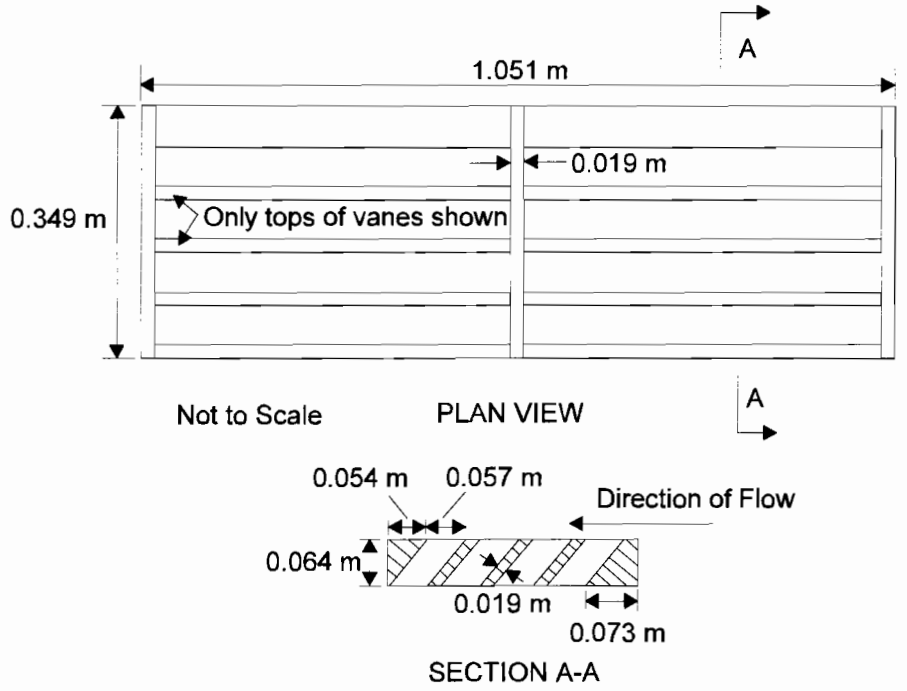

Figure 5.9 Drain 4 Grates

Also, an 0.203-m diameter downspout was used with Drain 4, instead of the 0.152-m downspout used with Drain 2 and Drain 2B. Like Drain 2B, Drain 4 was positioned perpendicular to the curb with the shallow part of the pan next to the curb.

The dimensions of the grates used with Drain 4 were 0.349 m long (in the direction of flow) and 1.051 m wide (Figure 5.9). The grate had four slots inclined in the direction of flow at an angle of about 50°. The slots were divided by a 0.191-m wide longitudinal bar at the center of the grate. Each slot was 0.054 m long in the direction of flow. The vanes which created the slots were 0.019 m thick.

The model was used at full scale for the experiments of Drain 4. All components of the drain were built of clear plexiglass so that the behavior of the flow inside the drain pan could be observed visually. A photograph of the Drain 4 model is shown in Figure C.10 in Appendix C.

5.2.2 Procedures

Fifty-one tests were conducted for Drain 4. No piping was installed on the drain downspout. This configuration is believed to be most representative of the connection of the drain downspout to subsequent piping system used by TxDOT. As shown in Figure 5.10, the downspouts of the drains are connected to the piping system by means of a reducer. Because there is no physical connection between the drain downspout with the reducer, some differential movement is allowed between the drain and the piping system. Therefore, the discharge end of the drain downspout is at atmospheric pressure, as it is when no pipe is connected to the downspout.

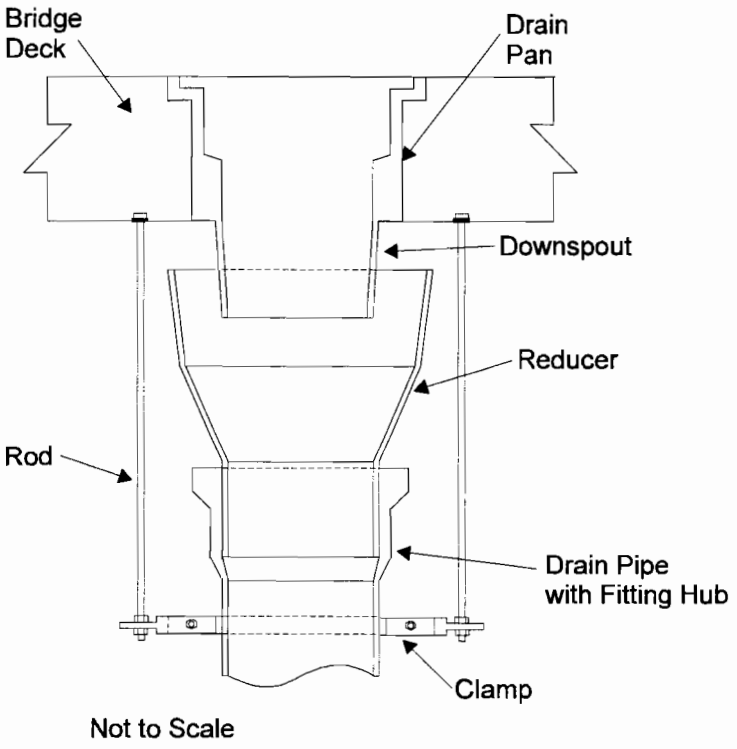

Figure 5.10 Connection of Deck Drain Downspout to Piping System

The longitudinal slopes used in the hydraulic tests were 0.004, 0.01, 0.02, 0.04, and 0.06. These slopes were chosen to represent the range of longitudinal slopes allowed by TxDOT. The transverse slopes used were 0.0208 (1:48) and 0.0417 (1:24), which are typical transverse slopes

for nonsuperelevated roadways. The approach flow rates in the tests varied from 0.014 to 0.20 m^3/s. The procedures used for the tests on Drain 4 were the same as those used for Drain 2B (Section 5.1.2). A photograph of a typical test performed on Drain 4 is shown in Figure C.11 in Appendix C.

5.2.3 Results and Analysis

The experimental data for Drain 4 are plotted in Figures 5.11 and 5.12. The data are tabulated in Table B.5 of Appendix B. Figure 5.11 is a plot of captured flow rate as a function of the calculated normal depth of the approach flow for S_x = 0.0208. Figure 5.12 is a similar plot

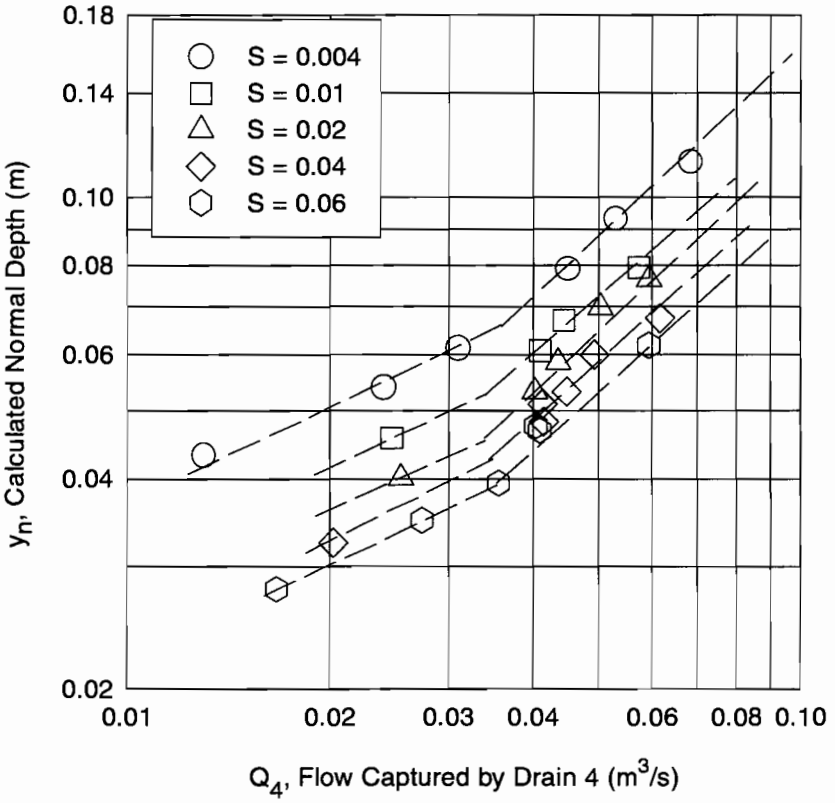

Figure 5.11 Drain 4 Experimental Data for S_x = 0.0208

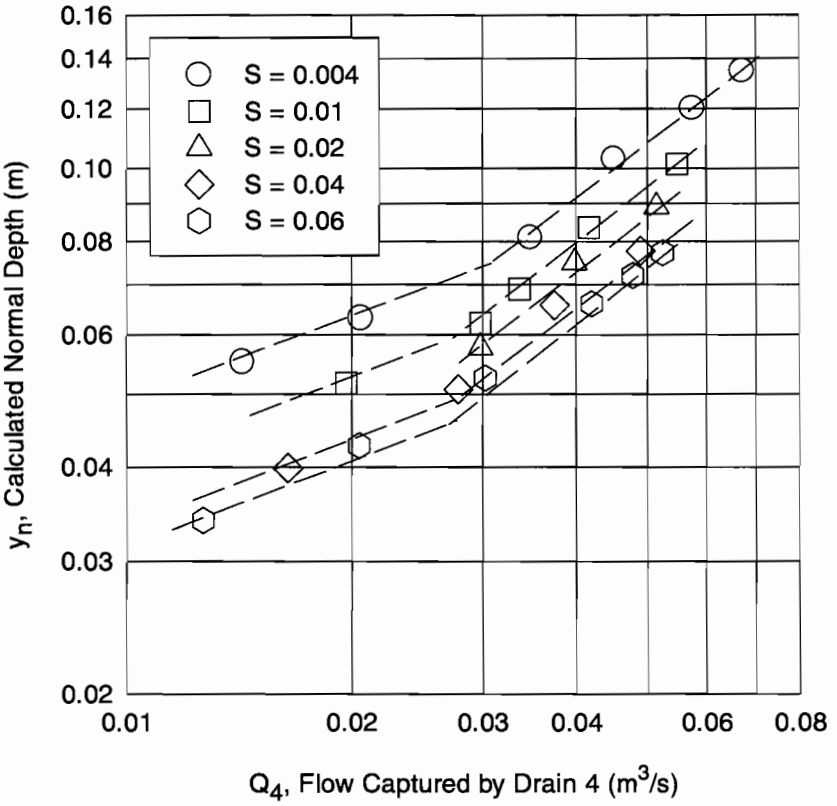

Figure 5.12 Drain 4 Experimental Data for S_x = 0.0417

for S_x = 0.0417. The dashed lines in the figures represent the trends of the data for a given longitudinal slope. The design of Drain 4 is much more efficient than either Drain 2 or Drain 2B. The lowest flow rates shown in Figures 5.11 and 5.12 correspond approximately to the 100% efficiency capacity of the drain when all of the approach flow was being captured. No tests were attempted at flow rates less than the 100% efficiency capacity of the drain because there is no correlation between calculated normal depth and captured flow rate for approach flow rates less than the 100% efficiency capacity of the drain.

It was observed during the tests conducted on Drain 4 that considerable splashing occurred at the shallow end of the drain for certain conditions. Dye tests revealed that water was actually entering the drain through the first slot of the grate, but the momentum of the approach flow caused some of the water to flow back up through the most downstream slot, as illustrated

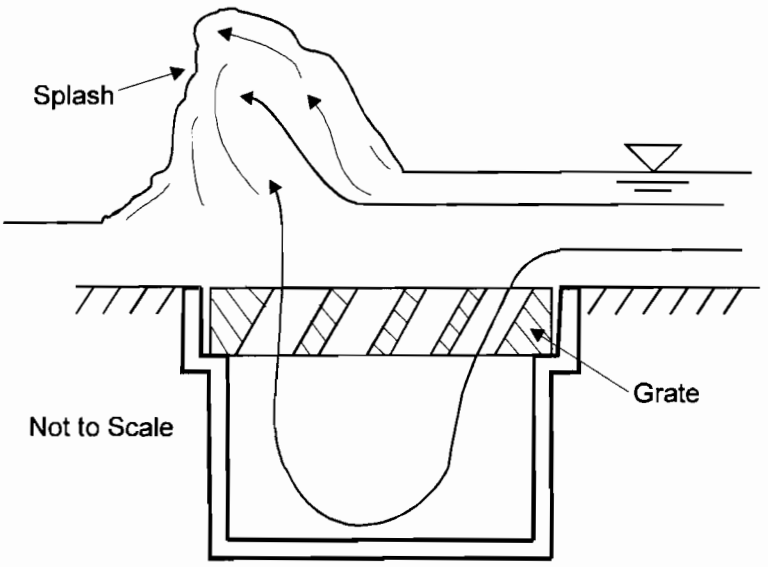

Figure 5.13 Cross Section of Drain Pan Showing Splashing Caused by Flow Exiting the Drain Pan Through the Grate

in Figure 5.13. Figure C.12 in Appendix C is a photograph of a test performed on Drain 4 illustrating the splashing occurring at the shallow end of the drain. The water flowing back through the grate from the drain pan caused a disturbance in the flow, forcing flow which was passing over the grate to rise over the disturbance. The resulting splash was up to 0.1 m in height under certain conditions. The splashing did not occur for the steepest longitudinal slopes tested, presumably because the velocity of the water flowing over the top of the grate was too great to rise over the water flowing through the grate from inside the drain pan, effectively washing out the splash. In any case, the amount of water involved in the splashing was insignificant compared to both the captured flow and the carryover flow. The splashing did not seem to have any adverse affect on the capacity of the drain.

Even though the data trend lines in Figures 5.11 and 5.12 are shown as smooth curves, each set of data actually has a slight break in the trend at Q_4 of approximately 0.027 m^3/s. Thus, the first set of empirical curves was obtained by fitting a separate empirical equation to the data in each region. The multiple regression analyses were performed with Statgraphics, using the same variables as for Drain 2B (Section 5.1.3). There was some uncertainty as to where the

dividing line should be between the two sets of regression equations. Thus, analyses were performed for several different dividing points. The best results were obtained by using data with captured flow rates less than 0.027 m^3/s for one equation with the higher flow rates being used for a second equation.

The best equation obtained from the regression analysis for the low flows was

$$Q_{4,low} = 8.63 y_n^{2.44} \frac{S^{0.42}}{S_x^{0.93}} \tag{5.3}$$

Equation 5.3 had a correlation coefficient (R^2) of 0.96, with a standard error of 0.0014 m^3/s. The equation developed from the regression analysis for the higher flows was

$$Q_{4,high} = 0.420 y_n^{1.24} \frac{S^{0.19}}{S_x^{0.51}} \tag{5.4}$$

Equation 5.4 had a correlation coefficient of 0.98 and a standard error of 0.0020 m^3/s. A comparison of the predictions of Equations 5.3 and 5.4 with the experimental data for Drain 4 is shown in Figure 5.14.

For the purposes of developing Equations 5.3 and 5.4, the break between the two equations was taken as a captured flow of 0.027 m^3/s. However, a designation of the break point using the captured flow rate is inconvenient for determining which equation to use for design because the captured flow rate is unknown at the beginning of the design procedure. Therefore, a more convenient definition of the break point was sought, one which would be a function of the roadway geometry. Equating Equations 5.3 and 5.4 gives

$$y_n = 0.081 \frac{S_x^{0.35}}{S^{0.19}} \tag{5.5}$$

as the dividing line between the two equations. Equation 5.3 should be used for y_n less than that given by Equation 5.5 while Equation 5.4 should be used for larger y_n.

As an alternative, it was decided to fit a single equation to all of the data from Drain 4. The best equation obtained from the regression analysis performed on the entire data set was

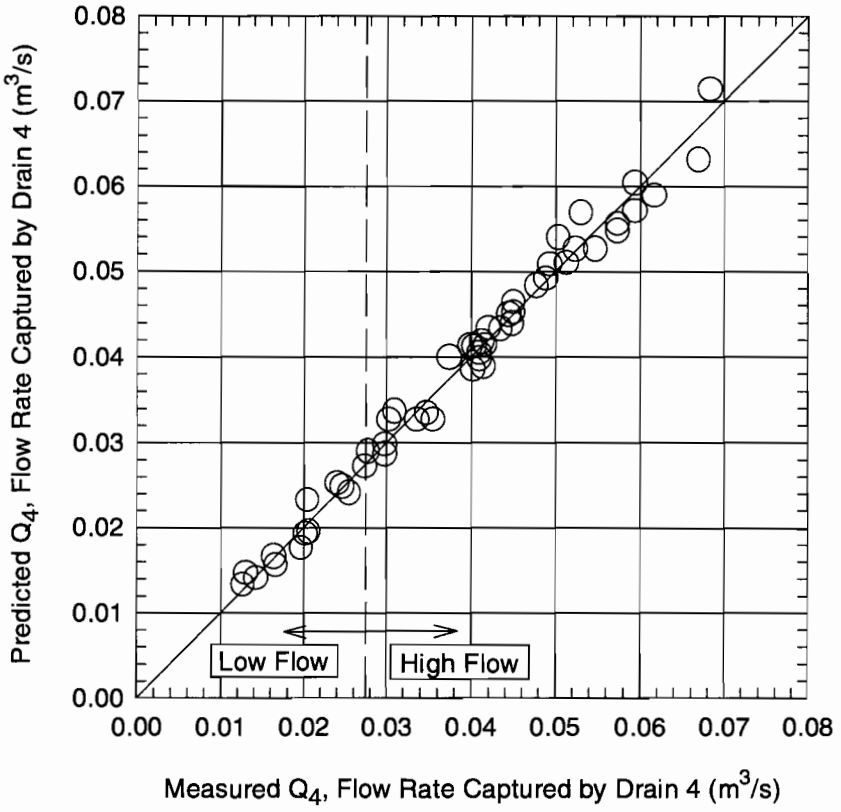

Figure 5.14 Comparison of Equations 5.3 and 5.4 with Experimental Data from Drain 4

$$Q_4 = 0.874 y_n^{1.57} \frac{S^{0.26}}{S_x^{0.63}} \tag{5.6}$$

Figure 5.15 shows a comparison of the predictions of Equation 5.6 with the experimental data. Equation 5.6 had a correlation coefficient of 0.98 and a standard error of 0.0029 m^3/s. Like the equation developed for Drain 2B (Equation 5.1), the upward concavity evident in the data shown in Figure 5.15 implies that a quadratic curve would provide a better fit for the data. Equation 5.6 is of the form $Q_4 = f(y_n, S, S_x)$; therefore, an equation was sought of the form $Q_4 = g(f)$ which would provide a better fit to the data. The best equation found was

$$Q_4 = 0.0057 + 1.41f - 6.0f^2 \tag{5.7}$$

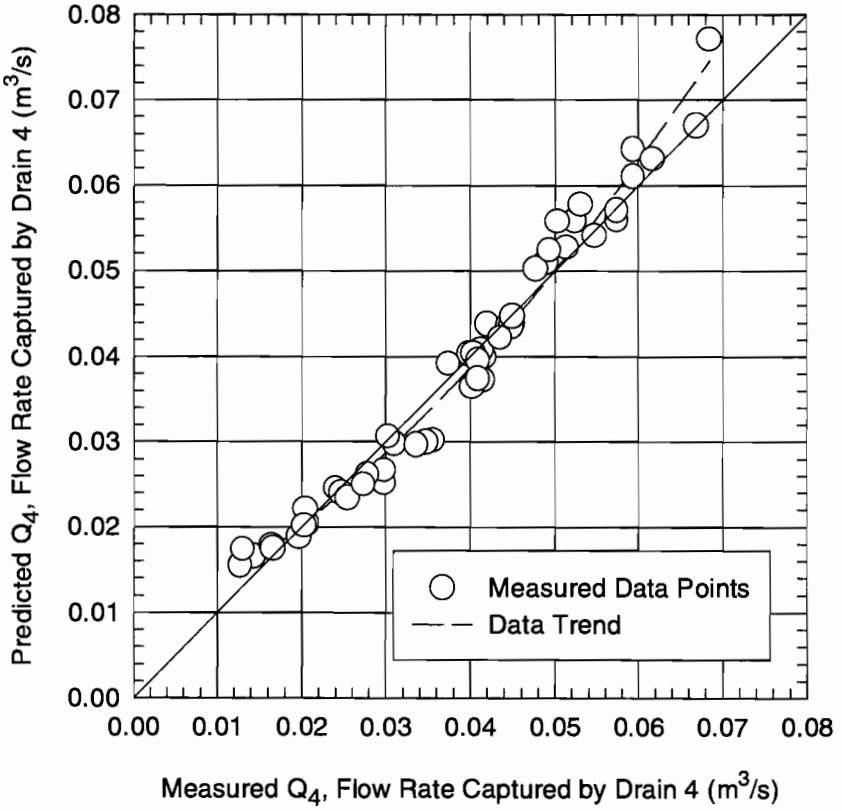

Figure 5.15 Comparison of Equation 5.6 with Experimental Data from Drain 4

where $f = 0.874 y_n^{1.57} S^{0.26} S_x^{-0.63}$. The correlation coefficient of Equation 5.7 is 0.99, and the standard error is 0.0022 m^3/s. As shown in Figure 5.16, Equation 5.7 is a better fit to the data than Equation 5.6.

5.2.4 Summary of Design Method and Limits of Applicability

Several different design equations were developed for Drain 4. Equations 5.3 and 5.4 may be used to predict the capacity of the drain using either Q = 0.027 m^3/s or Equation 5.5 as the dividing line between the two equations. Equations 5.3 and 5.4 provide the most accurate predictions of the capacity of the drain, especially for lower flow rates. However, Equations 5.6 and 5.7 may also be used to predict the capacity of the drain, although with slightly less accuracy

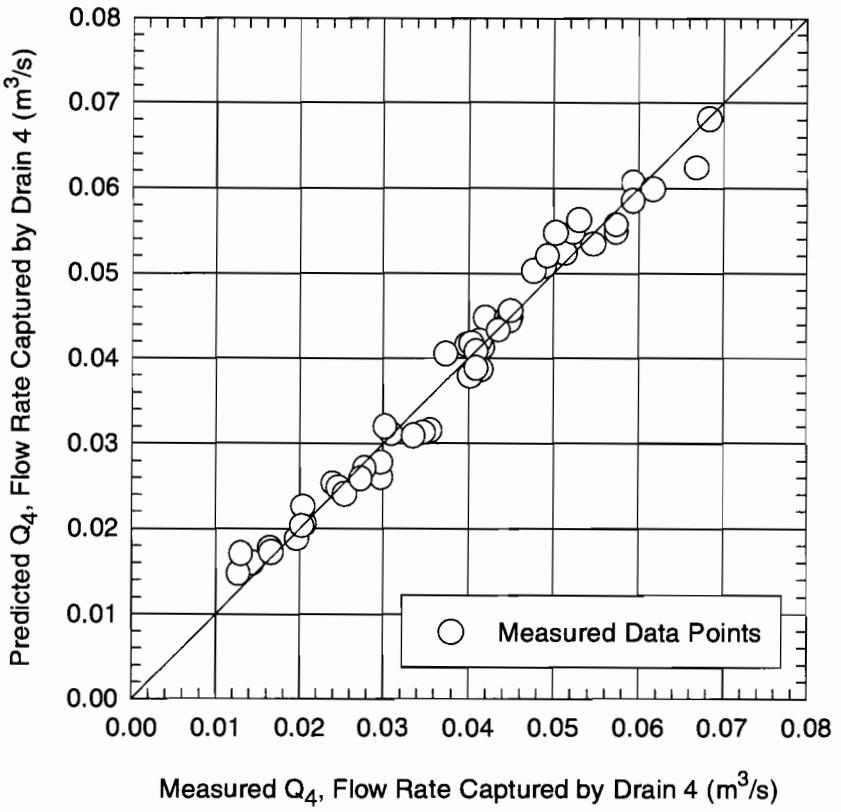

Figure 5.16 Comparison of Equation 5.7 with Experimental Data from Drain 4

than Equations 5.3 and 5.4. If one equation is to be used to predict the capacity of the drain over the entire range of captured flow rates, Equation 5.7 has slightly greater accuracy than Equation 5.6.

As with all of the empirical equations given in this report, Equations 5.3 to 5.7 should be used only for the conditions for which they were developed and tested. They should be used only for longitudinal slopes between 0.004 and 0.06, transverse slopes from 0.0208 (1:48) to 0.0417 (1:24), approach flow rates between 0.014 and 0.2 m^3/s, calculated normal depths between 0.027 and 0.134 m, and drain captured flow rates between 0.014 and 0.068 m^3/s. It is essential that these limits be observed because the capacity of the drain may decrease relative to the empirical equations for conditions outside of their range of applicability.

5.2.5 Comparison of the Hydraulic Behavior of Drain 4 and Drain 2B

A comparison of Figures 5.3 and 5.4 with Figures 5.12 and 5.13 immediately reveals that the hydraulic capacity of Drain 4 is far greater than that of Drain 2B. It is evident that the design improvements made to Drain 4 (larger and deeper pan, larger orifice, and deeper grate with inclined vanes) were very effective in increasing its capacity. For example, for a longitudinal roadway slope of 0.004, a transverse slope of 0.0417, and an approach flow rate of 0.122 m^3/s, Drain 2B captured 0.025 m^3/s. For the same roadway geometry and an approach flow rate of 0.117 m^3/s, Drain 4 captured 0.049 m^3/s, an increase of approximately 100%.

6. CONCLUSIONS

The primary objectives of the research project described in this report were to determine hydraulic characteristics of and design equations for two types of curb inlets and two types of bridge deck drains used by the Texas Department of Transportation (TxDOT). The curb inlets tested were TxDOT Type C and Type D flush depressed curb inlets (see Figure 4.1). The bridge deck drains tested were designated Drain 2B and Drain 4. Drain 2B is a TxDOT standard design used on many bridges and overpasses in the State of Texas (see Figure 5.1). Drain 4 is a new bridge deck drain design developed from information obtained from the results of the tests conducted on Drain 2B (see Figures 5.8 to 5.9).

All of the inlets and drains investigated in this research project were being designed by TxDOT based on existing design methods for curb inlets and bridge deck drains, but none had been tested to determine if the design methods adequately predicted the capacities of the inlets and drains. Most curb inlet and bridge deck drain design methods were developed empirically for specific inlet and drain geometries. Therefore, the applicability of these empirical methods to different inlet and drain geometries was uncertain.

Type C and Type D curb inlets are unique because of the short distance from the inlet lip to the back wall of the inlet box (0.152 m for Type C and Type D inlets; 0.457 to 0.610 m for most curb inlets). One of the primary concerns with the design of these inlets was that the water passing over the inlet lip might not have enough room to fall freely into the inlet box. It was believed that a backwater effect could be caused by the flow striking the back wall of the inlet box, causing water to back out into the street and decreasing the capacity of the inlets. Therefore, one of the objectives of this project was to determine if this backwater effect existed for Type C and Type D inlets, and if so, to quantify its effect on the capacity of the inlets.

The literature review presented in Chapter 2 revealed the knowledge gaps to be filled by this project. Although several different design methods for curb inlets were located during the literature review, none of the methods were developed for an inlet geometry closely similar to TxDOT Type C and Type D inlets. Furthermore, none specifically addressed backwater effects

caused by the inlet box. Therefore, experiments were required to determine the hydraulic characteristics of TxDOT Type C and Type D inlets and to compare the performance of the inlets with available design methods. Because no suitable design method was found in the literature, empirical design equations were developed specifically for Type C and Type D inlets.

The literature review revealed most of the available literature for grated inlets refers to grated street inlets, not to bridge deck drains. The hydraulic characteristics of grated street inlets are significantly different than those of bridge deck drains because the geometries of the inlet boxes and subsequent piping systems of grated street inlets and bridge deck drains are dissimilar. The only reference located which dealt specifically with bridge deck drains was Holley et al. (1992) (see Section 2.2.1). Holley et al. tested the same bridge deck drain as Drain 2B as part of a previous TxDOT research project. In that previous project, the drain was designated "Drain 2." The only difference between Drain 2 and Drain 2B was the orientation of the drain pan. While both inlets were placed in the bridge deck with their long axis normal to the curb, Drain 2 was placed with the outlet of the drain pan next to the curb; Drain 2B was placed with the outlet of the drain pan away from the curb (see Section 5.1 and Figures 5.1-5.2). Because the orientation of the drain pan has a significant effect on the hydraulics of the drain, it was found that the empirical equations developed by Holley et al. for Drain 2 did not apply to Drain 2B. The orientation of Drain 2 was preferable from a hydraulic standpoint, because the part of the drain with the greatest capacity (the deep part of the pan containing the outlet) was next to the curb, where the greatest percentage of the approach flow is concentrated. Nevertheless, the drain is usually installed in the field in the orientation of Drain 2B. Therefore, empirical design information was necessary for Drain 2B.

All of the design equations developed for inlets and drains in this project were based on data from physical hydraulic tests performed on models of the inlets and drains. The curb inlets were tested at 3/4 scale, while the bridge deck drains were tested at full scale. The inlets were tested on a roadway model located at the Center for Research in Water Resources at the University of Texas at Austin. The total length of the roadway model is 18.9 m. Since the inlet

and drain models were placed near the downstream end of the roadway, there was usually enough distance to allow uniform flow to be established upstream of the inlets and drains. The width of the model roadway was 3.20 m, which is the 3/4-scale width of a 4.27-m roadway lane. The roughness coefficient of the model surface was 0.018 (prototype). A venturi meter was used to measure the approach flow into the model, and V-notch weirs were used to measure the captured flow and the carryover flow. All of the flow measurement devices were calibrated at the start of the project, and their calibrations were checked periodically during the experimental work.

6.1 CONCLUSIONS FOR FLUSH DEPRESSED CURB INLETS

The experiments on Type C and Type D curb inlets revealed that no backwater effect exists for these inlets. The primary reason for the absence of backwater effects seems to be that under most conditions, the captured flow enters the inlet in the supercritical flow regime. Even for subcritical approach flow rates, the presence of the depression transitions and the fully depressed section can cause the flow to accelerate and enter the supercritical regime as it passes into the depressed section. Because the flow entering the inlet is supercritical, the effect of disturbances in the flow cannot be transmitted back into the street without drowning out the supercritical flow and changing it to subcritical. Although a small roller was usually created as the flow struck the back wall of the inlet box, the water in the roller simply fell into the inlet opening and was captured. No backwater effect was observed for any of the conditions tested in this research project.

Experiments on Type C and Type D curb inlets were performed at 100% efficiency and at less than 100% efficiency. 100% inlet efficiency means that the inlet is intercepting all of the approach flow; less than 100% efficiency means that there is carryover flow. The inlet opening lengths tested for both inlet types were 1.52 m and 4.57 m. The experimental data were compared against design methods developed by Izzard (1950), Li et al. (1951b), and Johnson and Chang (1984). None of the design methods tested was acceptable for predicting the capacity of the inlets.

Since Izzard's design method is used by TxDOT for the design of curb inlets, the most emphasis was placed on the comparison of Izzard's method with the experimental results. Like most curb inlet design methods, Izzard's method involves the use of separate equations for 100% inlet efficiency and less than 100% inlet efficiency. The use of the less than 100% efficiency equation requires the use of the 100% efficiency equation to calculate L_r, the inlet length required for 100% efficiency. The comparison of the experimental data from the 100% efficiency tests with the predictions of Izzard's 100% efficiency equation revealed that Izzard's equation overestimated the capacity of the inlets. Izzard's less than 100% efficiency equation gave acceptable agreement with the experimental data for 5-ft inlet lengths, but overestimated the capacity of the 4.57-m inlet lengths.

Because the 1.52-m inlet lengths showed the best (but still not acceptable) agreement with Izzard's 100% efficiency equation, and hence had the best (though not necessarily acceptable) predictions of L_r to be used in the less than 100% efficiency equation, it was hypothesized that Izzard's less than 100% efficiency equation might be an acceptably accurate equation for the curb inlets, provided that a good prediction of the value of L_r was available to use in Izzard's equation. Therefore, an empirical 100% efficiency equation was sought for the inlets. It was found that at 100% efficiency, a different linear relationship exists between the calculated normal depth (y_n) and the flow captured per unit of inlet length (q_L) for each inlet length tested, with no appreciable segregation of the inlet types. Therefore, two different linear 100% efficiency equations were developed, one for 1.52-m inlet lengths and one for 4.57-m inlet lengths (Equations 4.2 and 4.3). No distinction was necessary between Type D and Type C inlets.

When the new empirical 100% efficiency equations were used along with Izzard's less than 100% efficiency equations, acceptable agreement was obtained with the experimental data for both inlet lengths tested. Therefore, it was proved that Izzard's less than 100% efficiency equation was an acceptably accurate predictor of the less than 100% efficiency capacity of the inlets, as long as an accurate prediction of the 100% efficiency capacity was available to use in

Izzard's equation. However, it was recognized that the use of different empirical 100% efficiency equations for each inlet length is inconvenient. It was desired to develop a single empirical 100% efficiency equation which would be applicable for a range of inlet lengths.

To develop an empirical 100% efficiency equation for a range of inlet lengths, the use of the effective length concept developed by Holley et al. (1992) was explored. The basic premise of the effective length concept is that the net effect of the upstream and downstream depression transitions is to increase the capacity of the inlet, thus causing the inlet to behave as if its effective inlet length were longer than its physical length. Calculations performed using the trends of the experimental data showed that the depression transitions cause the inlets to behave at 100% efficiency as if their inlet openings were 3.05-m longer than the length of the actual openings. Thus, the effective length of an inlet is equal to the physical inlet opening length plus 3.05-m. A new empirical 100% efficiency equation was developed on the basis of the inlet's effective length (Equation 4.6) and showed good agreement with the less than 100% efficiency experimental data when used in Izzard's less than 100% efficiency equation.

In order to verify the applicability of the effective length concept, tests were conducted on undepressed curb inlets. Since these inlets have no depression transitions, the effective inlet length is equal to the physical inlet opening length. The experiments on undepressed curb inlets fit the predictions of the effective length 100% efficiency equation and Izzard's less than 100% efficiency equation very well, with the exception of the 1.52-m 100% efficiency data. The behavior of the 1.52-m undepressed inlet at 100% efficiency illustrated the principle of diminishing returns associated with increasing lengths of curb inlets.

This research project resulted in the development of a design method for TxDOT Type C and Type D curb inlets. The inlets are designed on the basis of their effective lengths, which are 3.05 m longer than the physical length of their inlet opening. A new empirical 100% efficiency equation was developed. To predict the less than 100% efficiency capacity of the inlets, the new empirical 100% efficiency equation is used along with Izzard's less than 100% efficiency equation for depressed curb inlets. The design method is applicable for inlet lengths between

1.52 m and 4.57 m, for longitudinal slopes between 0.004 and 0.06, for transverse slopes of 0.0208 (1:48) and 0.0417 (1:24), for approach flows up to 0.26 m^3/s, and for captured flow rates up to 0.25 m^3/s.

6.2 CONCLUSIONS FOR BRIDGE DECK DRAINS

The first phase of the experimental work on bridge deck drains in this project was aimed at developing a discharge relationship for Drain 2B. Experiments were conducted on Drain 2B for various approach flow rates and transverse and longitudinal roadway slopes. The experiments revealed that, like Drain 2 tested by Holley et al. (1992), Drain 2B exhibited a transition from weir control to orifice flow. However, the transition for Drain 2B was much more gradual than the sharp transition which occurred for Drain 2. The difference in the hydraulic characteristics of the two drains was caused by the orientation of the drain pan. In general, the capacity of Drain 2B was less than that of Drain 2, primarily because the shallow part of Drain 2B (the part with the least capacity) was located next to the curb, where the greatest percentage of approach flow is concentrated. However, the experiments showed that the capacities of Drain 2 and Drain 2B are approximately equal for low approach flow rates, when both drains are in the weir control regime.

Because the transition from weir control to orifice control was gradual for Drain 2B, it was possible to fit one equation to the entire range of experimental data (both weir control and orifice control). The design equation which was developed for Drain 2B (Equation 5.2) is a function of the roadway geometry (longitudinal and transverse slopes) and the calculated normal depth of the approach flow. This equation was able to predict the capacity of Drain 2B with a standard error of 0.00096 m^3/s. Equation 5.2 is applicable for longitudinal roadway slopes between 0.004 and 0.06, for transverse slopes from 0.0208 to 0.0417, for approach flow rates from 0.006 to 0.12 m^3/s, and for captured flow rates between 0.005 and 0.025 m^3/s.

The experiments on Drain 2B revealed that its capacity for higher approach flow rates was significantly less than that of Drain 2. The orientation of Drain 2B is less than optimum from a hydraulic standpoint. During the experimental work, it was observed that the capacity of

a drain in the orientation of Drain 2B could be improved with the use of a deeper, larger drain pan. Consequently, TxDOT hydraulic design personnel developed a new bridge deck drain design with a larger drain pan and a grate with transverse bars inclined in the direction of the approach flow (see Figures 5.8 to 5.9). This drain was designated Drain 4 in this research project. Drain 4 is 0.041 m deeper than Drain 2B at its shallow end and 0.038 m deeper than Drain 2B at its deep end. Furthermore, Drain 4 has an 0.203-m outlet pipe, compared to the 0.152-m outlet of Drain 2B.

The experiments on Drain 4 revealed that the design changes were extremely effective in increasing the capacity of the drain. In general, Drain 4 had a much greater capacity than Drain 2B. The most important design changes which increased the capacity of Drain 4 seem to be the deeper drain pan and the larger outlet pipe.

For Drain 4, separate design equations were developed for lower and higher flows (Equations 5.3 and 5.4). The equations are a function of the longitudinal and transverse roadway slopes and the calculated normal depth of the approach flow. The standard errors of the equations for weir flow and orifice flow are 0.0014 and 0.0020 m^3/s, respectively. An equation (Equation 5.5) was developed to predict the dividing line between low and high flows for the two equations. In addition, a single equation was fit to the entire range of data for Drain 4. The equation was also a function of the roadway slopes and the calculated normal depths (Equation 5.7). The standard error of Equation 5.7 is 0.0022 m^3/s. All of the equations developed for Drain 4 are applicable for longitudinal slopes between 0.004 and 0.06, for transverse slopes from 0.0208 to 0.0417, for approach flow rates between 0.014 and 0.20 m^3/s, and for captured flow rates between 0.014 and 0.068 m^3/s.

REFERENCES

AISC. *Manual of Steel Construction. Load and Resistance Factor Design*, First Edition. American Institute of Steel Construction, Chicago, 1986, p. 1-167.

Bauer, W. J. and D. C. Woo. "Hydraulic Design of Depressed Curb-Opening Inlets," *Highway Research Record*, No. 58, 1964, pp. 61-80.

Bos, M. G. *Discharge Measurement Structures*, International Institute for Land Reclamation and Improvement, Publication 20, Wageningen, The Netherlands, 1989, pp. 45-46, 54-58, 153, 158-164.

Burgi, P. H., and D. E. Gober. "Hydraulic and Safety Characteristics of Selected Grate Inlets," *Transportation Research Record*, No. 685, 1978, pp. 29-31.

Chang, F. F. M., D. C. Woo, and R. D. Thomas. "Bicycle-Safe Grate Inlets," *Urban Stormwater Hydraulics and Hydrology*, Proceedings of the Second International Conference on Urban Storm Drainage, 1982, pp. 101-109.

Federal Highway Administration (FHWA). Johnson, F. L. and F. F. M. Chang. *Hydraulic Engineering Circular No. 12. Drainage of Highway Pavements*, FHWA-TS-84-202, 1984, 136 pp.

Forbes, H. J. C. "Capacity of Lateral Stormwater Inlets," *The Civil Engineer in South Africa,* Vol. 18, No. 9, September, 1976, pp. 195-205.

Henderson, F. M. *Open Channel Hydraulics*, Macmillan, New York, 1966, p. 36.

Holley, E. R., C. Woodward, A. Brignetti, and C. Ott. "Hydraulic Characteristics of Recessed Curb Inlets and Bridge Drains," *Research Report 1267-1F*, Project 3-5-91/2-1267, Center for Transportation Research, The University of Texas at Austin, 1992, 80 pp.

Hotchkiss, H. H., D. E. Bohac, and J. Truby. "New Lessons about the Hydraulic Performance of Highway Storm Sewer Inlets," *Hydraulic Engineering*, Proceedings of the 1991 National Conference of the Hydraulics Division of the American Society of Civil Engineers, ASCE, New York, 1991, pp. 103-108.

Izzard, C. F. "Hydraulics of Runoff from Developed Surfaces," *Proceedings, 26th Annual Meeting,* Highway Research Board, 1946, pp. 129-150.

Izzard, C. F. "Tentative Results on Capacity of Curb Opening Inlets," *Research Report No. 11-B*, Highway Research Board, 1950, pp. 36-51.

Izzard, C. F. "Simplified Method for Design of Curb-Opening Inlets," *Transportation Research Record*, No. 631, 1977, pp. 39-46.

Johns Hopkins University. *The Design of Storm-Water Inlets*, Report of the Storm Drainage Research Committee of the Storm Drainage Research Project, Baltimore, 1956, pp. 143-181.

Kindsvater, C. E., and R. W. C. Carter. "Discharge Characteristics of Rectangular Thin-Plate Weirs." *Journal of the Hydraulics Division*, Proceedings of the American Society of Civil Engineers, Vol. 87, No. HY6, June, 1957.

Larson, C. L. "Experiments on Flow Through Inlet Gratings for Street Gutters," *Research Report No. 6-B*, Highway Research Board, 1948, pp. 17-26.

Li, W. H., K. K. Sorteberg, and J. C. Geyer. "Hydraulic Behavior of Storm-Water Inlets. I. Flow Into Gutter Inlets in a Straight Gutter Without Depression." *Sewage and Industrial Wastes*, Vol. 23, No. 1, January, 1951a, pp. 129-141.

Li, W. H., K. K. Sorteberg, and J. C. Geyer. "Hydraulic Behavior of Storm-Water Inlets. II. Flow Into Curb-Opening Inlets." *Sewage and Industrial Wastes*, Vol. 23, No. 6, June, 1951b, pp. 143-159.

Li, W.H. "Hydraulic Theory for Design of Storm-Water Inlets," *Proceedings, 33rd Annual Meeting*, Highway Research Board, 1954, pp. 83-91.

Roberson, J. A., J. J. Cassiday, and M. H. Chaudhry. *Hydraulic Engineering,* Houghton Mifflin, Boston, 1988, pp. 410-411.

Smith, S.L and E.R. Holley, *The Effects of Various Piping Configurations on the Capacity of a Bridge Deck Drain, Research Report 1409-2F*, Project 0-1409, Center for Transportation Research, The University of Texas at Austin, 1995, 104 pp.

Streeter, V. L., and E. B. Wylie. *Fluid Mechanics*, 8th Edition, McGraw-Hill, New York, 1985, pp. 367-370.

Uyumaz, A. "Discharge Capacity for Curb-Opening Inlets," *Journal of Hydraulic Engineering*, ASCE, Vol. 118, No. 7, July, 1992, pp. 1048-1051.

Wasley, R. J. "Hydrodynamics of Flow Into Curb-Opening Inlets," *Technical Report No. 6*, Stanford University, 1960, 108 pp. + appendices.

Wasley, R. J. "Hydrodynamics of Flow Into Curb-Opening Inlets," *Journal of the Engineering Mechanics Division*, Proceedings of the American Society of Civil Engineers, Vol. 87, No. EM4, August, 1961, pp. 1-18.

APPENDIX A. LIST OF SYMBOLS

Symbol	Definition (Dimensions)
a	depth of curb inlet depression (L)
a′	equivalent depth of depression for depressed curb inlets (L)
A	cross-sectional area of flow in the roadway (L^2)
A_1	cross-sectional area of venturi meter approach pipe (L^2)
A_2	cross-sectional area of venturi meter throat (L^2)
B	width of V-notch weir approach channel (L)
C	empirical coefficient in Li et al.'s depressed curb inlet equations (L)
C_d	venturi meter discharge coefficient
C_{ev}	V-notch weir effective discharge coefficient
D	pipe diameter (L)
d_{50}	median sand grain size (L)
E_o	ratio of flow in depression to the total approach flow
F_w	Froude number of flow at a distance W normal to the curb face
Fr	Froude number
g	gravitational acceleration (L/T^2)
h	hydraulic head (elevation head + pressure head) (L)
H	total head (elevation head + pressure head + velocity head) (L)
h_1	head on V-notch weir (L)
h_e	effective head on V-notch weir (L)
K	empirical coefficient in Li et al.'s curb inlet equations
K	coefficient in venturi meter equation
K_h	head correction for surface tension and viscosity effects on V-notch weir (L)
L	length of curb inlet opening (L)
L_a	additional effective curb inlet length contributed by transitions (L)

L_{eff}	total effective length of curb inlet (L)
L_r	length of curb inlet opening required to capture 100% of approach flow (L)
$L_{r,eff}$	effective length of curb inlet required to capture 100% of approach flow (L)
L_2	length of downstream depression transition (L)
M	empirical coefficient in Li et al.'s depressed curb inlet equations
n	Manning's roughness coefficient
n_r	ratio of Manning's n of model to that of prototype
P	height of bottom of weir notch above channel invert (L)
P_w	wetted perimeter of roadway flow
q_L	captured flow per unit of inlet length (L^2/T)
$q_{L,eff}$	captured flow per unit of effective inlet length (L^2/T)
Q	flow captured by curb inlet (L^3/T)
Q_a	approach flow rate (L^3/T)
Q_{co}	carryover flow rate (L^3/T)
Q_r	ratio of flow rate in model to that in prototype
Q_s	flow rate outside of the depressed section of a curb inlet (L^3/T)
Q_w	flow rate contained in depressed section of a depressed curb inlet (L^3/T)
Q_2	flow rate captured by Drain 2 (L^3/T)
Q_{2B}	flow rate captured by Drain 2B (L^3/T)
Q_4	flow rate captured by Drain 4 (L^3/T)
R_h	hydraulic radius of flow in the roadway (L)
Re	pipe flow Reynolds number
S	longitudinal roadway slope
S_e	equivalent transverse slope for depressed curb inlets
S_f	friction slope of roadway flow
S_x	transverse roadway slope
T	ponded width of approach flow (L)

T_l	reference ponded width less than T (L)
V_L	velocity in longitudinal direction (L/T)
V_r	ratio of velocity in model to that in prototype
V_T	velocity in transverse direction (L/T)
W	width of curb inlet depression (L)
x	distance along the inlet lip measured from upstream end of curb inlet (L)
y	depth of flow in depressed gutter (L)
y_c	critical depth of approach flow (L)
y_m	measured depth of approach flow (L)
y_n	calculated normal depth of approach flow (L)
y_l	reference flow depth less than y_n (L)
Δh	difference in piezometric head between venturi meter entrance and throat (L)
Λ_r	length scale ratio of model to prototype
ν	kinematic viscosity of water (L^2/T)
θ	V-notch weir notch angle
θ	angle between curb face and depressed gutter
θ_o	angle between curb face and undepressed gutter

APPENDIX B. EXPERIMENTAL DATA

The tables in this appendix summarize the experimental data for curb inlets and bridge deck drains. Tables B.1-B.3 present data for curb inlets and Tables B.4-B.5 present data for bridge deck drains. The definition of the variables from left to right in Tables B.1-B.3 are as follows:

- L = length of inlet opening
- Eff = indicates whether test was performed at 100% efficiency (*) or less than 100% efficiency (<)
- S = longitudinal slope
- S_x = transverse slope
- Q_a = approach flow rate (m^3/s)
- Q = captured flow rate (m^3/s)
- Q_{co} = carryover flow rate (m^3/s)
- y_m = measured flow depth upstream of the inlet (m)
- y_n = calculated normal depth of flow upstream of the inlet (m)
- T = measured ponded width upstream of the inlet (m)
- $y_{u/s}$ = measured depth just upstream of the inlet opening (m)
- $y_{d/s}$ = measured depth just downstream of the inlet opening (m)

The definition of the variables from left to right in Tables B.4-B.5 are as follows:

- S = longitudinal slope
- S_x = transverse slope
- Q_a = approach flow rate (m^3/s)
- Q = captured flow rate (m^3/s)
- Q_{co} = carryover flow rate (m^3/s)
- y_m = measured flow depth upstream of the inlet (m)
- y_n = calculated normal depth of flow upstream of the inlet (m)
- T = measured ponded width upstream of the inlet (m)

All data in the appendices have been scaled to prototype conditions. Blank entries indicate no measurements were taken.

Table B.1 Data for Type C Curb Inlets

TEST	L (m)	Eff	S	S_x	Q_e (m^3/s)	Q (m^3/s)	Q_{co} (m^3/s)	y_m (m)	y_n (m)	T (m)	$y_{u/s}$ (m)	$y_{d/s}$ (m)
C01	1.52	<	0.004	0.021	0.2400	0.1256	0.1086	0.133	0.123	4.27	0.175	0.159
C02	1.52	<	0.004	0.021	0.1076	0.0829	0.0300	0.096	0.091	4.27	0.147	0.131
C03	1.52	<	0.01	0.021	0.2361	0.1098	0.1219	0.117	0.103	4.27	0.167	0.121
C04	1.52	<	0.01	0.021	0.1806	0.0983	0.0838	0.104	0.093	4.27	0.167	0.101
C05	1.52	<	0.02	0.021	0.1246	0.0741	0.0552	0.079	0.071	3.45	0.139	0.097
C06	1.52	<	0.02	0.021	0.2424	0.0979	0.1369	0.101	0.091	4.27	0.163	0.183
C07	1.52	<	0.04	0.021	0.1281	0.0698	0.0626	0.076	0.063	4.07	0.135	0.093
C08	1.52	<	0.04	0.021	0.1589	0.0762	0.0852	0.075	0.068	4.07	0.135	0.101
C09	1.52	<	0.06	0.021	0.1166	0.0653	0.0560	0.065	0.056	4.07	0.131	0.109
C10	1.52	<	0.06	0.021	0.2451	0.0835	0.1519	0.083	0.075	4.27	0.147	0.143
C11	1.52	*	0.06	0.021	0.0144	0.0150	0.0	0.027	0.025	3.33	0.093	0.020
C12	1.52	*	0.04	0.021	0.0185	0.0191	0.0	0.035	0.031	2.52	0.097	0.028
C13	1.52	*	0.02	0.021	0.0228	0.0232	0.0	0.041	0.037	1.87	0.101	0.036
C14	1.52	*	0.01	0.021	0.0367	0.0355	0.0	0.057	0.051	2.48	0.113	0.069
C15	1.52	*	0.004	0.021	0.0423	0.0402	0.0	0.064	0.064	3.01	0.121	0.073
C16	1.52	*	0.04	0.021	0.0172	0.0177	0.0	0.033	0.029	2.76	0.093	0.032
C17	1.52	*	0.08	0.021	0.0031	0.0000	0.0	0.013	0.013	2.03	0.040	0.000
C18	1.52	*	0.06	0.042	0.0361	0.0351	0.0	0.044	0.047	1.13	0.113	0.040
C19	1.52	*	0.04	0.042	0.0468	0.0448	0.0	0.055	0.056	1.39	0.125	0.061
C20	1.52	*	0.02	0.042	0.0601	0.0583	0.0	0.072	0.071	1.71	0.139	0.081
C21	1.52	*	0.01	0.042	0.0675	0.0655	0.0	0.085	0.084	2.03	0.147	0.085
C22	1.52	*	0.004	0.042	0.0815	0.0819	0.0	0.119	0.107	2.56	0.163	0.113
C23	1.52	<	0.004	0.042	0.2316	0.1488	0.0778	0.164	0.157	3.87	0.211	0.203
C24	1.52	<	0.004	0.042	0.1439	0.1182	0.0289	0.137	0.132	3.21	0.183	0.163
C25	1.52	<	0.01	0.042	0.1433	0.1133	0.0333	0.119	0.111	2.84	0.171	0.163
C26	1.52	<	0.01	0.042	0.2320	0.1369	0.0924	0.139	0.133	3.37	0.203	0.244
C27	1.52	<	0.02	0.042	0.2433	0.1215	0.1156	0.112	0.119	2.97	0.199	0.203
C28	1.52	<	0.02	0.042	0.1031	0.0870	0.0191	0.089	0.085	2.28	0.159	0.109
C29	1.52	<	0.05	0.042	0.1724	0.0874	0.0864	0.096	0.088	2.16	0.143	0.163
C30	1.52	<	0.05	0.042	0.2381	0.0940	0.1398	0.109	0.099	3.09	0.163	0.163
C31	1.52	<	0.07	0.021	0.1542	0.0700	0.0872	0.064	0.061	4.07	0.135	0.121
C32	1.52	<	0.07	0.042	0.1535	0.0803	0.0782	0.087	0.079	3.05	0.143	0.163
C33	4.57	*	0.004	0.021	0.0950	0.0959	0.0	0.091	0.087	4.07	0.151	0.073
C34	4.57	*	0.01	0.021	0.0716	0.0698	0.0	0.069	0.065	3.09	0.125	0.045
C35	4.57	*	0.02	0.021	0.0546	0.0519	0.0	0.052	0.052	2.52	0.117	0.045
C36	4.57	*	0.05	0.021	0.0263	0.0269	0.0	0.036	0.033	2.48	0.101	0.024
C37	4.57	*	0.07	0.021	0.0099	0.0000	0.0	0.029	0.021	2.72	0.065	0.008
C38	4.57	*	0.06	0.042	0.0751	0.0743	0.0	0.060	0.063	1.55	0.135	0.040
C39	4.57	*	0.04	0.042	0.1035	0.1041	0.0	0.075	0.076	1.95	0.151	0.057
C40	4.57	*	0.02	0.042	0.1379	0.1410	0.0	0.095	0.096	2.48	0.163	0.077
C41	4.57	*	0.01	0.042	0.1763	0.1761	0.0	0.125	0.120	2.97	0.183	0.089
C42	4.57	*	0.004	0.042	0.2040	0.2018	0.0	0.151	0.151	3.49	0.199	0.109
C43	4.57	<	0.004	0.021	0.2408	0.1911	0.0456	0.129	0.123	4.27	0.175	0.135
C44	4.57	<	0.01	0.021	0.2406	0.1731	0.0628	0.111	0.104	4.27	0.171	0.121
C45	4.57	<	0.02	0.021	0.2404	0.1529	0.0813	0.095	0.091	4.27	0.163	0.121
C46	4.57	<	0.04	0.021	0.2400	0.1462	0.0897	0.088	0.080	4.27	0.147	0.101
C47	4.57	<	0.06	0.021	0.2400	0.1394	0.0967	0.083	0.073	4.27	0.143	0.081
C48	4.57	<	0.06	0.042	0.2371	0.1743	0.0593	0.107	0.096	2.72	0.155	0.081
C49	4.57	<	0.04	0.042	0.2371	0.1802	0.0509	0.112	0.103	2.44	0.163	0.121
C50	4.57	<	0.02	0.042	0.2494	0.2168	0.0289	0.119	0.120	3.01	0.191	0.121
C51	4.57	<	0.01	0.042	0.2488	0.2277	0.0166	0.143	0.136	3.41	0.199	0.143
C52	4.57	<	0.004	0.042	0.2494	0.2361	0.0078	0.161	0.161	3.87	0.207	0.143

Table B.2 Data for Type D Curb Inlets

TEST	L (m)	Eff	S	S_x	Q_a (m^3/s)	Q (m^3/s)	Q_{co} (m^3/s)	y_m (m)	y_n (m)	T (m)	$y_{u/s}$ (m)	$y_{d/s}$ (m)
D01	1.52	*	0.004	0.0208	0.0427	0.0419	0.0	0.067	0.064	3.05		
D02	1.52	*	0.01	0.0208	0.0326	0.0318	0.0	0.055	0.049	2.32	0.105	0.057
D03	1.52	*	0.02	0.0208	0.0246	0.0250	0.0	0.041	0.039	1.87	0.093	0.049
D04	1.52	*	0.04	0.0208	0.0146	0.0168	0.0	0.029	0.028	1.63	0.081	0.028
D05	1.52	*	0.06	0.0208	0.0090	0.0101	0.0	0.023	0.021	2.03	0.061	0.004
D06	1.52	*	0.06	0.0417	0.0285	0.0279	0.0	0.044	0.043	1.05	0.105	0.016
D07	1.52	*	0.04	0.0417	0.0370	0.0357	0.0	0.052	0.052	1.25	0.117	0.028
D08	1.52	*	0.02	0.0417	0.0523	0.0511	0.0	0.067	0.067	1.63	0.121	0.061
D09	1.52	*	0.01	0.0417	0.0634	0.0612	0.0	0.083	0.081	1.99	0.135	0.077
D10	1.52	*	0.004	0.0417	0.0702	0.0688	0.0	0.099	0.100	2.40	0.151	0.085
D11	1.52	<	0.004	0.0417	0.1677	0.1197	0.0519	0.140	0.140	3.33	0.175	0.163
D12	1.52	<	0.01	0.0417	0.1659	0.1092	0.0593	0.123	0.117	2.88	0.183	0.203
D13	1.52	<	0.02	0.0417	0.1659	0.0967	0.0710	0.100	0.103	2.64	0.167	0.163
D14	1.52	<	0.04	0.0417	0.2568	0.0936	0.1579	0.117	0.107	2.48	0.163	0.183
D15	1.52	<	0.06	0.0417	0.2266	0.0844	0.1402	0.109	0.093		0.151	0.203
D16	1.52	<	0.06	0.0208	0.2279	0.0735	0.1494	0.073	0.072	4.27	0.139	0.183
D17	1.52	<	0.04	0.0208	0.1361	0.0640	0.0774	0.069	0.064	4.07	0.135	0.143
D18	1.52	<	0.02	0.0208	0.2418	0.0870	0.1507	0.097	0.091	4.27	0.163	0.163
D19	1.52	<	0.01	0.0208	0.2424	0.1004	0.1377	0.113	0.104	4.27	0.163	0.203
D20	1.52	<	0.004	0.0208	0.1113	0.0768	0.0390	0.091	0.092	4.27	0.143	0.125
D21	4.57	<	0.004	0.0208	0.2484	0.1880	0.0544	0.128	0.124	4.27	0.171	0.139
D22	4.57	<	0.01	0.0208	0.1648	0.1363	0.0310	0.097	0.089	4.27	0.147	0.109
D23	4.57	<	0.02	0.0208	0.2564	0.1595	0.0897	0.100	0.093	4.27	0.163	0.105
D24	4.57	<	0.04	0.0208	0.1599	0.1137	0.0507	0.077	0.068	4.03	0.135	0.077
D25	4.57	<	0.06	0.0208	0.1802	0.1156	0.0647	0.067	0.067	4.27	0.135	0.081
D26	4.57	<	0.06	0.0417	0.1451	0.1295	0.0205	0.083	0.080	1.91	0.139	0.081
D27	4.57	<	0.04	0.0417	0.2509	0.1843	0.0601	0.117	0.105	2.48	0.163	0.113
D28	4.57	<	0.02	0.0417	0.2309	0.2024	0.0238	0.115	0.116	2.92	0.183	0.121
D29	4.57	<	0.01	0.0417	0.2597	0.2270	0.0185	0.144	0.139	3.41	0.195	0.143
D30	4.57	<	0.004	0.0417	0.2601	0.2346	0.0144	0.165	0.164	3.87	0.199	0.143
D31	4.57	*	0.004	0.0417	0.1887	0.1874	0.0	0.148	0.145	3.53	0.187	0.085
D32	4.57	*	0.01	0.0417	0.1671	0.1679	0.0	0.121	0.117	2.92	0.175	0.081
D33	4.57	*	0.02	0.0417	0.1332	0.1369	0.0	0.093	0.095	2.44	0.163	0.061
D34	4.57	*	0.04	0.0208	0.0380	0.0374	0.0	0.041	0.040		0.101	0.057
D35	4.57	*	0.06	0.0208	0.0203	0.0216	0.0	0.031	0.029	2.88	0.085	0.012

Table B.3 Data for Type O Curb Inlets

TEST	L (m)	Eff	S	S_x	Q_s (m^3/s)	Q (m^3/s)	Q_{cn} (m^3/s)	y_m (m)	y_n (m)	T (m)	$y_{u/s}$ (m)	$y_{d/s}$ (m)
O01	4.57	*	0.004	0.0208	0.0441	0.0431	0.0	0.068	0.065	3.05		
O02	4.57	*	0.01	0.0208	0.0281	0.0291	0.0	0.051	0.047	2.28	0.053	0.0
O03	4.57	*	0.02	0.0208	0.0185	0.0209	0.0	0.037	0.035	1.71	0.040	0.0
O04	4.57	*	0.04	0.0208	0.0166	0.0177	0.0	0.031	0.029	1.83	0.040	0.0
O05	4.57	*	0.06	0.0208	0.0101	0.0142	0.0	0.025	0.023	2.24	0.032	0.0
O06	4.57	*	0.06	0.0417	0.0339	0.0339	0.0	0.047	0.047	1.09	0.053	0.0
O07	4.57	*	0.04	0.0417	0.0429	0.0427	0.0	0.055	0.055	1.31	0.061	0.0
O08	4.57	*	0.02	0.0417	0.0540	0.0532	0.0	0.068	0.068	1.63	0.069	0.0
O09	4.57	*	0.01	0.0417	0.0686	0.0690	0.0	0.087	0.084	1.91	0.081	0.0
O10	4.57	*	0.004	0.0417	0.0901	0.0936	0.0	0.112	0.111	2.64	0.097	0.0
O11	4.57	<	0.004	0.0208	0.2478	0.1568	0.0833	0.132	0.124	4.27	0.113	0.101
O12	4.57	<	0.01	0.0208	0.0856	0.0704	0.0193	0.076	0.071	3.49	0.073	0.061
O13	4.57	<	0.02	0.0208	0.1965	0.1012	0.0936	0.092	0.084	4.11	0.093	0.081
O14	4.57	<	0.04	0.0208	0.1328	0.0753	0.0624	0.071	0.064	3.99	0.081	0.073
O15	4.57	<	0.06	0.0208	0.0725	0.0499	0.0250	0.051	0.047	3.83	0.061	0.045
O16	4.57	<	0.06	0.0417	0.1741	0.1076	0.0688	0.095	0.085	2.24	0.093	0.081
O17	4.57	<	0.04	0.0417	0.1070	0.0911	0.0209	0.075	0.076	1.95	0.085	0.081
O18	4.57	<	0.02	0.0417	0.1907	0.1394	0.0507	0.105	0.108	2.80	0.121	0.121
O19	4.57	<	0.01	0.0417	0.2293	0.1702	0.0548	0.139	0.132	3.33	0.131	0.143
O20	4.57	<	0.004	0.0417	0.2564	0.2030	0.0464	0.167	0.164	4.03	0.143	0.143
O21	1.52	<	0.004	0.0208	0.1597	0.0511	0.1102	0.111	0.105	4.27	0.093	0.121
O22	1.52	<	0.01	0.0208	0.1718	0.0419	0.1322	0.099	0.091	4.27	0.093	0.121
O23	1.52	<	0.02	0.0208	0.1735	0.0398	0.1330	0.087	0.080	4.27	0.085	0.073
O24	1.52	<	0.04	0.0208	0.1815	0.0355	0.1343	0.079	0.072	4.27	0.081	0.073
O25	1.52	<	0.06	0.0208	0.1757	0.0318	0.1431	0.071	0.065	4.27	0.077	0.065
O26	1.52	<	0.04	0.0417	0.1234	0.0427	0.0844	0.081	0.081	2.03	0.097	0.081
O27	1.52	<	0.02	0.0417	0.1751	0.0569	0.1168	0.104	0.105	2.68	0.117	0.040
O28	1.52	<	0.01	0.0417	0.1626	0.0591	0.1047	0.121	0.116	2.80	0.121	0.081
O29	1.52	<	0.004	0.0417	0.1572	0.0690	0.0891	0.141	0.136	3.25	0.121	0.163
O30	1.52	*	0.004	0.0208	0.0103	0.0101	0.0	0.039	0.037	1.71	0.040	0.0
O31	1.52	*	0.01	0.0208	0.0094	0.0092	0.0	0.033	0.031	1.47	0.036	0.0
O32	1.52	*	0.02	0.0208	0.0092	0.0092	0.0	0.029	0.027	1.21	0.032	0.0
O33	1.52	*	0.04	0.0208	0.0060	0.0064	0.0	0.019	0.020	0.97	0.028	0.0
O34	1.52	*	0.06	0.0208	0.0049	0.0049	0.0	0.016	0.017	0.89	0.045	0.0
O35	1.52	*	0.06	0.0417	0.0060	0.0062	0.0	0.024	0.024	0.61	0.028	0.0
O36	1.52	*	0.04	0.042	0.0086	0.0080	0.0	0.029	0.029	0.73	0.032	0.0
O37	1.52	*	0.02	0.042	0.0111	0.0107	0.0	0.037	0.037	0.89	0.040	0.0
O38	1.52	*	0.01	0.042	0.0162	0.0156	0.0	0.052	0.049	1.09	0.049	0.0
O39	1.52	*	0.004	0.042	0.0191	0.0189	0.0	0.060	0.061	1.39	0.053	0.0

Table B.4 Data for Drain 2B

TEST	S	S_x	Q_a (m^3/s)	Q_{2B} (m^3/s)	Q_{co} (m^3/s)	y_m (m)	y_n (m)	T (m)
2B1	0.004	0.0208	0.0156	0.0133	0.0016	0.042	0.043	2.00
2B2	0.004	0.0208	0.0072	0.0073	0.0008	0.033	0.033	1.52
2B3	0.004	0.0208	0.0231	0.0171	0.0052	0.048	0.050	2.29
2B4	0.004	0.0208	0.0374	0.0216	0.0178	0.062	0.060	2.96
2B5	0.01	0.0208	0.0374	0.0212	0.0181	0.052	0.051	2.51
2B6	0.01	0.0208	0.0245	0.0180	0.0072	0.043	0.043	2.07
2B7	0.01	0.0208	0.0141	0.0125	0.0020	0.036	0.035	1.68
2B8	0.02	0.0208	0.0140	0.0125	0.0020	0.033	0.031	1.40
2B9	0.02	0.0208	0.0355	0.0204	0.0173	0.045	0.044	2.14
2B10	0.02	0.0208	0.0232	0.0168	0.0068	0.040	0.037	1.77
2B11	0.04	0.0208	0.0231	0.0161	0.0077	0.034	0.033	1.46
2B12	0.04	0.0208	0.0136	0.0118	0.0023	0.027	0.027	1.22
2B13	0.04	0.0208	0.0055	0.0054	0.0003	0.020	0.019	0.91
2B14	0.06	0.0208	0.0055	0.0054	0.0007	0.018	0.018	0.88
2B15	0.06	0.0208	0.0305	0.0170	0.0149	0.032	0.034	1.54
2B16	0.06	0.0208	0.0231	0.0152	0.0083	0.028	0.030	1.52
2B17	0.06	0.0417	0.0231	0.0123	0.0109	0.039	0.039	0.94
2B18	0.06	0.0417	0.0059	0.0054	0.0010	0.022	0.023	0.61
2B19	0.06	0.0417	0.0132	0.0096	0.0037	0.030	0.032	0.79
2B20	0.04	0.0417	0.0131	0.0103	0.0033	0.032	0.034	0.82
2B21	0.04	0.0417	0.0100	0.0085	0.0020	0.029	0.031	0.73
2B22	0.04	0.0417	0.0317	0.0152	0.0176	0.045	0.048	1.19
2B23	0.02	0.0417	0.0317	0.0177	0.0155	0.055	0.054	1.28
2B24	0.02	0.0417	0.0059	0.0059	0.0008	0.030	0.029	0.70
2B25	0.02	0.0417	0.0169	0.0123	0.0046	0.041	0.043	0.98
2B26	0.01	0.0417	0.0169	0.0132	0.0038	0.046	0.049	1.16
2B27	0.01	0.0417	0.0078	0.0076	0.0008	0.036	0.037	0.88
2B28	0.01	0.0417	0.0256	0.0171	0.0094	0.054	0.057	1.37
2B29	0.004	0.0417	0.0255	0.0180	0.0085	0.065	0.068	1.58
2B30	0.004	0.0417	0.0165	0.0132	0.0031	0.054	0.058	1.30
2B31	0.004	0.0417	0.0064	0.0061	0.0005	0.037	0.040	0.94
2B32	0.005	0.0208	0.0420	0.0216	0.0225	0.061	0.060	
2B33	0.005	0.0208	0.0303	0.0232	0.0371	0.070	0.068	
2B34	0.01	0.0208	0.0587	0.0227	0.0374	0.062	0.060	
2B35	0.02	0.0208	0.0887	0.0237	0.0677	0.060	0.062	
2B36	0.04	0.0208	0.0676	0.0213	0.0479	0.046	0.049	
2B37	0.06	0.0208	0.0524	0.0193	0.0357	0.042	0.041	
2B38	0.06	0.0417	0.0492	0.0167	0.0356	0.050	0.052	
2B39	0.04	0.0417	0.0466	0.0180	0.0319	0.055	0.055	
2B40	0.02	0.0417	0.0691	0.0232	0.0479	0.075	0.073	
2B41	0.01	0.0417	0.0539	0.0231	0.0338	0.079	0.075	
2B42	0.004	0.0417	0.0628	0.0237	0.0393	0.091	0.095	
2B43	0.04	0.0417	0.1224	0.0245	0.0944	0.075	0.079	
2B44	0.06	0.0417	0.1234	0.0250	0.0927	0.072	0.073	
2B45	0.06	0.0208	0.1202	0.0242	0.0944	0.053	0.056	
2B46	0.04	0.0208	0.1237	0.0249	0.0936	0.057	0.061	

Table B.5 Data for Drain 4

TEST	S	S_x	Q_s (m^3/s)	Q_{2B} (m^3/s)	Q_{co} (m^3/s)	y_m (m)	y_n (m)	T (m)
4_01	0.004	0.0417	0.1187	0.0574	0.0549	0.121	0.120	2.96
4_02	0.004	0.0417	0.0785	0.0450	0.0315	0.103	0.103	2.50
4_03	0.004	0.0417	0.0412	0.0348	0.0082	0.081	0.081	1.98
4_04	0.01	0.0417	0.0428	0.0336	0.0103	0.071	0.069	1.68
4_05	0.01	0.0417	0.0709	0.0416	0.0293	0.087	0.084	2.01
4_06	0.01	0.0417	0.1187	0.0547	0.0583	0.104	0.101	2.41
4_07	0.02	0.0417	0.1187	0.0514	0.0610	0.091	0.089	2.19
4_08	0.02	0.0417	0.0752	0.0399	0.0336	0.079	0.075	1.80
4_09	0.02	0.0417	0.0374	0.0298	0.0082	0.060	0.058	1.40
4_10	0.04	0.0417	0.0376	0.0278	0.0110	0.053	0.051	1.22
4_11	0.04	0.0417	0.0748	0.0374	0.0367	0.066	0.066	1.68
4_12	0.04	0.0417	0.1170	0.0489	0.0635	0.074	0.078	1.92
4_13	0.06	0.0417	0.1170	0.0477	0.0642	0.072	0.072	1.77
4_14	0.06	0.0417	0.0927	0.0420	0.0481	0.065	0.066	1.65
4_15	0.06	0.0417	0.0505	0.0303	0.0220	0.053	0.053	1.34
4_16	0.06	0.0208	0.0773	0.0404	0.0344	0.052	0.048	3.02
4_17	0.06	0.0208	0.0471	0.0356	0.0145	0.043	0.039	2.74
4_18	0.06	0.0208	0.0744	0.0409	0.0325	0.052	0.047	3.20
4_19	0.04	0.0208	0.0853	0.0448	0.0386	0.056	0.053	3.20
4_20	0.04	0.0208	0.1171	0.0493	0.0627	0.062	0.060	3.20
4_21	0.04	0.0208	0.0657	0.0415	0.0243	0.049	0.048	2.93
4_22	0.02	0.0208	0.0605	0.0402	0.0214	0.056	0.053	2.47
4_23	0.02	0.0208	0.0776	0.0435	0.0326	0.059	0.058	2.68
4_24	0.02	0.0208	0.1247	0.0503	0.0662	0.071	0.070	3.11
4_25	0.01	0.0208	0.1242	0.0574	0.0654	0.084	0.079	3.20
4_26	0.01	0.0208	0.0787	0.0444	0.0336	0.069	0.067	3.14
4_27	0.01	0.0208	0.0605	0.0409	0.0205	0.062	0.061	2.56
4_28	0.004	0.0208	0.0389	0.0310	0.0099	0.062	0.061	2.96
4_29	0.004	0.0208	0.0775	0.0450	0.0315	0.079	0.079	3.20
4_30	0.004	0.0208	0.1197	0.0530	0.0610	0.093	0.093	3.20
4_31	0.004	0.0208	0.1954	0.0684	0.1270	0.116	0.112	3.20
4_32	0.004	0.0417	0.1611	0.0669	0.0941	0.135	0.135	3.20
4_33	0.06	0.0208	0.1557	0.0594	0.0963	0.070	0.062	3.20
4_34	0.06	0.0417	0.1404	0.0524	0.0880	0.082	0.077	1.86
4_35	0.06	0.0417	0.0158	0.0127	0.0030	0.034	0.034	0.79
4_36	0.06	0.0417	0.0290	0.0205	0.0098	0.046	0.043	1.04
4_37	0.06	0.0208	0.0186	0.0167	0.0022	0.028	0.028	1.34
4_38	0.06	0.0208	0.0341	0.0274	0.0085	0.037	0.035	1.68
4_39	0.004	0.0208	0.0155	0.0131	0.0015	0.042	0.043	2.07
4_40	0.004	0.0208	0.0279	0.0240	0.0050	0.053	0.054	2.26
4_41	0.004	0.0417	0.0149	0.0143	0.0000	0.052	0.055	1.34
4_42	0.004	0.0417	0.0213	0.0206	0.0012	0.062	0.063	1.55
4_43	0.01	0.0417	0.0323	0.0298	0.0042	0.065	0.062	1.55
4_44	0.01	0.0417	0.0198	0.0197	0.0015	0.050	0.052	1.25
4_45	0.04	0.0417	0.0197	0.0165	0.0035	0.038	0.040	1.01
4_46	0.04	0.0208	0.0230	0.0202	0.0030	0.033	0.033	1.55
4_47	0.04	0.0208	0.0766	0.0413	0.0339	0.052	0.051	2.90
4_48	0.04	0.0208	0.1604	0.0617	0.0987	0.074	0.067	3.20
4_49	0.02	0.0208	0.1586	0.0594	0.0992	0.078	0.076	3.20
4_50	0.02	0.0208	0.0285	0.0255	0.0047	0.044	0.040	1.95
4_51	0.01	0.0208	0.0285	0.0247	0.0053	0.049	0.046	2.16

APPENDIX C. PHOTOGRAPHS

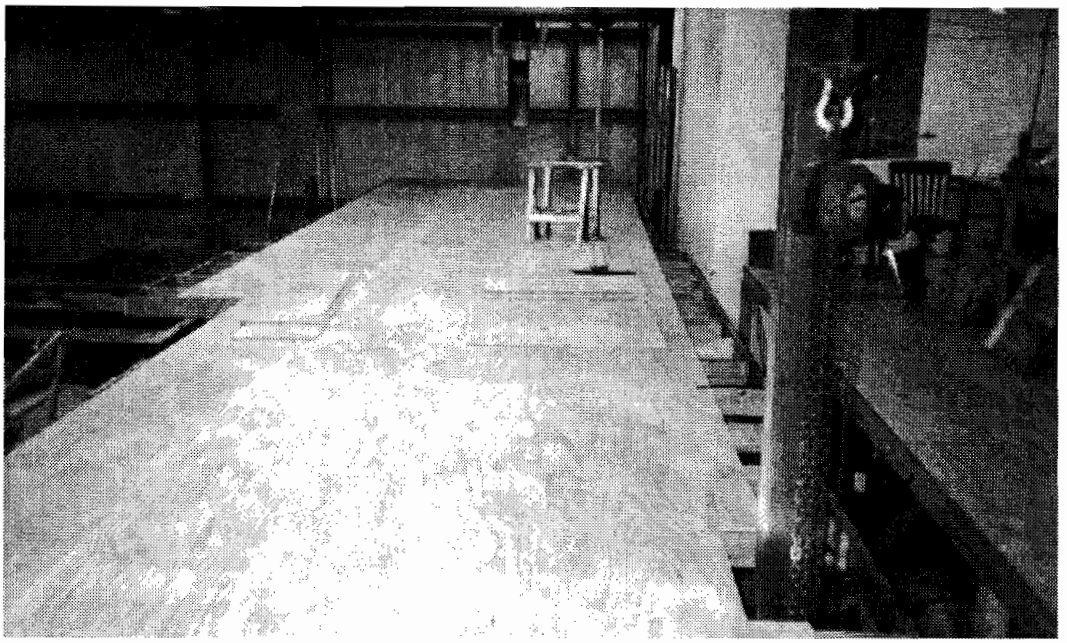

Figure C.1 Plywood Deck Under Construction, Looking Upstream

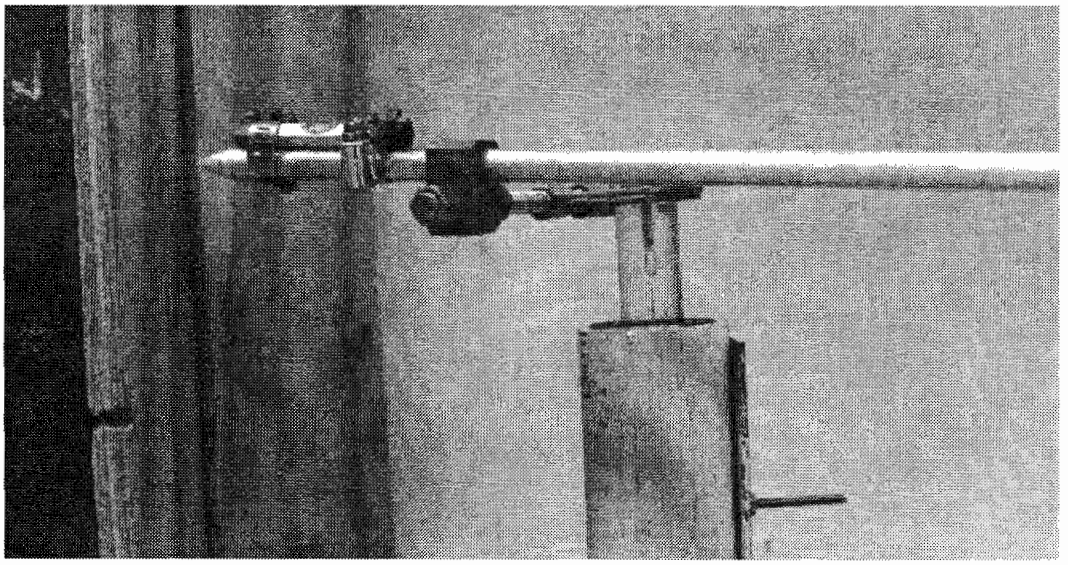

Figure C.2 Pointer mechanism

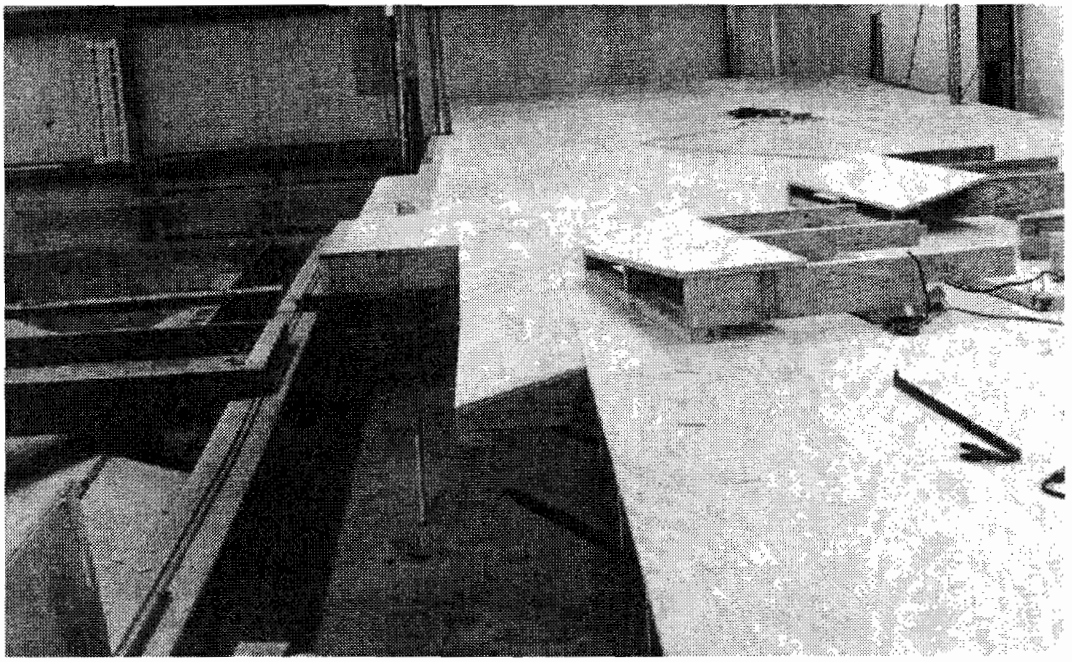

Figure C.3 Modular Curb Inlet Pieces Under Construction

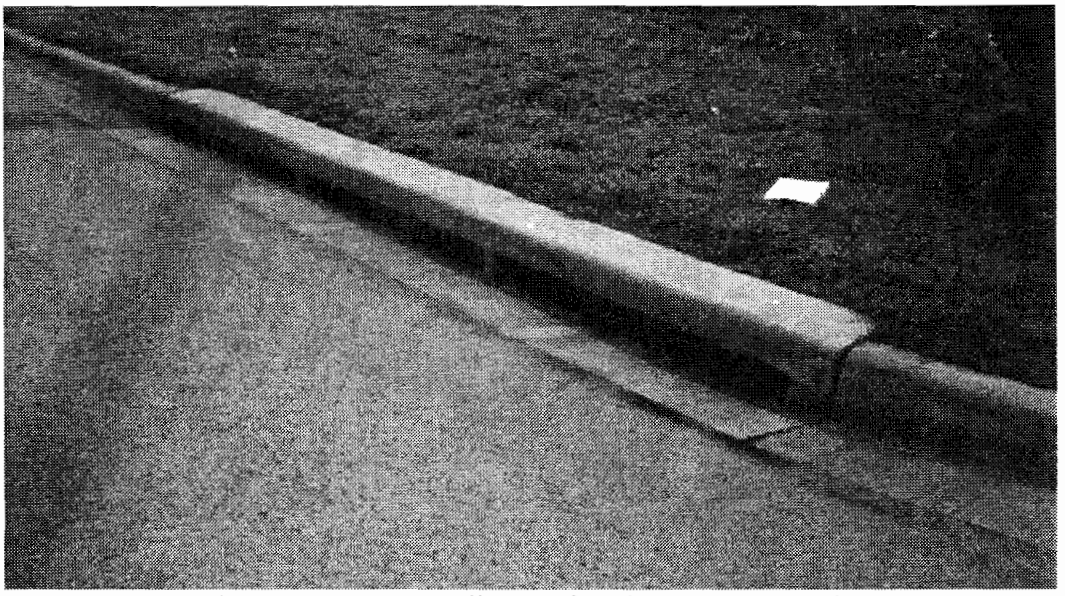

Figure C.4 Field Installation of 15-ft Type D Curb Inlet

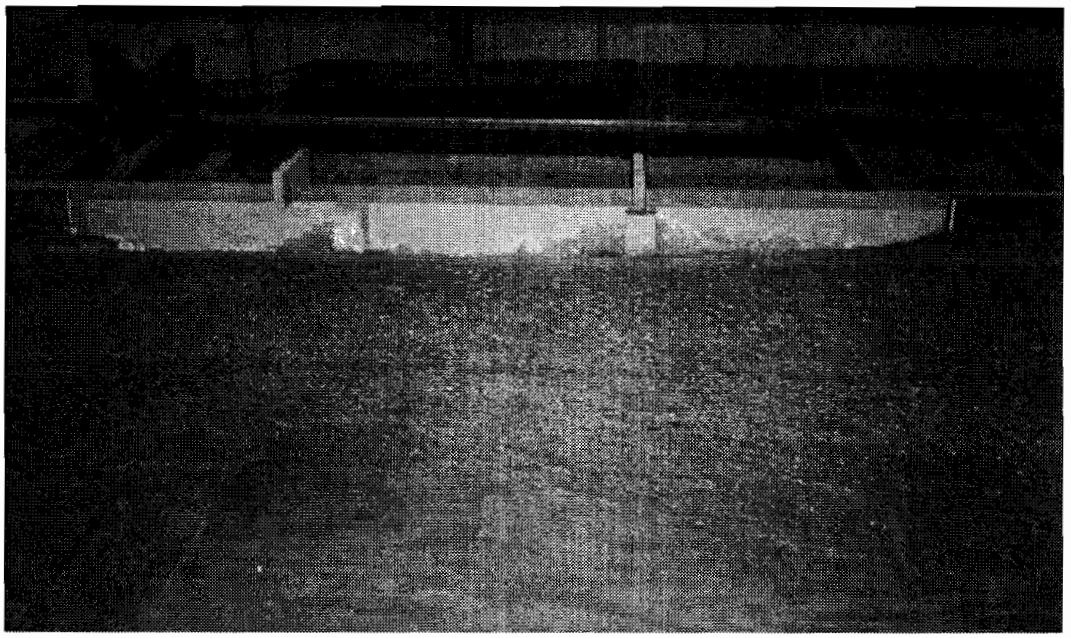

Figure C.5 Typical Less Than 100% Efficiency Test Conducted on 15-ft Inlet

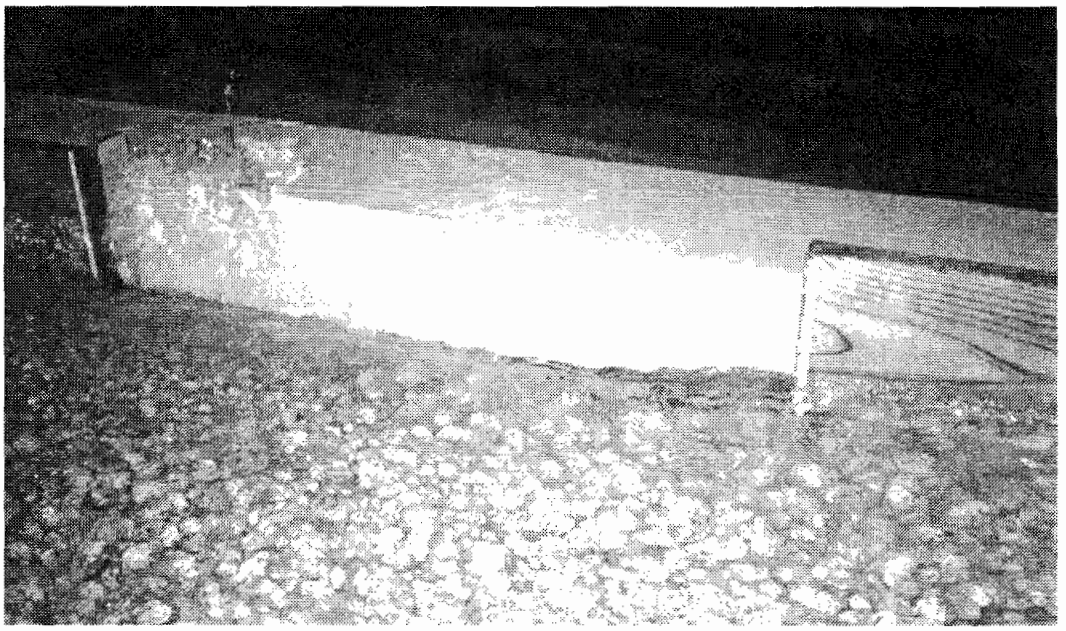

Figure C.6 Less Than 100% Efficiency Test Conducted on 5-ft Inlet, Illustrating Splashing at Downstream End of Inlet

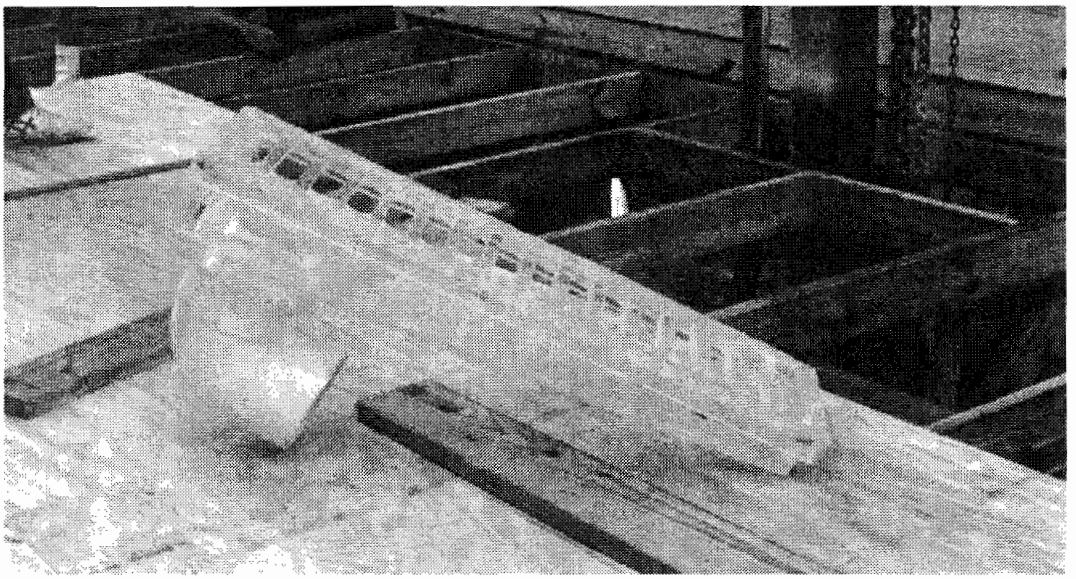

Figure C.7 Plexiglass Model of Drain 2B

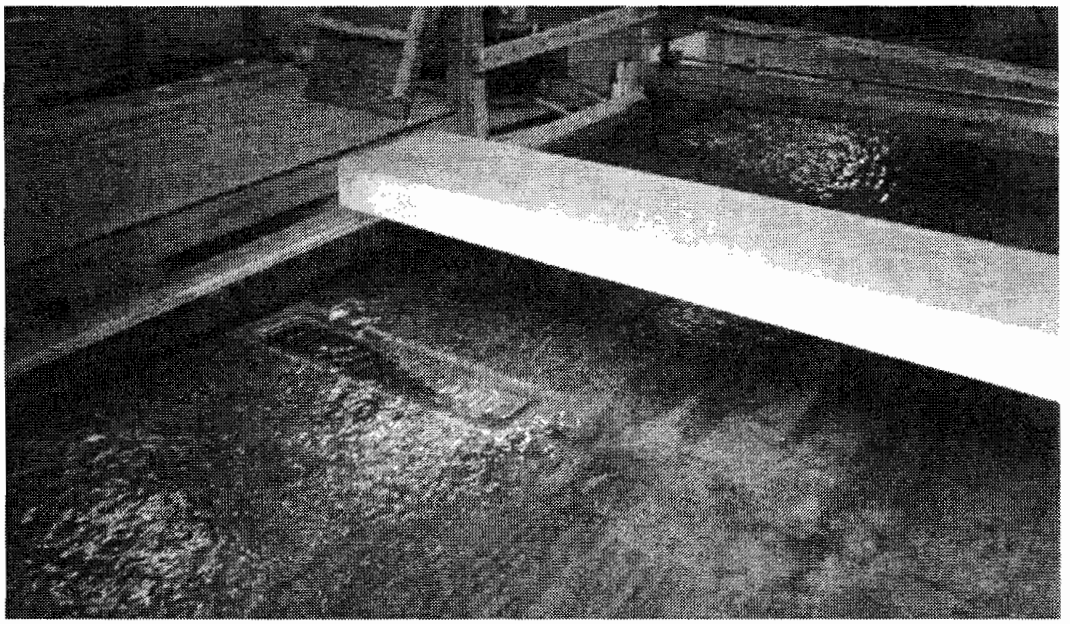

Figure C.8 Typical Test Conducted on Drain 2B, Looking Downstream

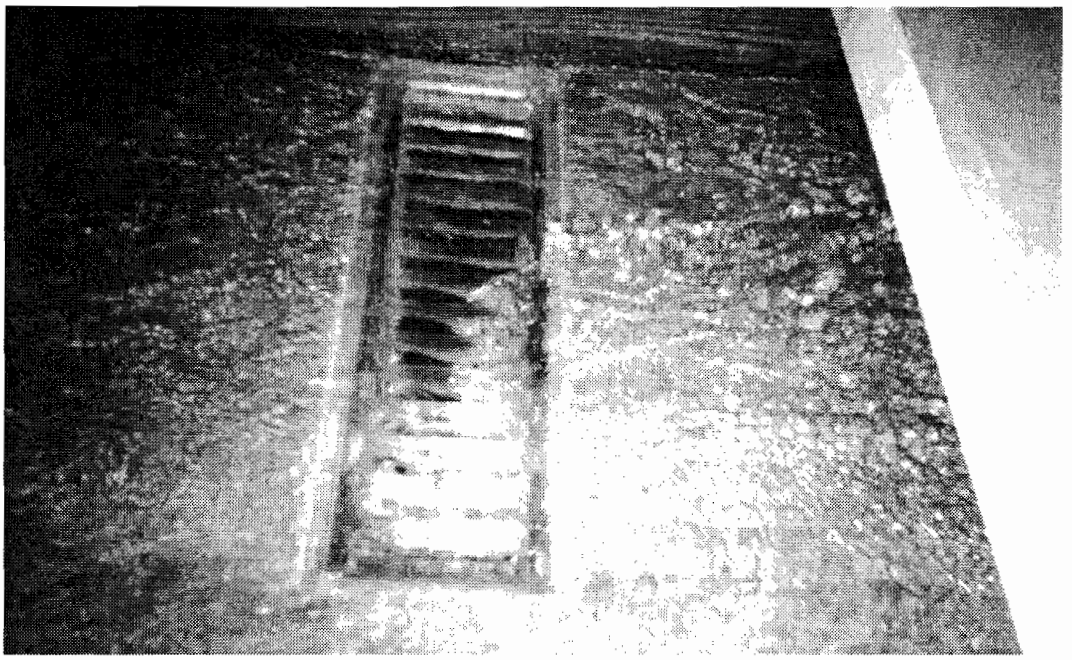

Figure C.9 Drain 2B, Partially Submerged

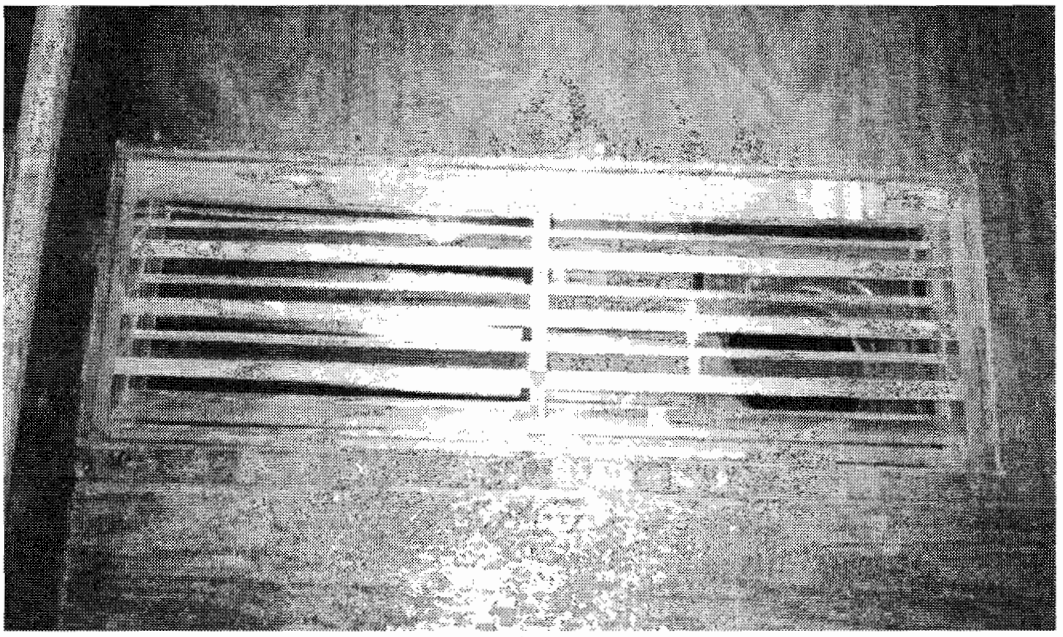

Figure C.10 Plexiglass Model of Drain 4

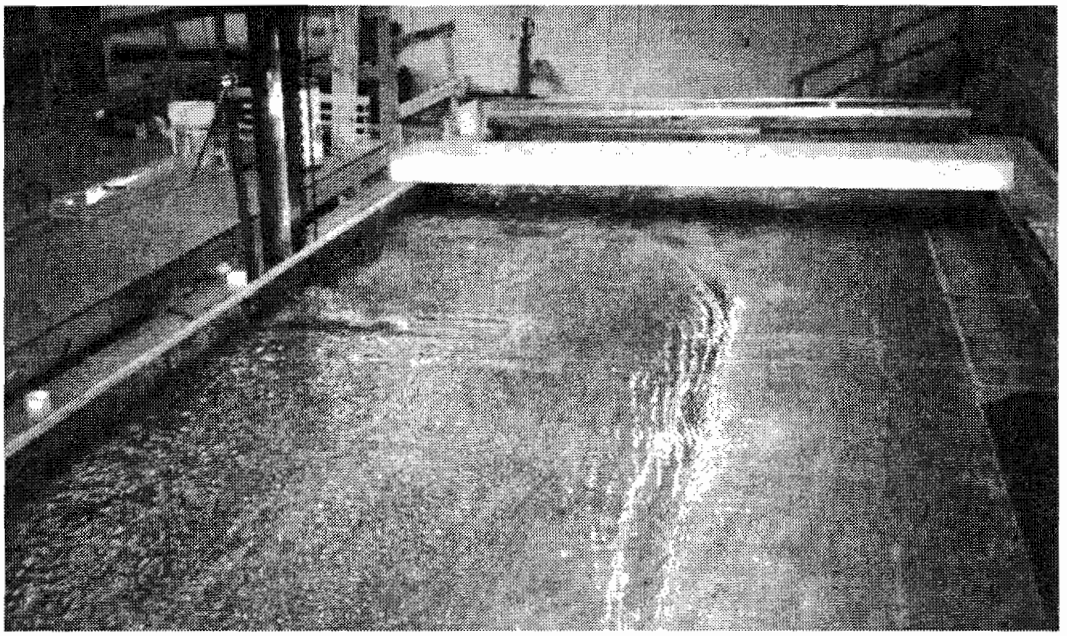

Figure C.11 Typical Test Conducted on Drain 4

Figure C.12 Test Conducted on Drain 4, Illustrating Splash Occuring at the Shallow End of the Drain Pan